7

E7.6-10130

NASA CR-144506
ERIM 101900-63-F

Final Report

S-192 ANALYSIS: CONVENTIONAL AND SPECIAL DATA PROCESSING TECHNIQUES

J. MORGANSTERN, R. NALEPKA, R. CICONE,
J. SARNO, P. LAMBECK, AND W. MALILA

SEPTEMBER 1975

(E76-10130) S-192 ANALYSIS: CONVENTIONAL AND SPECIAL DATA PROCESSING TECHNIQUES Final Report, 8 Mar. 1973 - 30 Sep. 1975 (Environmental Research Inst. of Michigan) 186 p HC $7.50

N76-16552

Unclas
CSCL 05B G3/43 00130

Prepared for

NATIONAL AERONAUTICS AND SPACE ADMINISTRATION

Johnson Space Center
Houston, Texas 77058

Contract NAS9-13280
Technical Monitor: Mr. Larry B. York

ENVIRONMENTAL
RESEARCH INSTITUTE OF MICHIGAN
FORMERLY WILLOW RUN LABORATORIES, THE UNIVERSITY OF MICHIGAN
BOX 618 • ANN ARBOR • MICHIGAN 48107

TECHNICAL REPORT STANDARD TITLE PAGE

1. Report No.	2. Government Accession No.	3. Recipient's Catalog No.
ERIM 101900-61-F		

4. Title and Subtitle	5. Report Date
S-192 ANALYSIS: CONVENTIONAL AND SPECIAL DATA PROCESSING TECHNIQUES	SEPTEMBER 1975
	6. Performing Organization Code

7. Author(s)	8. Performing Organization Report No.
J. Morgenstern, R. Nalepka, R. Cicone, J. Sarno, P. Lambeck and W. Malila	101900-61-F

9. Performing Organization Name and Address	10. Work Unit No.
Environmental Research Institute of Michigan P.O. Box 618 Ann Arbor, Michigan 48107	11. Contract or Grant No. NAS9-13280
	13. Type of Report and Period Covered FINAL REPORT; 8 March 1973 through 30 September 1975

12. Sponsoring Agency Name and Address	14. Sponsoring Agency Code
NASA/Johnson Space Center Houston, Texas 77058	

15. Supplementary Notes

Mr. Larry B. York has been Technical Monitor for NASA.

16. Abstract

Results of an investigation into the utility of conventional and special processing techniques as applied to SKYLAB S-192 multispectral scanner data for the automatic extraction of resource information are reported. As a part of this investigation, S-192 data gathered over test sites in Southeast Michigan were analyzed. This analysis showed the data to be somewhat deficient especially in terms of the limited signal range in most SDOs and also in regard to SDO-SDO misregistration. Further analysis showed that the scan-line-straightening algorithm increased the misregistration of the data. As a result, the processing on this contract was carried out using conic format data. The effects of such misregistration on classification accuracy was analyzed via simulation and found to be significant. Results of employing conventional as well as special, unresolved object, processing techniques were disappointing due, at least in part, to the limited signal range and noise content of the data. Application of a second class of special processing techniques, signature extension techniques, yielded better results. Two of the more basic signature extension techniques seemed to be useful in spite of the difficulties.

17. Key Words	18. Distribution Statement
Remote Sensing Earth Resources Pattern Recognition	Approval for public release distribution unlimited.

19. Security Classif. (of this report)	20. Security Classif. (of this page)	21. No. of Pages	22. Price
UNCLASSIFIED	UNCLASSIFIED		

PREFACE

This final report presents results of an investigation carried out at the Environmental Research Institute of Michigan (ERIM), to analyze the SKYLAB S-192 multispectral scanner data and to assess the utility of special (unresolved object and signature extension) processing and information extraction techniques for the remote sensing of Earth resources.

The research covered in this report was performed under Contract NAS9-13280 and covers the period between March 1973 and September 1975. During this period Mr. L. B. York has been Technical Monitor for NASA. Expenses for the preparation of data and some of the processing were shared by this contract and ERIM's subcontract to Michigan State University's Contract NAS9-13332 which utilized data collected over the same test site. The program was directed by R. R. Legault, Vice-President of ERIM; J. D. Erickson, Head of the ERIM Information Systems and Analysis Department; and R. F. Nalepka, Principal Investigator and Head of the ERIM Multispectral Analysis Section. W. A. Malila was Co-Principal Investigator. The ERIM number for this report is 101900-61-F.

Part of this investigation was to test information extraction techniques for SKYLAB S-192 data, and compare those results with results obtained from processing LANDSAT and aircraft multispectral scanner data as well. Unfortunately, the Southeast Michigan test site was cloud covered during every LANDSAT-1 pass from June to September, so it was impossible to obtain LANDSAT data over the test site during some time in the growing season that would in some way be comparable to the S-192 data set being studied, thus it was not possible to comparably process LANDSAT data for this investigation.

The authors wish to thank Dr. L. V. Manderscheid of Michigan State University, East Lansing for making available the ground information for the test site. Special acknowledgement is due to R. B. Crane and J. Gleason of the ERIM Multispectral Analysis Section (MAS) staff for their technical assistance and suggestions on the data misregistration studies which were carried out.

The technical work for the study of effects of misregistration (Section 4) was conducted by R. Cicone and the signature extension work (Section 5) was carried out by P. Lambeck. Numerous other MAS technical staff members contributed to the success of this investigation as well. Throughout this contract period secretatial assistance has been provided by Ms. D. Dickerson, L. Parker, G. Sotomayor and E. Hugg.

CONTENTS

CONTENTS (Continued)

CONTENTS (Continued)

FIGURES

FIGURES (Continued)

TABLES

TABLES (Continued)

SUMMARY

The objective of this investigation was to examine the utility of special processing techniques as applied to Skylab S-192 data for the automatic extraction of resource information. These special processing techniques include signacure extension algorithms to extend the applicability of signatures over distance,time, and/or measurement conditions and mixture classifiers to estimate proportions of spatially unresolved objects. As a part of this investigation, S-192 data gathered over Southeast Michigan were analyzed and three sites were studied 1) a 90 square mile agricultural area in Ingham County, 2) an urban and rural area in the vicinity of Lansing, and 3) an urban and rural area in the vicinity of Ypsilanti.

Upon receipt of the data we examined the data quality, investigating in each SDO (Scientific Data Output) signal-to-noise characteristics and dynamic range. Aircraft scanner data gathered over the agricultural site the morning of S-192 data collection were examined also and used as a basis for comparison. The results of the examination of S-192 data quality were essentially in keeping with the published S-192 performance evaluations [4]. A conclusion reached was that all spectral bands had a very limited range of values in relation to the noise content of the data; four of the bands were sufficiently noisy so as to be of doubtful use in classification processing. Also examined was the spatial registration of the scanner data. The SDO-to-SDO misregistration in conic data was measured and shown to be greater than one pixel in some instances. More importantly, further analysis showed that the effect of scan-line-straightening was to compound and increase the misregistration of the S-192 data: a maximum misregistration of 2.2 pixels was calculated. Not only is the misregistration of scan-line-straightened data not easily correctable but the additional misregistration seriously reduces the number of pure pixels available for training.

Analytical and simulation studies were then performed to investigate the effects of misregistration on classification accuracy. The results showed that, for pixels which imaged more than one ground class in one or more channels, the error rate was substantial and increased as the degree of misregistration increased. Also shown was that, while the correct classification rate for pure (one class) pixels did not change significantly as misregistration increased, the number of such pure pixels markedly decreased as misregistration increased. Because of the increased, uncorrectable misregistration in scan-line-straightened data, the recognition processing for this contract was carried out with conic data. Using the conic data, we were able to substantially correct for misregistration by selecting a set of 13 SDOs (one for each band) and shifting some relative to others such that the maximum misregistration was one third of a pixel.

In preparation for recognition processing of the agricultural test site using conventional techniques, a set of training statistics was extracted using a supervised clustering method applied to pure (one class) pixels from half the area. In this manner, several recognition signatures were defined for each class, the number depending on actual physiological and physical phenomena as well as on economic designations. Having established the signatures, the utility of the 13 spectral bands for recognition processing in the agricultural area was determined. Using a computer algorithm which computed the average pairwise probability of misclassification, the 13 bands were rank ordered with the result that the four bands previously identified as having poor signal quality were adjudged to be among the worst bands. The two best bands, by far were 1.55-1.73 μm (SDO 12) and 0.93-1.05 μm (SDO 19). The result of classifying the agricultural site using conventional techniques and the 7 best bands provided an overall correct classification rate of 75% for the pure (one-class) pixels for the local (training) area and 63% for the nonlocal (test) area. A second measure of performance, the overall estimation of class proportions, was based on aggregated classification counts of all pixels in the area. These results, which are given as the root mean square error of the estimates summed over all classes, were E=4.7% for the local area and E=6.9% for the non-local area.

In both cases, great confusion was noted in a triad of corn, trees and brush. The classification of the data was affected by a combination of the limited signal range in the data and the apparent spectral similarity of many of the ground classes. The latter effect was attributed to the contrast reducing effect of atmospheric haze and the fact that, at the time of year the data was collected, there was a large range of conditions for several classes (e.g., some of the corn had tasseled and some had not) leading therefore to added spectral similarity among classes. The errors in the proportion estimation were also affected by the large number of mixture (more than one class) pixels in the scene. A brief study indicated that more than 70% of the scene was composed of such mixture pixels. In general a disproportionate number of such pixels were classified as corn, resulting in a substantial overestimation of corn in the scene.

The utility of signature extension techniques for S-192 data was tested using the Lansing and Ypsilanti sites for training and test, respectively. Signature extension techniques are potentially useful for reducing costs and data processing time for large area surveys and are an important part of multispectral data processing. Several signature extension techniques developed at ERIM for use on LANDSAT and/or aircraft data were utilized to process data for the signature extension test site located some 70 miles from the signature extension training area. The test area was chosen particularly because a layer of haze covering this site was very evident in the S-190B imagery; thus, this was a test under very different atmospheric conditions as well as a test over distance. Training statistics were gathered using an unsupervised clustering technique and clusters were identified for urban, residential, vegetation, water, concrete, bare soil and sparse vegetation. A classification attempt without the use of signature extension techniques resulted in poor accuracy while the use of signature extension techniques improved classification accuracy. The best results were obtained using the dark object algorithm. In a qualitative sense these results matched those obtained using local clusters (i.e., clusters generated at the signature extension site).

Further classification was carried out on both training sites previously mentioned using the other special classifier. This classifier, the unresolved object or mixtures classifier, first identifies each pixel as being either pure or a mixture of several classes and, if it is a mixture, estimates the proportions of pure ground covers in that resolution element. Such a classifier would seem to be well suited to a data set where more than 70% of the pixels were mixture pixels. The results of using this approach on both sites was unsatisfactory, due apparently to the previously mentioned limited signal range, contrast and and spectral discriminability of the data. Thus, no general conclusions were drawn with regard to the utility of the mixtures classifier on S-192 data.

Results of this investigation indicate that deficiencies in the S-192 data will tend to limit its ultimate utility. To minimize deleterious effects of channel-to-channel misregistration in any future use of S-192 data, use of conic format data is recommended. Furthermore, the design of future multispectral scanner and data processing systems should take into account the experience gained in processing and analyzing S-192 data. To this end, two recommendations are made. First, finer spatial resolution should be considered for future sensors; this would alleviate the problems caused by having a large proportion of mixture pixels in the scene and the attendant problem of having so few pure pixels on which to base training statistics. The second recommendation is that future systems provide a means to adjust scanner gain and offset parameters to better match the radiance characteristics of individual scenes and thus make fuller use of the available scanner dynamic range.

1
INTRODUCTION

Remote sensing of earth resources using multispectral scanners and automatic information extraction techniques has been shown over the past several years to be a feasible and viable tool for providing information required by resource managers in many disciplines. Early multispectral scanners used low-flying aircraft platforms for data collection. In 1972, multispectral remote sensing systems became spaceborne with the launching of the first LANDSAT (initially called the Earth Resources Technology Satellite). As it steadfastly orbited the earth, it was capable of providing information from four broad spectral bands. Moreover, its orbit characteristics allowed it to overfly the same site every 18 days, allowing for timely collection of data as well as enabling the use of temporal information.

SKYLAB, the first U.S. orbiting manned space station, carried as part of its payload a new multispectral scanner, designated as sensor S-192. The S-192 is more sensitive spectrally than LANDSAT, having 13 bands across the visible, near-infrared and thermal-infrared portions of the spectrum. The purpose of this contract was to analyze the data collected with the S-192 and adapt previously developed information extraction techniques for such data, especially in regard to problems associated with signature extension and subresolution element classification. Signature extension techniques potentially provide the ability to use training data from one scene gathered under different conditions. Subresolution element classification refers to techniques designed to estimate the proportion of the constituent ground covers in resolution elements containing two or more different ground covers.

The data used in this study were acquired on August 5, 1973 at approximately 10:02 EST (15:02 GMT) over an area of Southeast Michigan stretching between Lansing and Detroit. A five by 18 mile rural area comprising the townships of Locke, Leroy and White Oak in Ingham County was designated as the agricultural intensive study site for the contract, and detailed ground information for this area was collected. The principal ground covers of the test site are corn, various pastures, grasses, wheat stubbles and weeds, dense woodlots, scrub and brush areas and bare soil. Appendix III more fully describes the test site. As for the weather on the morning of the overflight, a nonuniform haze layer was covering this test site area according to ground observers.

Subsidiary data other than that collected by the S-192 that were used for this study include imagery from the SKYLAB EREP S-190A multiband camera and the S-190B fine resolution camera, screening film (video presentation) of each channel of the S-192, and 9-inch false color infrared photography acquired by a high altitude aircraft. Also, at the time of S-192 data acquisition, the ERIM C-47 aircraft carrying the ERIM M-7 12-band multispectral scanner made repeated passes over the test site, collecting MSS data from several altitudes. Color, false color IR, and black and white IR photography were also collected by the C-47 during these underflights. LANDSAT data for the area for the 1973 growing season was unavailable since the area was cloud covered on all passes of that satellite.

For this study, SKYLAB S-192 data were obtained in two formats: scan-line-straightened data and unstraightened or conic format data. In both cases the data were radiometrically corrected and had been processed at Johnson Space Center to reduce the effects of low and high frequency noise.

The remaining sections of this report discuss many aspects of the investigation in some detail. In Section 2 the analysis of the S-192 data is discussed. Questions related to signal-to-noise, dynamic range, and band-to-band registration are addressed and S-192 and M-7 signal characteristics

are compared. Section 3 presents and analyzes classification results achieved over the Southeast Michigan agricultural test site. The effects of channel-to-channel misregistration as determined via simulation are discussed in Section 4. The classification results achieved in applying signature extension and subresolution element processing techniques are described in Sections 5 and 6, respectively. Section 7 provides conclusions and recommendations arising out of the investigation.

2
DATA QUALITY ANALYSIS

2.1 INTRODUCTION

This section discusses the SKYLAB S-192 multispectral scanner and the quality of the data recorded from it. A thorough understanding of the workings of the scanner and the characteristics of the resultant data is necessary to successfully process the data and interpret the results. At the end of the section, the S-192 data characteristics are compared to those of another scanner, the aircraft mounted ERIM M-7 scanner.

2.1.1 DESCRIPTION OF S-192

The S-192 is extensively described elsewhere [1] and in Appendix I; here we describe it briefly to introduce the concepts necessary for understanding the material in this report.

The S-192 has a conical scan, with a scan frequency of 94.79 scans/seconds, using only the forward 116^{o} of the scan for obtaining earth resources information. The scanner instantaneous field of view is 0.182 mrad (approximately 81 m on the ground at spacecraft orbital altitude) and successive scan lines overlap by about 10%. The data are oversampled by 10% along the scan line as well, so the effective pixel (picture element) size is about 72m x 72m. Data over the Southeast Michigan test site were collected at an altitude of 441,429 meters. While the data are originally collected as conic scan lines, i.e., along an arc of a circle, the data are processed at NASA/Johnson Space Center to produce scan-line-straightened data to conform with the majority of data display forms. This aspect of the data will be extensively discussed later.

There are 13 detectors on the S-192, and the wavebands covering the visible, near infrared, and thermal infrared portions of the spectrum are listed in Appendix I. The data from each detector were sampled and recorded in the SDOs (channels) noted in the table. Each pixel, or picture element,

contains 22 SDOs. The data were sampled so that the 13 detectors produced 22 channels as follows: for all odd numbered SDOs, their detectors' signals were sampled at the same instant during the scan, time t. For all even numbered SDOs, the appropriate detectors were simultaneously sampled at a later instant, $(t + \Delta t)$, one half pixel along the scan line after time t. Thus eight of the detectors are sampled twice for each data point, and the thermal detector odd SDO sample is recorded both in SDO 15 and SDO 21. Those detectors which are sampled twice for each pixel (e.g., SDOs 1 and 2) are referred to as high sample rate bands while the other detectors are referred to as low sample rate bands.

The following sections will describe and analyze the data from the S-192 in terms of signal characteristics, spatial registration and resolution, and will discuss their impact on processing of S-192 data.

2.1.2 SIGNAL CHARACTERISTICS

The processing of the S-192 data was begun by analyzing the information content of the data channels. While we are interested in using differences in reflectance (and/or emittance and temperature) characteristics to discriminate between the ground covers of interest, the data values recorded on the tape are only indirectly related to the ground reflectance (or thermal) characteristics, being acted upon by the atmosphere, the sensor optics and electronics, and the digitizing electronics [2]. Here we consider just the effect of the system electronics on the radiant energy collected by the scanner. In the end, the desired output from a system of this sort are signals which, for different object classes, are distinct enough to allow classification of the data based upon pattern recognition techniques. The components of the system effects which can be analyzed and discussed are the sensitivity and linearity of the individual detectors and the detector output utilization of the dynamic range of values available. There is also the consideration of system noise, especially in relation to the signal levels being output by the detectors. Finally, the apparent registration of the system should also be inspected.

The first part of this section describes various measurements made on the S-192 data. Where it is difficult or impossible to derive absolute measures for several of these components, measures of the S-192 relative to those of another multispectral scanner will allow us to obtain a better feel for the performance of the S-192. The remainder of this section, therefore, discusses these same measurements as made on the ERIM M-7 aircraft mounted scanner data and the results for the two scanners are compared.

To begin with, screening imagery and digital gray scale printouts (graymaps) of each SDO were visually analyzed for noise characteristics. It was seen that while most channels appeared to be of good quality, three detectors (SDOs 5,6; 7,8; 18) contained a high degree of scan-line dependent noise and two detectors (SDOs 15,16,21; 22) were so noisy that there was no visible structure in the data. By scan line dependent noise we mean that striations along the arc of the conic scan were quite prominent. Figure 2.1 displays a piece of screening film for one SDO from each group, and Figure 2.2 indicates the portions of the spectrum covered by the three groups of SDOs. As noted, the two detectors in the last group are the thermal band, 10. - 12.68 μm and the .41 - .45 μm band respectively. In the case of the thermal band, it has been reported [3] that the noise equivalent temperature for the thermal detector for this data set is 2.6°K. It is entirely possible that this noise level exceeds the temperature changes occurring in the scene so that there is essentially no information in this band. It was further noted that one of the noisier detectors is the .66 - .73 μm band which covers the region of chlorophyl absorption. This is unfortunate since this band is usually a key band in the processing of multispectral data for agricultural areas. It was also noted from viewing these graymaps that most roads and other features useful for location of fields were not readily evident.

SDO 12: 1.55-1.73 μm

SDO 18: .45-.50 μm

SDO 22: .41-.45 μm

FIGURE 2.1. SCREENING FILMS FOR S-192 DATA. Examples of clear data, some scan line noise, very noisy data.

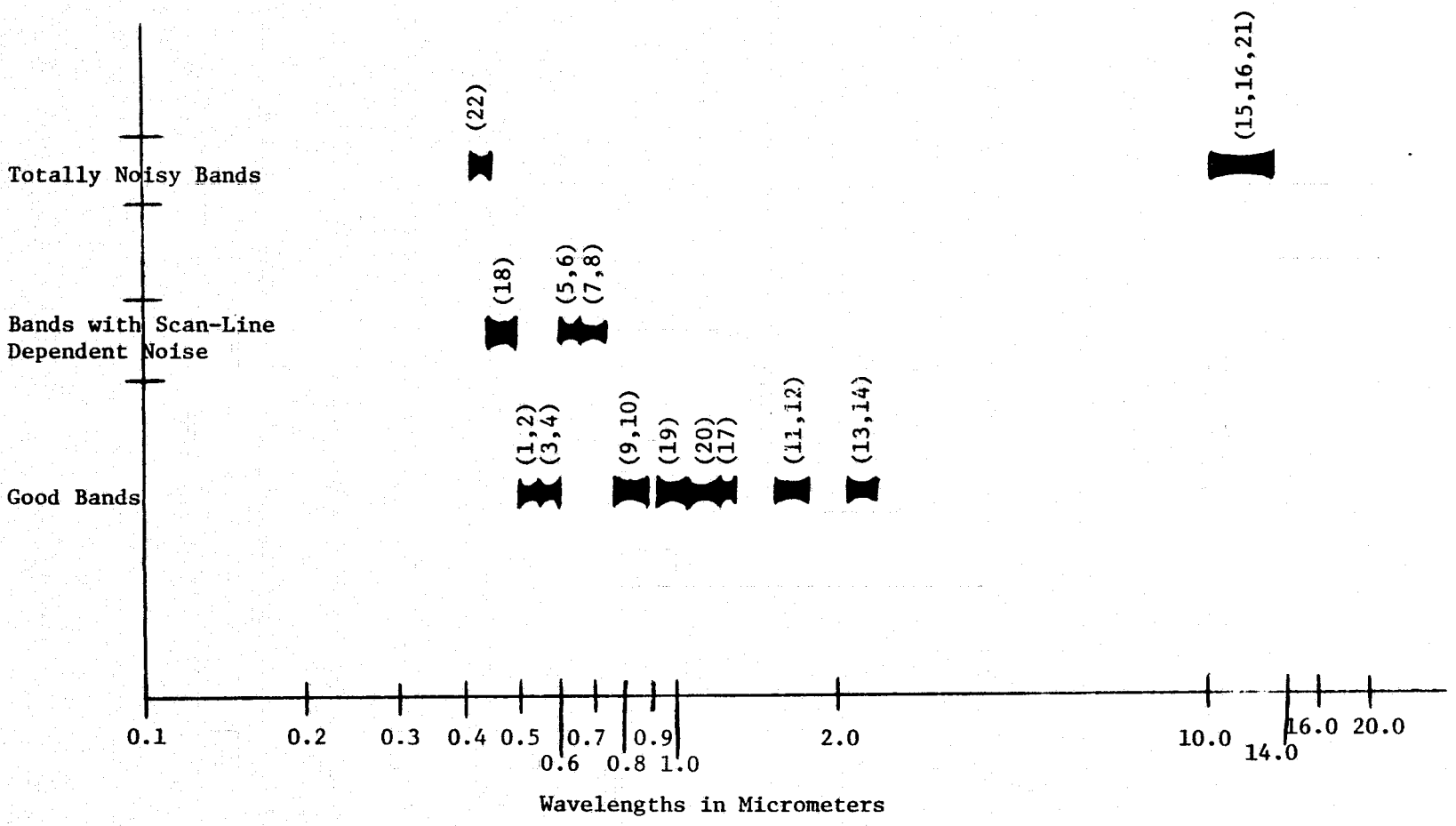

FIGURE 2.2. SPECTRAL LOCATION OF GOOD AND NOISY S-192 BANDS (SDO Numbers Given Parenthetically)

Following this, a more analytic analysis of S-192 signal quality was carried out. The first, dynamic range of the data, was obtained by examining histograms of pixels from an area 600 lines long by 700 points wide. The area sampled included urban, water, forested and rural areas and included the agricultural test site. The results, as listed in Table 2.1, were tabulated in two ways. In examining the histograms it was not clear at which point on the tails one no longer had data but rather was just viewing infrequent noise spikes. Accordingly two rules were used for determining the range: for the first, the limit was taken as occurring at the first empty bin of the histogram; for the second, the data values between the tenth and 90th percentile were used. In the latter case, we are looking at the range of values for 80%, or most, of the data. Here the dynamic range was between 6% and 12% of the available range of 256 counts; no SDO had more than 5 bits of significance.

To obtain a fuller picture of the situation, these results need to be compared to the noise content in the data, as well as the separability of signals representing different ground classes.

Measuring the noise characteristics of the scanner, i.e., noise from electronic sources not including scene dependent sources, requires analyzing data from a uniform reflector. The closest thing to a uniform reflector that the data set included was a large lake. We developed statistics, means and standard deviations in each SDO, from the pixels of the lake. We use them here with the following strictures. Because of weeds and other suspended vegetation in the water, patches of shallow water and some atmospheric back-scattering at the blue end of the visible spectrum, the estimates of the noise given by the standard deviation will be greater than the true condition. At longer wavelengths these effects are diminished and the accuracy of the estimate improves. In Table 2.2 we present the mean and standard deviation measured; the signal:noise calculated is the ratio of these two quantities. One further measure, range:noise, is the ratio of the dynamic range to the

TABLE 2.1. S-192 DATA QUALITY ANALYSIS:
DYNAMIC RANGE IN COUNTS

In each column, the first entry indicates the data values, the second is the number of counts.

DETECTOR	SDOs[1]	DYNAMIC RANGE[2]	DYNAMIC RANGE[3]
1	22	76-126, 50	89-105, 16
2	18	[4]90-140, 50	95-117, 22
3	1,2	48-98, 50	57-70, 13
4	3,4	18-71, 53	29-42, 13
5	5,6	14-81, 67	29-48, 19
6	7,8	37-110, 73	67-86, 19
7	9,10	21-126, 105	64-94, 30
8	19	41-125, 84	75-105, 30
9	20	22-123, 101	74-97, 23
10	17	16-118, 102	73-96, 23
11	11,12	13-99, 86	44-63, 19
12	13,14	4-95, 91	20-42, 22
13	21,15,16	126-177, 51	140-156, 16

Maximum Range Available: 0-255

[1]For the doubly sampled detectors, results were calculated for both SDOs and found to be in agreement -- as would be expected. Hence they are reported together.

[2]Used continuous rule

[3]Used 10% to 90% rule

[4]Trimodal distribution; reported is the major distribution

TABLE 2.2 S-192 DATA QUALITY ANALYSIS: SIGNAL:NOISE

DETECTOR	SDOs[1]	SIGNAL MEAN	STANDARD DEVIATION	SIGNAL:NOISE	RANGE:NOISE
1	22	95.8	5.6	17.1	2.9
2	18	102.4	11.7	8.8	1.9
3	1,2	56.5	2.8	20.1	4.6
4	3,4	29.3	2.8	10.5	5.4
5	5,6	32.4	5.2	6.2	3.7
6	7,8	42.1	4.8	8.8	4.0
7	9,10	26.4	8.3	3.2	3.6
8	19	23.5	5.0	4.7	6.0
9	20	26.1	6.4	4.1	3.6
10	17	18.1	5.3	3.4	4.3
11	11,12	14.4	3.3	4.4	5.8
12	13,14	10.3	4.4	2.3	5.0
13	21,15,16	144.3	4.8	30.1	3.3

[1]For the doubly sampled detectors, results were calculated for both SDOs and found to be in agreement -- as would be expected. Hence they are reported together.

noise and indicates the number of "noise σs" wide the data range is in each band. For this calculation we used the dynamic range according to the 10% rule, since we are interested in the majority of the data points. It is noteworthy that the bands specified as exceedingly noisy at the beginning of the analysis have the lower range:noise values, although their signal:noise may be good.

To complete the analysis of signal quality we would like to get a feel for the detector sensitivity. However, it will be possible to do this only in a relative sense. By locating, for different ground classes, the same areas on the ground in both the S-192 and M-7 data sets, signatures may be calculated and either distances between the distributions or probabilities of misclassification (the degree of overlap between pairs of signatures) may be calculated and used to compare the separability of signals between the two scanners.

Two areas* were located in the test site and signatures, mean and covariance matrices, were calculated from the pixels in each field. These two fields were chosen solely because they were the two largest occurrences of different classes that appeared in both the S-192 and the M-7 data sets. We wanted the largest fields possible so as to have a sufficient number of pixels in the S-192 data set and thus to well estimate the signatures for these fields. The corn field was very large and as a result 59 field center pixels were identified and used for the signature calculation. The woodlot, on the other hand, was not small but still only nine field-center pixels could be identified for the woodlot. To measure the distance between the signatures we have chosen to calculate a form of the Bhattacharyya distance. The distance calculated was**

$$D = (\mu_C - \mu_T)\left(\frac{\Sigma_C + \Sigma_T}{2}\right)^{-1}(\mu_C - \mu_T)^T$$

*Fields chosen were a large corn field in Section 16, Leroy Township and a large hardwood woodlot in Section 4, Leroy Township.

**The full form of the Bhattacharyya distance is:

$$B = \frac{1}{8}(\mu_C - \mu_T)\left(\frac{\Sigma_C + \Sigma_T}{2}\right)^{-1}(\mu_C - \mu_T)^T + \frac{1}{2}\left|\frac{1}{2}(\Sigma_C + \Sigma_T)\right| \Big/ \left|\Sigma_C\right|^{1/2}\left|\Sigma_T\right|^{1/2}$$

where μ_C and μ_T are the mean vectors of corn and trees respectively

and $\sum_C$ and $\sum_T$ are the covariance matrices for corn and trees.

To enable us to analyze the situation even more closely, we calculated D_i for each channel or

$$D_i = \frac{(\mu_{Ci} - \mu_{Ti})^2}{\frac{1}{2}(\sigma_{Ci}^2 + \sigma_{Ti}^2)}$$

and the results are given in Table 2.3 below. Obviously, the larger the distance calculated, the greater the separation between the two distributions.

TABLE 2.3 DISTANCE BY DETECTOR BETWEEN CORN FIELD AND WOODLOT FOR S-192

DETECTOR	SDOs	D_i
1	22	0.45
2	18	0.47
3	1,2	1.42
4	3,4	0.06
5	5,6	0.0003
6	7,8	3.3
7	9,10	4.42
8	19	5.20
9	20	3.03
10	17	0.20
11	11,12	3.3
12	13,14	0.40
13	21,15,16	0.05

Readily apparent is the large disparity in the table's values. In general those bands which had been identified as being noisy have very small distance values (D_i), the exception being band 6 (.67 - .73 μm) which is in the spectral region of chlorophyl absorption. Other bands with small distances merely indicate very little separability in these bands for these two object classes. In Section 2.3 these results were compared to those obtained by analyzing signatures of these same two areas calculated from the M-7 data set. This provides some measure of how well or how poorly the distributions are separated in the S-192 data.

In summary, S-192 data has been analyzed in several ways and has been shown to have limited signal range, especially in relation to the system noise. By the word system is meant the combined optics and electronics of the data collection facility and also the data preprocessing facility. Conclusions on how accurately such data can be classified, however, are not easily drawn from this information. By comparing S-192 data characteristics to those of another multispectral scanner we may obtain a better understanding of the situation. In Section 2.3, such a comparison is made.

2.1.3 SPATIAL REGISTRATION

Multispectral remote sensing and multivariate analysis have at their core the concept that many channels of information regarding one data point (pixel) can be used to more accurately classify it. One necessary condition, obviously, is that all the channels of information used must refer to the same point or condition. For example, if most channels of a pixel of multispectral data image an area of class 1, while some other of the channels image an area of class 2, it may not be possible to correctly classify the pixel. Thus, all channels of information must be spatially registered, i.e., all imaging the same area on the ground, if one is to achieve good results. If the data are seriously misregistered it may be possible to process the data in such a way as to substantially correct the problem. We analyzed both the conic data and the scan-line-straightened data for misregistration. It turned out that the scan line straightening procedure further misregisters the data so that the conic data are more registered than the scan-line-straightened data. Details of two analyses are presented below.

2.1.3.1 Misregistration in Conic Data

By the S-192 system design, all even-numbered SDOs are perfectly registered one with the other; the same is true for all odd numbered SDOs. Further, there is a one-half pixel misregistration between the odd numbered SDOs and the even numbered SDOs due to the sampling technique used. Further misregistration is introduced by scanner electronics, by different response times for different detectors, and/or by improperly skewed record heads on the spacecraft tape recorder. These combine to produce the misregistration observed in the conic data.

Misregistration in conic data, i.e., misregistration caused by scanner and related recording electronics, has been documented by Braithwaite and Lambeck [3,4]. The measurements carried out were made using scans of the lunar surface and were accurate to a quarter pixel. These results showed that SDOs 17, 19, and 20 lagged one half pixel from where they would be expected. To investigate the registration properties of the data set being processed, a short manual investigation was carried out for the conic data set utilizing the fact that significant reflective changes occur at land/water interfaces in many of the bands. These results were in agreement with those cited above, again with a quarter pixel error in measurement.

To obtain more precise answers as to what the spatial misregistration characteristics of the conic data were, a more analytical technique was developed. The technique used is thoroughly presented in Appendix IV; here we summarize it briefly so that the discussion of the results will be understandable.

To determine the misregistration between two channel , the cross correlation was determined over a range of fractional pixel shifts. The cross-correlation function then has a maximum at the shift representing the actual misregistration. Initial tests of the method indicated that the values near the peak closely approximated a quadratic curve. To obtain a more accurate estimate of the shift at which the peak actually occurs, a quadratic curve was fit to the three shift values nearest the peak. From the coefficients of this curve, the peak of the cross-correlation function was estimated.

Table 2.4 contains the estimated misregistration between 17 of the original 22 Skylab SDOs. The SDOs (15,16,18,21,22) which do not appear in the table were not used in this investigation, because they were not sufficiently correlated with any other channels to obtain meaningful results.

TABLE 2.4. SKYLAB S-192 SENSOR MISREGISTRATION (PIXELS)

	1	2	3	4	5	6	7	8	9	10	11	12	13	14	17	19	20
1		-.50	.05	-.45	-.01	-.51	-.14	-.64	-.33	-.83	-.12	-.62	-.07	-.57	.23	.30	-.55
2			+.55	-.05	.49	-.01	.36	-.14	.17	-.33	.38	-.12	.43	-.07	.73	.80	-.05
3				-.50	-.06	-.56	-.19	-.69	-.38	-.88	-.17	-.67	-.12	-.62	.18	.25	-.60
4					.44	-.06	.31	-.19	.12	-.38	.33	-.17	.38	-.12	.68	.75	-.10
5						-.50	-.13	-.63	-.32	-.82	-.11	-.61	-.06	-.56	.24	.31	-.54
6							.37	-.13	.18	-.32	.39	-.11	.44	-.06	.74	.81	-.04
7								-.50	-.19	-.69	.02	-.48	.07	-.43	.37	.44	-.41
8									.31	-.19	.52	.02	.57	.07	.87	.94	.09
9										-.50	.21	-.29	.26	-.24	.56	.63	-.22
10											.71	.21	.76	.26	1.06	1.13	.28
11												-.50	.05	-.45	.35	.42	-.43
12													.55	.05	.85	.92	.07
13														-.50	.30	.37	-.48
14															.80	.87	.02
17																.07	-.78
19																	-.85
20																	

The misregistration was not actually determined by direct measurement for all of the pairs of channels represented in the table. The misregistration was first measured between seven pairs of even and odd numbered high sample rate SDOs (1-2, 3-4, 5-6, 7-8, 9-10, 11-12, 13-14). In all cases, the average measurement taken over 5 lines of data was almost exactly 0.5. These measurements indicated that the misregistration between these pairs of channels could be safely assumed as being 1/2 pixel. Measurements were made using 10 lines of conical data on an additional seventeen pairs of correlated ($\rho \geq .5$ for a large sample of pixels) channels chosen from among the odd numbered high sample rate channels and the remaining low sample rate channels. A multiple linear regression was performed on these seventeen measurements to obtain estimates of the misregistration between nine pairs of channels from which estimates of all of the remaining pairs were derived. The sum of the squared deviations between the 17 actual measurements and their predicted values from the regression analysis was 0.0015. This low figure indicates the consistency of the results obtained from the different pairs of channels. As a further test, measurements of the misregistration between nine pairs of channels taken from a different set of 10 lines, were also made. The sum of the squared deviations between these measured values and the values shown in Table 2.4 was 0.0067.

To determine the misregistration between any two pairs of channels from Table 2.4, find the fractional pixel value in the table corresponding to the desired pair of channels. The sign of the entry in the table denotes the direction the channel given by the column must be shifted to register it with the row channel. Positive is defined as in the direction of scan and negative as the opposite direction. For example, channel 1 lags channel 2 and channel 2 also leads channel 3.

Results indicate that the algorithm which was developed is, in fact, quite accurate. The measurements made on the even and odd numbered high sample rate SDOs yielded the exact results expected. The measurements made on the 17 pairs of channels were consistent among themselves. The standard deviation of each of these estimates over the 10 lines of data which were employed were also quite small (less than .05 pixels). Measurements made on the second set of 10 lines were also consistent with those obtained from the first set of lines. These results indicate that the method is reliable.

Furthermore, it is possible to substantially correct for the misregistration for conic data, and to define a set of 10 SDOs, one for each detector called out in Section 2.1.3 as being useable, which are fairly well registered. This may be done by first shifting SDOs 17 and 19 one pixel in the scan direction relative to the other SDOs and then choosing the even numbered high sample rate SDOs 2, 4, 6, 8, 10, 12, and 14, and finally SDO 20 along with SDOs 17 and 19.

The next aspect of this discussion is to consider the effect of misregistered conical data on the scan-line-straightened data.

2.1.3.2 Spatial Misregistration for Scan Line Straightened Data

In the previous section we discussed the existence and extent of spatial misregistration in conic data. In this section we examine it for scan-line-straightened data and also examine the effects of the scan-line-straightening algorithm on spatial misregistration. It is shown that even in the absence of scanner-related misregistration, serious misregistration is created in the data by the scan-line-straightening algorithm.

For this analysis, it was not possible to use the cross correlation technique from the previous section because the technique requires some 500 continuous points on each scan line to be used in the algorithm to reduce boundary effects and these 500 pixels must have identical misregistration characteristics. That this last condition does not occur in the scan-line-straightened data will be evident from the discussion below.

By the S-192 system design, all even-numbered SDOs are perfectly registered one with the other; the same is true for all odd numbered SDOs. Further, there is a one-half pixel misregistration between the odd numbered SDOs and the even numbered SDOs due to the sampling technique used. Further misregistration is introduced by scanner electronics, by different response times for different detectors, and/or by improperly skewed record heads on the spacecraft tape recorder. These combine to produce the misregistration observed in the conic data.

When the scan-line-straightening algorithm rearranges the collected pixels into scan-line-straightened format, additional spatial misregistration is introduced. The following example gives a graphic account of the randomness of the resulting misregistration and the possible extent of it. Presented below, in Figure 2.3, are two pixels each from two consecutive conic scan lines and the manner in which they are assigned to a straightened scan line.

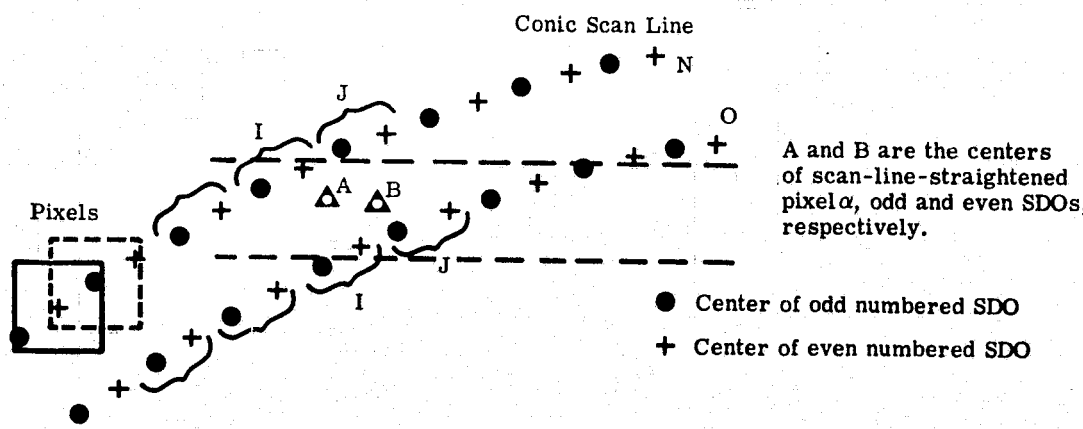

FIGURE 2.3. ASSIGNMENT OF SDOs IN SCAN-LINE-STRAIGHTENING

To begin the analysis, let us break the 22 SDOs into four subsets and examine each independently. The four subsets are: 1) ODD numbered LOW sample rate SDOs, 2) EVEN numbered LOW sample rate SDOs, 3) ODD numbered HIGH sample rate SDOs and 4) EVEN numbered HIGH sample rate SDOs. It is assumed that all SDOs in a subset will be assigned in the same way; this is so since the the assignment algorithm as well as the starting point on a scan line is the same for all SDOs.

All ODD numbered, LOW sample rate SDOs from pixel J in line N will be assigned to A of scan-line-straightened pixel α (A being the center of the resolution cell for the ODD SDOs of α). Similarly all EVEN numbered LOW sample rate SDOs from pixel I, scan line 0 will be assigned to B. (B being the even numbered SDOs of pixel α.)

When the high sample rate SDOs are straightened, the odd-even pair of SDOs for each detector are interleaved, then the samples are assigned to straightened lines and points and rebroken into an odd-even SDO pair again. Thus for this example, all EVEN numbered, HIGH sample rate SDOs from pixel I, scan line N, will be assigned to A and renamed to be the ODD numbered SDOs of pixel α. Similarly all ODD numbered HIGH sample rate SDOs from pixel J scan line 0 will be assigned to B and become the EVEN numbered SDOs for pixel α.

Within each of the two cases (paragraphs) cited above, the low sample rate and the high sample rate groups, the misregistration between the even SDOs and the odd SDOs will be that as found in the conic data -- for the along scan line direction. In the along track direction for the example in Figure 2.3 there will be one full pixel misregistration due just to the scan-line-straightening. This is the maximum that could be created for this particular effect.

The misregistration between a set of high sample rate SDOs and a set of low sample rate SDOs is indeterminate since it depends on whether or not the even-odd designation for the high sample rate SDOs in the straightened format has been switched from what it was in the conic format. Potentially, the along scan misregistration between low and high sample rate SDOs can be one whole pixel.

The above discussion has referred only to misregistration caused by the sampling scheme and the scan-line-straightening procedure. The occurrence of scanner electronic related misregistration is in addition to that cited above. This additional misregistration in the conic data is only along the scan line. In the scan-line-straightened data its direction is still along the tangent to the conical scan at the point of interest. We can state the total expected misregistration in scan-line-straightened data as:

$$R_x = 1 + M \sin\theta \qquad \text{(pixels)}$$

$$R_y = 1 + M \cos\theta \qquad \text{(pixels)}$$

where:

R_x is the component of misregistration in the straightened data along the scan line

R_y is the component of misregistration in the straightened data in the along track direction

M is the maximum misregistration in the conic data

θ is the angle between the line tangent to the conic scan at the point being considered and a line in the along track or flight direction.

This result will be used in the next section to show how misregistration affects the processing of data.

Another observation regarding misregistration in scan-line-straightened data is that it is not possible to correct the data, at least not using a simple algorithm as was used in the conic data. Further, it is not possible even to correct within any one of the four subsets previously cited, so that misregistration due to scanner electronics could be reduced even within one of the subset groups of SDOs. That this is the case may be easily shown by using Figure 2.4 below.

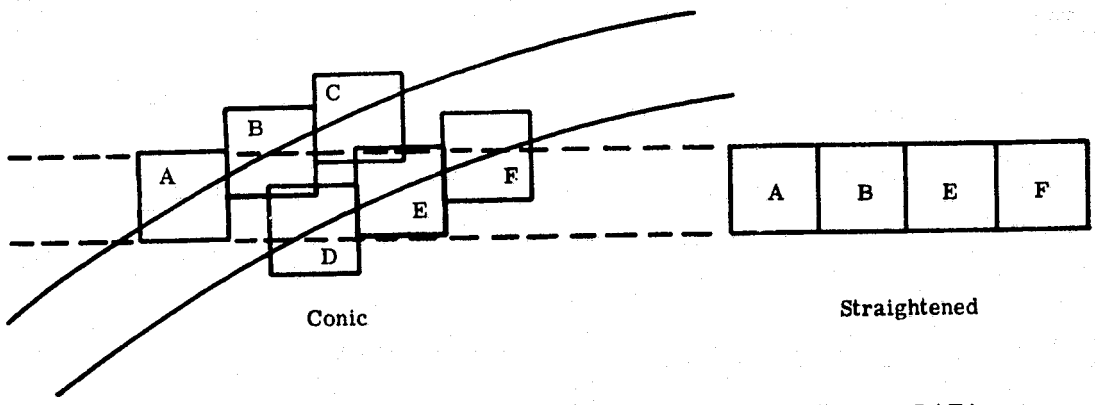

FIGURE 2.4. SCAN-LINE STRAIGHTENING WITH MISREGISTERED DATA

In the figure pixels A, B, E, and F will be assigned sequentially to a straightened scan line. Assume that one SDO, SDO k, is one pixel out of registration with the other SDOs. Thus SDO k of pixel B images the area of pixel A, and SDO k of pixel E images the area of pixel D. Any attempt to simply shift, for the scan line straightened data, SDO k one pixel relative to all the other SDOs will result in SDO k of pixel B being the area of pixel, D, and not pixel C as would be correct. It is possible that such a shifting technique would reduce the misregistration in some pixels, but it would increase the misregistration for other pixels and, more importantly, it would not be possible to know exactly which pixels were correct and which were not.

It is not possible, in general, to predict where these discontinuities might occur as it is a function of spacecraft altitude, velocity, and heading. In general, it can be stated that these discontinuities will occur as frequently as every pixel, at the ends of the scan lines, and falling off as one moves toward the middle of the scan line to a frequency of about every 15^{th} or 18^{th} pixel at the point on the scan line directly ahead of the spacecraft.

Finally, it is clear that the increased misregistration caused by the scan-line-straightening algorithm results in fewer pure field center pixels than for the conic data and in many more pseudo mixture pixels, i.e., pixels which have some SDOs imaging field center areas and other SDOs imaging field boundaries or even completely different fields. Even the mixture pixels will image different proportions of the classes in different SDOs.

A thorough analysis of the effects of misregistration on the processing of S-192 data is presented in Chapter 4.

The effects of misregistration due to the scan-line-straightening algorithm on S-192 data may be stated succinctly.

1. There is greatly increased misregistration in scan-line-straightened data over conic data.
2. Scanner-caused misregistration between any pairs of channels may not be easily corrected for in scan-line-straightened data.
3. Scan-line-straightened data will have fewer pure field center pixels than will conic data.

2.1.4 S-192 RESOLUTION AND THE IDENTIFICATION OF FIELD CENTER PIXELS

The resolution of the S-192 scanner for the spacecraft altitude at the time the Southeast Michigan data set was collected, yielded a resolution cell almost 81 meters square, or about 0.65 hectares (1.6 acres) per resolution element. Especially for this test site, where the average agricultural field size is 15-18 acres, many of the resolution elements in the scene will be imaging two or more fields. Obviously, in extracting training statistics it is important that the data points used be only those data points which are purely of the class being considered. Thus a need evolves to identify pure data points, or as they are more commonly called: field center points. The complement of the field center point is called a mixture data point.

Thus far, the discussion has dealt with resolution elements and not pixels. A pixel is not, for the S-192 (and generally speaking), the same as a resolution element. A pixel, or picture element, refers to one data point, one vector of observation, sampled from the detector outputs. The S-192 system oversamples by approximately 10% along the scan direction, and the overlap between successive conical scans is also about 10% at the midpoint in the scanners front field of view.

The ground size of a pixel is given to be 72 x 72 meters [1]. A brief analysis of actual pixel size was conducted in the following manner. Pairs of pixels in lakes were located on scan-line-straightened data graymaps. Care was taken to find pairs which were either on the same scan line, several hundred pixels apart, or located at the same scan point number several hundred scan lines apart. Points corresponding to the pixels selected were also located on USGS maps of Southern Michigan. Distances were accurately measured on the USGS maps

and on the graymaps; the result was that the pixels were measured to be 69 meters wide in the along-scan direction and 72 meters in the along track direction. Calculations based on geometrical considerations using only the angle of the scan cone and the altitude at the time of data acquisition yielded measures of 70 x 70 meters. The differences are not felt to be serious.

Having defined resolution elements, pixels, pure pixels and mixture pixels, the rest of this discussion is devoted to a procedure for identifying field center pixels. Preparatory to this, it should be understood that at ERIM individual fields are usually defined by the set of points $S = \{(x_i, y_i),$ x_i = line number of vertex i, y_i = point number at vertex i$\}$ which are the vertices of a generalized polygon which is the boundary of the field.

Simply speaking, identification of field center pixels is accomplished by the inscribing of a smaller similar polygon with the polygon which defines the field being considered. A pixel is identified as a field center pixel if its center is within the inscribed polygon. The distance the field center polygon is inset from the original is calculated so that even in the worst case all the pixels in the field center polygon are guaranteed to be resolving only areas within the field. It is important to remember here the distinction between pixel size and the size of the resolution cell.

In general, the inset calculation is a summation of many components, and in fact the inset may be different in the direction of scan than in the along track direction. We can generalize the inset (I: $\{I_x, I_y\}$) as follows:

$$I_\alpha = \frac{D_\alpha}{P_\alpha} \quad B + R_\alpha + L + S \qquad \text{pixels}$$

where

- α indicates x: scan direction or y: line or along track direction
- D_α is the size of the resolution cell in the direction of α
- P_α is the size of the picture element in the direction of α

B is the inset necessary to insure that the pixel does not include the boundary between fields. Typically B = 0.5 pixel.

R_α is the error due to misregistration effects, e.g., if one channel is misregistered from the others by R pixels, then this channel could still be imaging across the field boundary when the other channels are imaged entirely within the field. For conic data corrected for misregistration,

$$R_x = 0.32$$

$$R_y = 0.$$

For straightened data, from the previous section we have

$$R_x = 1 + M\sin\Theta$$

$$R_y = 1 + M\cos\Theta$$

from Table 2.4, M is found to be 1.13. To develop one measure for the whole scan line, we take the maximum values of SINΘ and COSΘ, which is one.
Thus:

$$R_x = 2.13$$

$$R_y = 2.13$$

L is due to any field location errors which may have occurred.

S is the error due to "movement" of individual pixels as a result of the nearest neighbor scan line straightening. For conic data, therefore, S = 0. For straightened data, S = 0.5 pixel.

Thus, the inset to be used for conic data would be:

$$I_x = \left(\frac{81}{72}\right) 0.5 + 0.92 + L = .90 + L \text{ pixels}$$

$$I_y = \left(\frac{81}{72}\right) 0.5 + 0. \quad + L = .58 + L \text{ pixels}$$

while the inset to be used for scan-line-straightened data would be:

$$I = I_x = I_y = \left(\frac{81}{72}\right) 0.5 + 2.13 + L + 0.5 = 3.21 + L \text{ pixels}$$

The significant increase in inset for the second case here is due to the increased misregistration between SDOs found in scan-line-straightened data. Figure 2.5 illustrates the use of insets for these two cases. In the conic data case a 20 pixel field has eight certain field center pixels while a field of 75 scan-line-straightened data pixels has only six pure field center pixels.

In summary, what has been presented here is the inset to be used to insure that any pixel identified as a pure, field center pixel is resolving only one ground class in all of its bands. This insures that the training statistics will refer only to pure conditions of the classes they represent.

2.1.5 PROCESSING CONIC DATA

The bulk of the processing carried out for this study was done on conic, not scan-line-straightened data. Using conic data meant that the misregistration in the data was not compounded by the scan-line-straightening algorithm. More importantly, it meant that remedial algorithms, as described at the end of Section 2.1.3.1, could be and were employed to significantly reduce the misregistration in the data.

The drawback to using conic data is that graymaps of individual SDOs are somewhat distorted. For most of our work, however, such graymaps proved adequate. For instances where undistorted maps were desired, a special implementation of the digital mapping program was used. In this mode, the data to be presented are broken into groups of 40-55 pixels for which the conical arc over those points can be approximated by a straight line. Then each swath of data are mapped, the symbols being printed diagonally on the printer, incrementing one print line every n characters. Additionally, conic pixels falling at points where there is overlap in the undistorted printed map can be deleted. While this does not produce as rectified a map as the scan-line-straightening algorithm employed at JSC, graymaps generated in this manner are only slightly distorted. On the whole, we found the mechanics of data manipulation when using conic data to be little different than when working with straightened data.

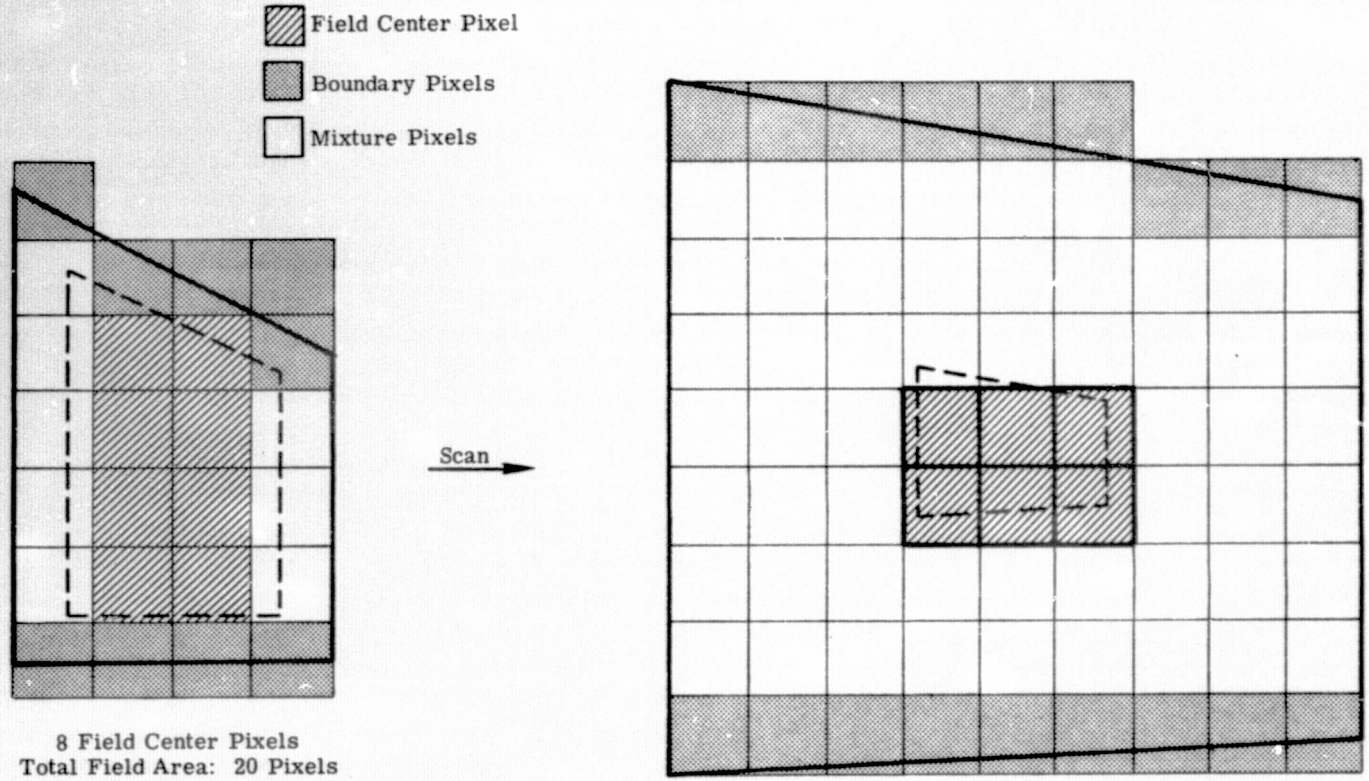

FIGURE 2.5. USE OF INSETS TO DEFINE FIELD CENTER PIXELS

2.2 M-7 MULTISPECTRAL SCANNER

The ERIM M-7 multispectral scanner is an aircraft mounted line scanner with the capability of recording data in 12 wavebands from the ultraviolet to the thermal infrared region of the spectrum [6]. Appendix II lists the spectral and optical characteristics of the M-7 scanner. For this study, the M-7 was used to acquire data over the test site at the same time as the S-192 data for this study was collected [7]. The M-7 data were acquired at an altitude of 2000 ft,* collecting data along several parallel North-South passes over the test site. The data used for this study was Run 2 over flight 1. Run 2 began at 1056 hrs. E.D.T., and ended at 1105 hrs. E.D.T., while the S-192 data set was acquired at 1102 hrs. E.D.T.

2.2.1 M-7 SIGNAL CHARACTERISTICS

The M-7 data were digitized and preprocessed as described in Appendix V and the data were then analyzed for signal characteristics. The analysis was carried out along the same lines as that for the S-192.
The dynamic range analysis is presented in Table 2.5 and the signal:noise analysis in Table 2.6. For this latter table, the only water body in the M-7 data set was a small farm pond. For the sake of rigorous comparison to the procedures of Section 2.1 the statistics derived from it are presented. However we should point out that since it is a very small water body and probably much shallower than Lake Lansing, the estimated noise for the M-7 is probably larger than the actual noise characteristic of the data. For the M-7 data, however, we can obtain a very accurate estimate of the scanner-related noise by analyzing the signals derived from the "dark level", i.e., that portion of the data generated while scanning the dark interior of the scanner housing, Since here the illumination is zero, any variation in the signal is due just to scanner system noise. The calculated noise from the dark level and from the water signature are presented in Table 2.7. To calculate the standard deviations reported in Table 2.5, the dark level of 1000 consecutive scan lines were analyzed. For the thermal band, the noise on the cold reference plate was used instead. It

*The original flight plan had been for data collection from an altitude of 5000 ft., however haze over the site necessitated collection at a lower altitude.

TABLE 2.5. M-7 SIGNAL CHARACTERISTICS: DYNAMIC RANGE

Total Available Range = 512 Counts

CHANNEL	DYNAMIC RANGE[1]	DYNAMIC RANGE[2]
1	71-284, 213	90-137, 47
2	65-301, 235	89-155, 66
3	64-388, 304	105-186, 81
4	76-369, 193	110-185, 75
5	59-317, 278	100-165, 65
6	57-318, 261	91-159, 68
7	63-343, 280	94-192, 98
8	56-362, 306	73-196, 123
9	10-208, 198	94-158, 64
10	10-207, 197	109-166, 57
11	12-270, 258	109-176, 69
12	60-287, 227	100-210, 110

[1]Used Continuous Rule

[2]Used 10% Rule

TABLE 2.6. M-7 SIGNAL CHARACTERISTICS: SIGNAL:NOISE

CHANNEL	WATER MEAN	STANDARD DEVIATION	SIGNAL:NOISE	RANGE:NOISE
1	102	5.0	20.4	9.4
2	103.5	5.6	18.5	11.8
3	120	6.2	19.4	13.1
4	111	5.6	19.8	13.4
5	88	5.6	15.7	11.6
6	86	5.1	16.9	13.3
7	88	6.7	13.1	14.6
8	68	6.7	10.1	18.4
9	21	2.9	7.2	22.1
10	19	2.8	6.8	20.4
11	24	6.3	3.8	11.0
12	84	4.3	19.5	25.6

TABLE 2.7. M-7 NOISE CHARACTERISTICS FROM DARK LEVEL SIGNALS

CHANNEL	MEAN	STANDARD DEVIATION	DARK LEVEL SIGNAL:NOISE	WATER SIGNAL:NOISE
1	26	1.3	20.0	20.4
2	22	1.2	18.3	18.5
3	21	.53	39.6	19.4
4	28	1.3	21.5	19.8
5	30	1.2	25.0	15.7
6	27	1.2	22.5	16.9
7	58	1.5	38.7	13.1
8	26	.9	28.9	10.1
9	52	1.5	34.7	7.2
10	39	1.0	39.0	6.8
11	30	1.5	20.0	3.8
12*	31	4.1	7.6	19.5

*Results for this band were analyzed from cold reference plate signals.

TABLE 2.8. DISTANCE BY CHANNEL BETWEEN A CORN AND A WOODLOT DISTRIBUTION FOR M-7 DATA

CHANNEL	D_i
1	6.02
2	7.1
3	2.6
4	9.1
5	7.3
6	8.0
7	8.7
8	9.5
9	10.4
10	5.2
11	3.7
12	6.0

can be seen that in some bands the noise measured from the water signature is much greater than the dark level noise. So it seems that using the water signature as the noise measurement results in an overestimation of the scanner noise.

The two selfsame corn field and woodlot areas which were used for the S-192 part of this analysis were located in the M-7 data set. Signatures were calculated and the same distance measure used previously was also calculated here. Table 2.8 below presents the results of this analysis. On the whole the two distributions appear to be very well separated in this data.

Comparisons of the two scanners for dynamic range, noise and signature separability will be made in the following section.

2.3 COMPARISON OF S-192 AND M-7 SIGNAL CHARACTERISTICS

The purpose in comparing data characteristics of the M-7 and S-192 multispectral scanners is not to prove one better than the other, but rather to better understand the capabilities of the new S-192 scanner. The M-7 has been widely used for several years and its capabilities and performance are well known while, on the other hand, the S-192 is only the second experimental spaceborne multispectral scanner and its performance and capabilities are unknown. By comparing these two scanners, we hope to better understand the S-192 and perhaps be able to suggest improvements or refinements for the next generation of spacecraft scanners.

Briefly, with reference to Tables 2.1 through 2.8, it is seen that the dynamic range of the two data sets is very different, especially that the S-192 data range in the better channels is no more than 5 bits. Also, looking at the dynamic range in relation to the level of noise (as expressed in statistics over bodies of water), the S-192 data range:noise is a quarter or a third that of the M-7 data.

As for the separability of ground classes of interest, this was investigated by determining the separability of two specific fields, one corn and one woodlot, which were scanned in both of the data sets.

A comparison of Tables 2.3 and 2.8 shows that, on the whole, the separability for the M-7 data is much greater than that for the S-192; one should remember in making the comparison that, because the measurement is of two Gaussian distributions and is given in terms of σ^2, that the actual probability of misclassification declines exponentially at a rapid rate as the distance slowly increases.

A further, finer comparison can be based on the fact that three of the S-192 and M-7 spectral bands are very similar. This identification was made upon inspection of spectral response curves for the two scanners. These bands are listed in Table 2.9

Of the three bands treated here, two are in the near-infrared and one in the visible (green) portion of the spectrum. For these three bands we can compare, in Table 2.9, the key quantities calculated for each scanner.

TABLE 2.9. BAND TO BAND COMPARISON OF M-7 AND S-192 RESULTS

	λ	DYNAMIC RANGE	RANGE: NOISE	SIGNAL: NOISE	CORN-WOODLOT SEPARABILITY (D_i)
S-192 Band 4:	.54 - .59	13	5.4	10.5	0.06
M-7 Band 6:	.55 - .60	68	13.3	16.9	8.0
S-192 Band 10:	1.15 - 1.28	28	4.3	3.4	0.20
M-7 Band 10:	1.00 - 1.50	57	20.4	6.8	5.2
S-192 Band 11:	1.55 - 1.73	19	5.8	4.4	3.0
M-7 Band 11:	1.50 - 1.80	69	11.0	3.8	3.7

From the above comparisons, it is clear that the S-192 data has a very limited range of data values, especially in relation to system noise. This small range:noise in turn severely inhibits the separability of classes of interest. Such problems with S-192 data appear to be due, in some part, to the effects of the atmosphere on radiation sensed by the scanner. In general, the atmosphere reduces data contrast and, in this instance, with a variable haze covering the test site area, the effect was more pronounced. Another factor which seems to make a difference between the two data sets is that on the one hand full use of available signal range on the M-7 was achieved by manual intervention both during data acquisition and during the digitizing process, while on the other the S-192 system was ubiquitously set to handle surface radiance over a wide range of atmospheric and ground conditions resulting in a very limited available range for any particular instance. Perhaps a more versatile acquisition system design would have upgraded the S-192 performance.

3
PROCESSING RESULTS FOR THE AGRICULTURAL TEST SITE

SKYLAB S-192 data over Southern Michigan was processed for two sites, showing two different applications of multispectral data. The first application was in the performance of an agricultural survey over the Southeast Michigan EREP test site. Both SKYLAB S-192 and aircraft M-7 scanner data were collected over the area and are discussed in Sections 3.1 and 3.2, respectively. The second, a land use evaluation for the urban-rural area around Lansing, Michigan, is detailed in Section 5.

3.1 PROCESSING RESULTS FOR S-192 AGRICULTURAL DATA

3.1.1 SIGNATURE EXTRACTION

The agricultural test site, detailed in Appendix III, comprised 90 sections (each about 1 mile square) in Ingham County, Michigan. The process of field location and identification was accomplished using a semi-automated technique described in Appendix VI. Briefly, field vertices were digitized from large-scale photography and transformed to data scan line and scan point coordinates. The same procedures used to identify pure field center pixels within each of the ground truth fields as described in Section 2.1.4, were applied in order to identify the field center pixels for each of the 90 ground truth sections. Table 3.1 shows the classes in the scene along with the number of field center pixels identified for those classes; the notation of local (north 40 sections) and non-local (south 50 sections) sections of the ground truth area refer to the manner in which the area was divided for training and testing purposes.

Some of the class names require explanation. Unplanted farm areas were listed in the ground truth as any of these categories: sod, grass, clover, grassy weeds, weeds, pasture, fallow and stubble. These were deemed to be similar in character differing only in the proportion of

TABLE 3.1 NUMBER AND DISTRIBUTION OF FIELD CENTER PIXELS

CLASS	NUMBER OF FIELD CENTER PIXELS FOR CLASS	
	LOCAL AREA (NORTH 40 SECTIONS)	NON-LOCAL AREA (SOUTH 50 SECTIONS)
CORN	344	549
TREES	24	260
BRUSH	68	39
SOYBEANS	19	52
ALFALFA	23	20
GRASS	398	264
STUBBLE	53	71
BARE SOIL	38	43
URBAN	69	0
FIELD BEANS	0	56
TOTAL	1036	1307

ground covered by the vegetation, and hence were lumped together in the category of forage. The category of trees was deemed to be dense stands of mature trees, while the term brush was used in the ground truth to indicate scrub forest, some less dense tree stands, and brushy areas.

Training was carried out using only pixels from the north 40 sections.* The use of the north area for training rather than the south area was an arbitrary choice. The use of 40 sections, rather than some subset of the 40,

*The signature extraction, classification and assessment of results for the S-192 data reported in this section was carried out under Contract NAS9-13332, a subcontract involving the performance of S-192 data processing for Michigan State University. [5].

was based on the desire to obtain training statistics for as many of the classes in the scene as possible and also to have a large number of pixels for each class so as to more accurately estimate the training statistics for each class. In extracting the training statistics, rather than lumping all pixels of common class together and thereby calculating one set of statistics for a class, we implemented a supervised clustering approach. In this manner, all the field center pixels of each class were clustered independently. Thus if a ground class, which is basically an economic distinction, varies physiologically so that several spectral signatures are necessary to fully represent the class, this method will yield a better set of training signatures. Table 3.2 lists the clusters obtained from this procedure.

TABLE 3.2 DERIVED TRAINING CLUSTERS FOR S-192 AGRICULTURAL DATA SET

CLUSTER	NUMBER OF PIXELS
CORN 1	134
CORN 2	28
CORN 4	129
CORN 5	28
ALFALFA	20
TREES 3	12
TREES 4	10
BRUSH	55
SOYBEANS	18
BARE SOIL	20
CLOVER	10
STUBBLE	32
WEEDS	43
GRASS 1	27
GRASS 2	17
GRASS 3	79
GRASS 6	22
PASTURE 7	50
PASTURE 8	49
PASTURE 9	20
PASTURE 10	20
URBAN 1	29
URBAN 2	14
URBAN 3	12

The signatures extracted in this manner were 12-channel signatures; SDO 18 (.45-.50 μm) was dropped from the processing at this point because besides containing no information (see Section 2), its wildly fluctuating data values were causing confusion in the analysis.

3.1.2 SIGNATURE ANALYSIS AND SELECTION OF OPTIMUM BANDS

The set of signatures was first analyzed to see if any of the apparent spectral subclasses were due solely to effects of the noisier channels. At the same time, they were examined to determine if some of the signatures, for the same class, might be combined. Since the cost of classifying a data set is directly related to the size of the signature set, it is important to reduce the size of the signature set whenever possible.

As a first step, all 24 signatures were input to program STEPL which calculates optimum channels. Care was taken so intra-class differences were ignored; the channels were selected on an inter-class basis only. The results, as shown in Table 3.3 below, indicate that three of the four bands (SDO's 6, 21, 22) identified initially as noisy or having poor signal quality, were also identified by the program as the least useful in discriminating among the object classes. The fourth band previously identified as too noisy to use, SDO 8 (.67-.73 μm), which covers the region of chlorophyl absorption and is thus a key band in the discrimination of vegetation class, was deemed by this program to be of use. This is perhaps so because the separation of classes in this band is still greater than the noise content of the band.

Next, with the aid of one- and two-channel signature plots and outputs from computer programs which measure pairwise probabilities of misclassification and also estimate theoretical performance matrices for sets of signatures, the signature set was reduced from 24 to 15 signatures. Six of the signatures were simply dropped: the three urban signatures because they were deemed to be primarily mixtures of grass, soil and trees and also because there were

TABLE 3.3 SDO RANKING BASED ON OPTIMUM BAND CRITERIA

RANK	1	2	3	4	5	6	7	8	9	10	11	12
SDO #	19	12	2	8	10	17	20	6	4	14	21	22
λ(μm)	.93-1.05	1.5-1.7	.50-.55	.66-.73	.770-.89	1.15-1.28	1.03-1.12	.60-.65	.54-.60	2.1-2.34	10.2-12.5	.40-.45
CUMULATIVE PAIRWISE PROBABILITY OF MISCLASSIFICATION	.21	.10	.07	.056	.048	.039	.034	.031	.028	.026	.024	.022

no other urban features in the test site to test them on, the clover signature because it was very similar to some of the grass signatures and there was no other clover in the test site, and the stubble and Pasture 7 clusters were found to be redundant with some of the grass clusters. Signatures combined on the basis of spectral similarity were: Pasture 8 with Pasture 10; Grass 6 with Pasture 9; and Grass 3 with Weeds.

This reduced set of signatures was input to Program STEPL for a final calculation of optimum bands. As reported in Table 3.4, the rank ordering is almost the same although the pairwise probability of misclassification has increased slightly, due to the several combination signatures in the set. Seven bands were selected for processing using a rule of thumb which says to select n channels where the decrease in the probability of misclassification is less than .005 between n channels and n+1 channels.

3.1.3 CLASSIFICATION RESULTS OF S-192 AGRICULTURAL DATA SET

The signature set described in the previous sections was applied to classify all 90 sections in the agricultural data set. Two bases for evaluation were used to analyze the results. The first basis was the pixel-by-pixel

TABLE 3.4 FINAL SELECTION OF OPTIMUM BANDS

RANK	1	2	3	4	5	6	7	8
SDO	12	19	2	10	17	8	20	4
λ(μm)	1.50-1.70	.93-1.05	.50-.55	.770-.89	1.15-1.28	.660-.73	1.03-1.19	.54-.60
PROBABILITY OF MISCLASSIFICATION	.21	.11	.088	.070	.058	.050	.043	.039

classification results for pixels of known class, i.e., the previously identified field center pixels. The second was an analysis of proportion estimation as taken from aggregated classification counts, which provides a more overall evaluation of the classification results.

Tables 3.5 and 3.6 present performance matrices for just the field center pixels in the north and south areas, respectively. The bottom lines of the tables show the total proportion of field center pixels classified to each recognition class, and present the ground truth proportion for comparison. Finally, estimates of the overall classification rates are offered.

Examination of the performance matrices shows that overall performance is only fair. One major problem is the high percentage of corn pixels being classified as trees/brush, as well as a large number of other pixels being classified as corn. The trees/brush classification is especially disappointing. Investigation of this showed the classes to be, simply, very similar spectrally. Some of the other apparently false recognitions are not entirely spurious. Several of the stubble pixels could indeed be bare or almost bare soil for example, or some of the brush pixels might be weedy or pasture spots in low density brush areas. In comparing the south area to

TABLE 3.5 PERFORMANCE MATRIX FOR CLASSIFICATION OF FIELD CENTER PIXELS FROM NORTH 40 SECTIONS

GROUND TRUTH CLASS	NO. PIXELS	PERCENT OF FIELD CENTER PIXELS ASSIGNED TO RECOGNITION CLASS: CORN	FORAGE	TREE/BRUSH	BARE SOIL	SOYBEAN	UNCLASSIFIED
CORN	344	73.0	6.4	18.1	0.3	1.7	0.6
FORAGE	474	8.9	81.4	3.8	3.6	1.7	0.6
(GRASS 398)		(7.3)	(83.7)	(4.6)	(2.5)	(1.3)	(0.8)
(ALFALFA 23)		(21.7)	(69.5)	(0.0)	(0.0)	(8.7)	(0.0)
(STUBBLE 53)		(15.1)	(69.8)	(0.0)	(13.2)	(1.9)	(0.0)
TREE/BRUSH	92	26.1	17.4	51.1	0.0	0.0	5.4
(TREES 24)		(4.2)	(20.8)	(75.0)	(0.0)	(0.0)	(0.0)
(BRUSH 68)		(33.8)	(16.2)	(42.6)	(0.0)	(0.0)	(7.4)
BARE SOIL	38	13.2	7.9	0.0	79.0	0.0	0.0
SOYBEAN	19	31.6	10.6	0.0	0.0	57.9	0.0
TOTAL	967	33.9	44.4	13.1	5.0	2.6	1.0
GROUND TRUTH (%)		35.6	49.0	9.5	3.9	2.0	0.0

RMS Error in Proportion Estimation (%) = 2.57 (Excluding Urban)

Overall Percent Correct Classification of Pixels = 75.0% (Excluding Urban)

TABLE 3.6 PERFORMANCE MATRIX FOR CLASSIFICATION OF FIELD CENTER PIXELS FROM SOUTH 50 SECTIONS USING SIGNATURES OBTAINED FROM 40 NORTHERN SECTIONS

GROUND TRUTH CLASS	NO. PIXELS	PERCENT OF FIELD CENTER PIXELS ASSIGNED TO RECOGNITION CLASS: CORN	FORAGE	TREE/BRUSH	BARE SOIL	SOYBEAN	UNCLASSIFIED
CORN	549	76.1	8.0	14.0	0.0	1.8	0.0
FORAGE	355	23.9	68.7	2.0	3.9	29.0	0.0
(GRASS 264)		(21.6)	(74.3)	(2.7)	(0.0)	(1.5)	(0.0)
(ALFALFA 20)		(80.0)	(20.0)	(0.0)	(0.0)	(0.0)	(0.0)
(STUBBLE 71)		(16.9)	(62.0)	(0.0)	(19.7)	(1.4)	(0.0)
TREE/BRUSH	308	31.5	12.3	51.9	0.0	2.6	1.6
(TREES 269)		(32.7)	(8.6)	(55.8)	(0.0)	(1.1)	(1.9)
(BRUSH 39)		(23.1)	(38.5)	(25.6)	(0.0)	(12.8)	(0.0)
BARE SOIL	43	4.7	30.2	2.3	62.8	0.0	0.0
SOYBEAN	52	15.4	65.4	0.0	0.0	19.2	0.0
FIELD BEAN	56	67.9	28.6	3.6	0.0	0.0	0.0
TOTAL	1363	47.5	28.6	18.1	3.0	2.4	0.4
GROUND TRUTH (%)		40.3	26.0	22.6	3.2	3.8	4.1

RMS Error in Proportion Estimation (%) = 3.97

Overall Percent Correct Classification of Pixels = 63.0%

the north, it is seen that the forage subclasses in the south area distinctly fall off in terms of classification accuracy, with most of the incorrectly classified pixels being called corn and soybeans. Soybean recognition also suffers. However, it was noticed in the aerial photography that soybeans were a highly variable ground cover for the data set at this time of year. There are probably too few soybean pixels in the sample to give an accurate accounting of the classification performance.

The analysis of the proportion estimation results for both north and south areas are presented in Table 3.7. These results are the classification counts over all pixels in each area. Given in the table for each area and ground class is the ground truth proportion; the proportion of pixels in the area classified as that class; and the RMS error of the estimate.

The striking features of this table are that corn is overestimated, and that the error rate is larger in the nonlocal (south) area.

Conclusions regarding these classification results will be given in Section 3.3, where comparison can be made with results obtained from processing aircraft scanner data from the same site.

3.2 RESULTS OF PROCESSING M-7 AGRICULTURAL DATA SET

For purposes of comparison with the S-192 data processing results, training and classification was carried out for the M-7 acquired data for a small 1.5 square mile area. The area selected for training and testing was located at mile three from the beginning of the flight line, line 2. (A complete description of the data, digitization and preprocessing is given in Appendix V.) This region was chosen because it was the first area in the data set which contained several large contiguous areas of corn, soybeans, woodlots and bare soil. All fields within the area were identified and used in this exercise. The classes, number of fields and number of pixels for each class appear as part of the results in Table 3.9.

TABLE 3.7 GROUND TRUTH PORPORTIONS AND RECOGNITION ESTIMATES FOR LOCAL (NORTH 40) AND NONLOCAL (SOUTH 50) RECOGNITION OVER LARGE AREAS

	North 40 Area			South 50 Area		
Ground Cover Class	Ground Truth	Recognition Counts	% RMS Error* by Class	Ground Truth	Recognition Counts	% RMS Error* by Class
Corn	26.5%	36.8%	13.8	33.3%	48.0%	17.0
Trees/Brush	17.2	14.3	7.3	16.5	13.3	7.2
Forage	47.4	40.5	9.7	35.5	30.9	11.0
Bare Soil	7.2	5.4	4.4	7.2	3.3	7.4
Soybeans	3.7	2.4	5.0	4.0	4.4	5.6
Other	3.1	0.4	5.9	4.7	0.0	7.8
RMS Error†	4.66%			6.89%		

*RMS error was calculated as: $E_{RMS_j} = \left(\frac{1}{n} \sum_{i=1}^{n} (p_{ij} - \hat{p}_{ij})^2 \right)^{1/2}$

for: j = Class j

n = Number of agricultural sections used

p_{ij} = True proportion of class j in Section i

$\hat{p}_{ij}$ = Estimated proportion of class j in Section i

†RMS error was calculated as: $E_{RMS} = \left(\frac{1}{m} \sum_{j=1}^{m} (p_j - \hat{p}_j)^2 \right)^{1/2}$

for m classes and j, p_j and $\hat{p}_j$ as above.

3.2.1 TRAINING PROCEDURES

Initial training for the M-7 data was accomplished by using an unsupervised clustering technique to process every ninth pixel in the area. This technique yielded 59 clusters. The output graymap of cluster assignments was examined and an association was established between clusters and actual ground covers. It was shown that four major object classes (corn, soybeans, trees, and hay) were represented by very few clusters, while the various other ground covers such as weeds, bare soil, cut hay, senescent vegetation, pastures, farmsteads, etc., which display a wide degree of variability, were represented by 85% of the clusters. By examining the statistics for the cluster groups we were able to generalize the larger of these clusters into eight broad classes, as noted in Table 3.8.

TABLE 3.8 COMBINING CLUSTERS BASED ON REPRESENTING COMMON OBJECT CLASSES

Class	No. of Clusters	Total No. of Points
1. Corn	2	2006
2. Soybeans	3	217
3. Trees	3	566
4. Hay	1	1771
5. Sparse Vegetation	8	252
6. Grass	4	889
7. Bare Soil	9	305
8. Dark or Wet Bare Soil	6	301
TOTAL	36	6307

Next the statistics (means and standard deviations) for the clusters in each group were combined to yield one signature for use in classification processing. In order to reduce classification costs, it was necessary to combine the clusters so as to greatly reduce the number of training signatures used in classification processing. Also, it was felt that for this data no loss of accuracy would result since it appeared from our analyses that there was very little overlap between class groups of clusters. As an additional safeguard, the program which calculates the new signature first performs a χ^2 test on each signature to measure its distance (in a probability sense) to the mean of the other signatures in the group and rejects signatures if the distance is too large.

The subset of seven bands chosen for processing this set of data are as follows (listed in order of increasing wavelength): 2 (.46-.49 μm); 3 (.48-.52 μm); 7 (.58-.64 μm); 9 (.67-.94 μm); 10 (1.0-1.4 μm); 11 (1.5-1.8 μm); and 12 (9.3-11.7 μm).

The data were then classified and evaluated. It was found that the overall classification rates were only fair and there was a major problem with tree false alarms in corn fields and also corn false alarms in tree areas. Further tests showed that these problems were not a result of having combined the individual clusters -- in fact classifying with the separate corn and tree clusters produced slightly poorer results.

As a final investigation, "classical" training techniques, that is calculation of a set of training statistics for each individual field using all the pixels in that field, were used for all corn fields, soybean fields, and woodlots. The set of signatures for each class were combined, after first omitting "outlying" signatures, (signatures whose mean was further than a specified distance from the mean of the combined signatures). It was found that signatures thus discarded were from anomalous fields -- so-called tree areas which were pasture with some trees, a soybean field that was very weedy or uneven in ground cover, etc. The final set of eight signatures therefore included five signatures derived from clustering and three signatures derived from the more "classical" approach.

Results using this set showed a marked increase in correct classification and are presented in Table 3.9. It was noted that the tree-corn confusion problem, though still evident, involved significantly fewer pixels than previously. In comparing the recognition map to aerial photography, many cases were noted where apparently incorrect classifications in a corn or soybean field, for example, were matched with spots of dead crops or weeds in the fields. Thus we arrive at a problem in trying to assess classification results using only classification counts: nonhomogeneous recognition in a nonhomogeneous area thought to be homogeneous, is likely to be correct classification. Therefore, it is believed that the numbers displayed are an understatement of the correct classification rate. Also pertaining to the interpretation of Table 3.9 is the observation that more anomalous ground covers, such as weeds or pasture, would be correctly classified if called any one of a number of training classes such as weeds, sparse vegetation or hay.

Because of time limitations we were not able to classify the entire data set to compare with the S-192 data set.

3.3 COMPARISON OF CLASSIFICATION RESULTS

Examination of the S-192 and M-7 classification results, Tables 3.5, 3.6 and 3.9, shows that the M-7 classification was substantially better than that accomplished using the S-192 data especially as regards tree recognition. This is not too surprising considering the problems caused in the S-192 data by coarser resolution cell size and atmospheric effects due to the longer path length for reflected radiation to reach the SKYLAB sensor. Also, five of the seven bands used in processing the M-7 data were not useable in the S-192 data set due either to excessive noise or to limited dynamic range for the data in those bands. Thus it is perhaps unfair to compare results obtained from the two sensors.

TABLE 3.9 PERFORMANCE MATRIX FOR M-7 MULTISPECTRAL SCANNER CLASSIFICATION OF TRAINING AREA FOR FIELD CENTER PIXELS

GROUND TRUTH CLASS	# FIELDS	# PIXELS	CORN	SOY-BEANS	TREES	HAY	GRASS	SPARSE VEG.	LIGHT BARE SOIL	DARK (WET) SOIL	UNCLASSIFIED
Corn	10	5767	85.0	0.9	6.4	4.3	3.2	0.5	.0	.0	.0
Soybeans	6	2248	4.5	77.0	3.2	2.9	12.4	.0	.0	.0	.0
Trees	8	2139	1.6	0.3	88.9	4.5	1.8	0.4	2.2	0.3	.0
Hay	7	3379	2.5	5.2	4.8	86.9	0.5	0.1	.0	.0	.0
Weeds	6	4371	10.3	.3	5.9	27.7	22.0	5.1	25.5	2.8	.0
Pasture	5	1524	8.7	.0	.5	1.3	79.7	8.6	1.0	.1	.0
Pasture/Woods	8	820	9.6	2.4	38.4	14.5	31.2	3.3	.5	.0	.0
Alfalfa	1	119	.0	72.3	.0	27.7	.0	.0	.0	.0	.0
Grass	2	394	5.3	0.8	6.3	0.8	79.4	2.5	4.3	0.5	.0
Bare Soil	7	1741	1.1	0.1	0.8	.0	5.0	11.1	24.2	57.6	.0
Field Beans	2	371	10.2	.0	3.8	1.1	14.6	66.3	1.1	3.0	.0
TOTALS	62	22873	25.5	9.1	13.6		39.6			12.2	.0
GROUND TRUTH (%)			25.2	9.8	9.4		48.0			7.6	.0

Overall Correct Classification = 84.1%

RMS Error in Proportion Estimation = 4.7%

However, an illustration which would point up the differences in the data collected, and hence the differences in the performance of the scanners could be effected via a comparison of the manner in which signals from the various ground classes fill up the signal space. This can be shown by using a sequence of two-dimensional ellipse plots. For simplicity, presented here are two such plots for each scanner. In each plot, Figures 3.1, 3.2 for the S-192 data and Figures 3.3 and 3.4 for the M-7 data, the channels displayed are the best bands for discrimination. What is plotted is the two-dimensional contour ellipse for a chi-square value of one. The scale of the plots differs for the two scanners -- the S-192 plots are twice the scale of the M-7 plots.

It is seen from comparing these figures that the S-192 data overlap a considerable amount, that is, the signals are compressed into a small portion of the available signal space. The ellipses shown are for a chi-square value of one meaning that only about 40% of the population of a two-channel distribution lies inside the ellipse as drawn (assuming the distributions to be Gaussian). It is readily apparent, then, that the 60% of the pixels outside the ellipse of the correct class will lie inside the ellipse of some other, probably incorrect class. It is surprising that the processing results were as good as they were. For the M-7 data, noting the change in the scale of the plots, it is seen that the ellipses are spread about a larger area of the signal space and are also somewhat distant from each other. The closeness of tree and corn distributions in each case indicate why this pair of classes was so troublesome.

In conclusion, it has been shown that the limited range of the data or, viewing it another way, the compression of the signals into a small portion of the signal space, is responsible for the high confusion rate in classifying the S-192 data.

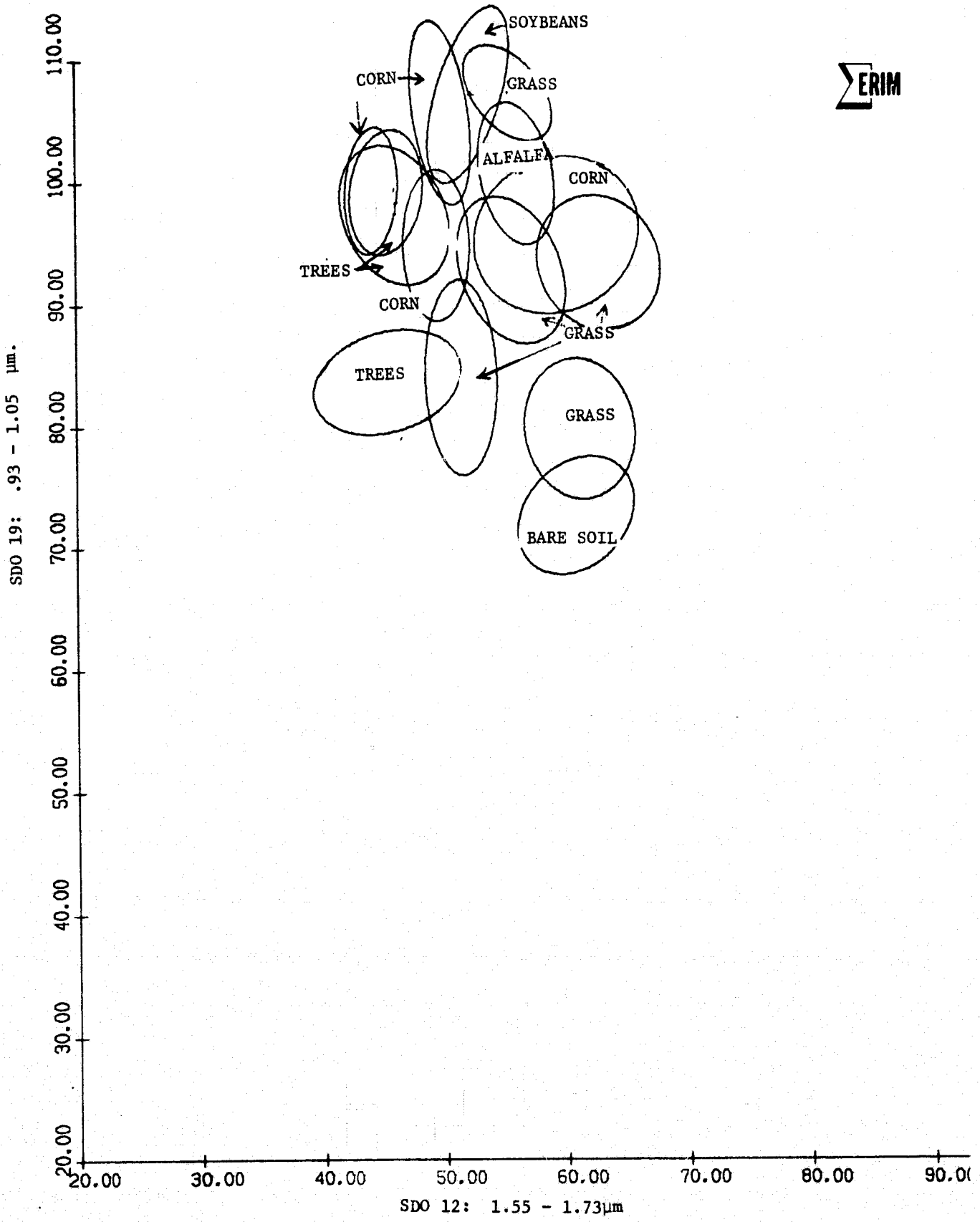

FIGURE 3.1 TWO-DIMENSIONAL SIGNATURE PLOTS FOR S-192 AGRICULTURAL DATA

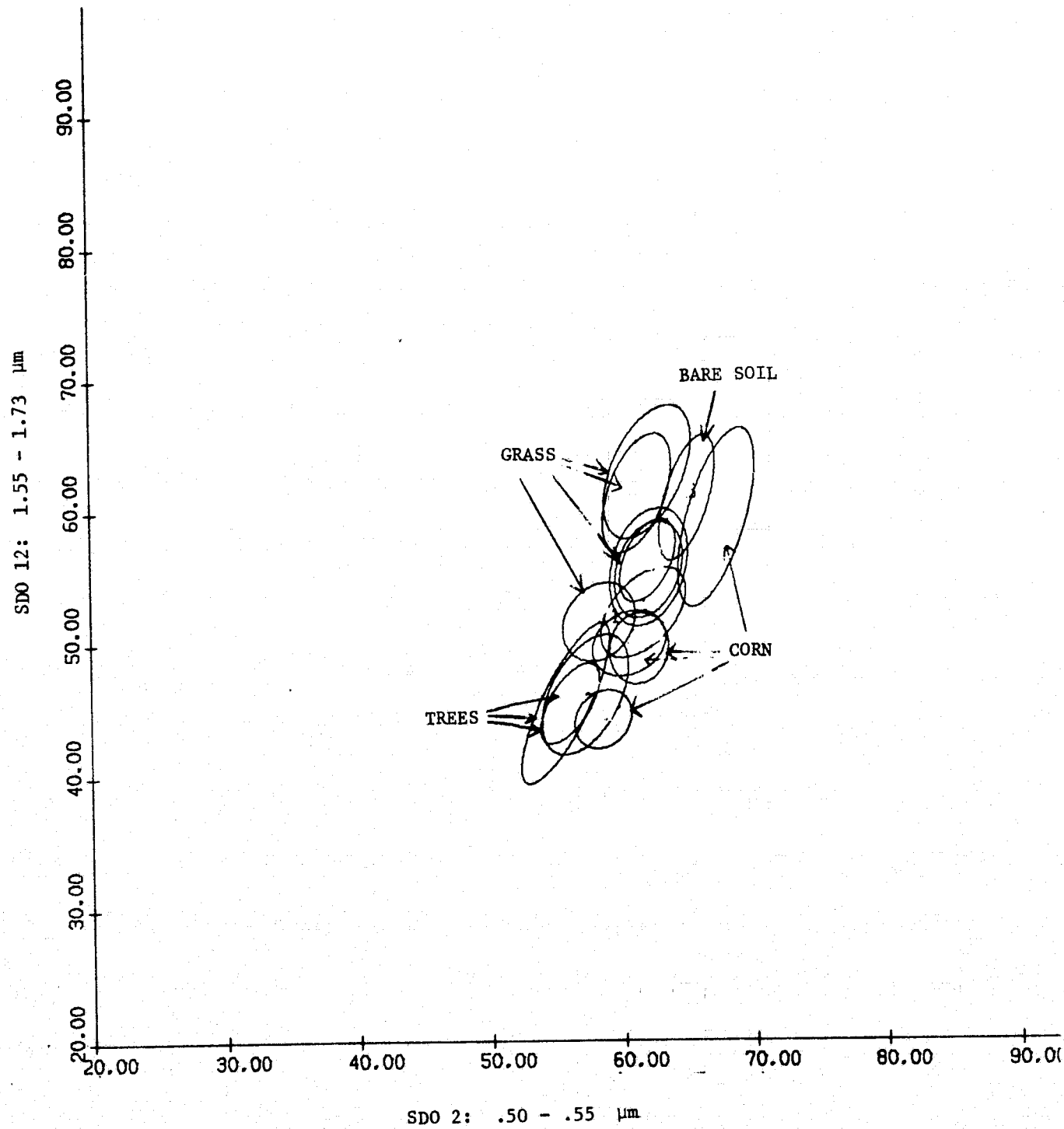

FIGURE 3.2 TWO-DIMENSIONAL SIGNATURE PLOTS FOR S-192 AGRICULTURAL DATA

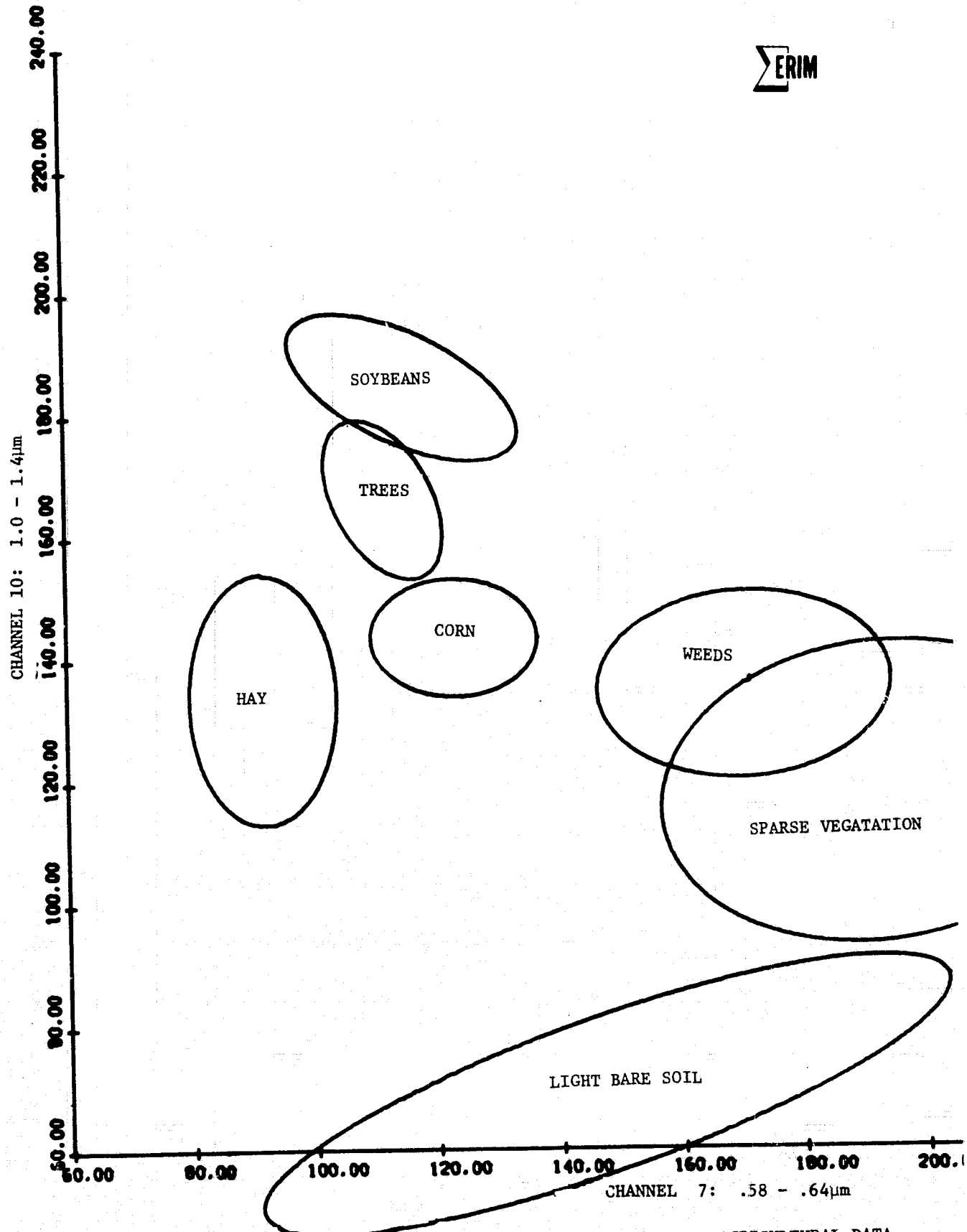

FIGURE 3.3 TWO-DIMENSIONAL SIGNATURE PLOTS FOR M-7 SCANNER AGRICULTURAL DATA

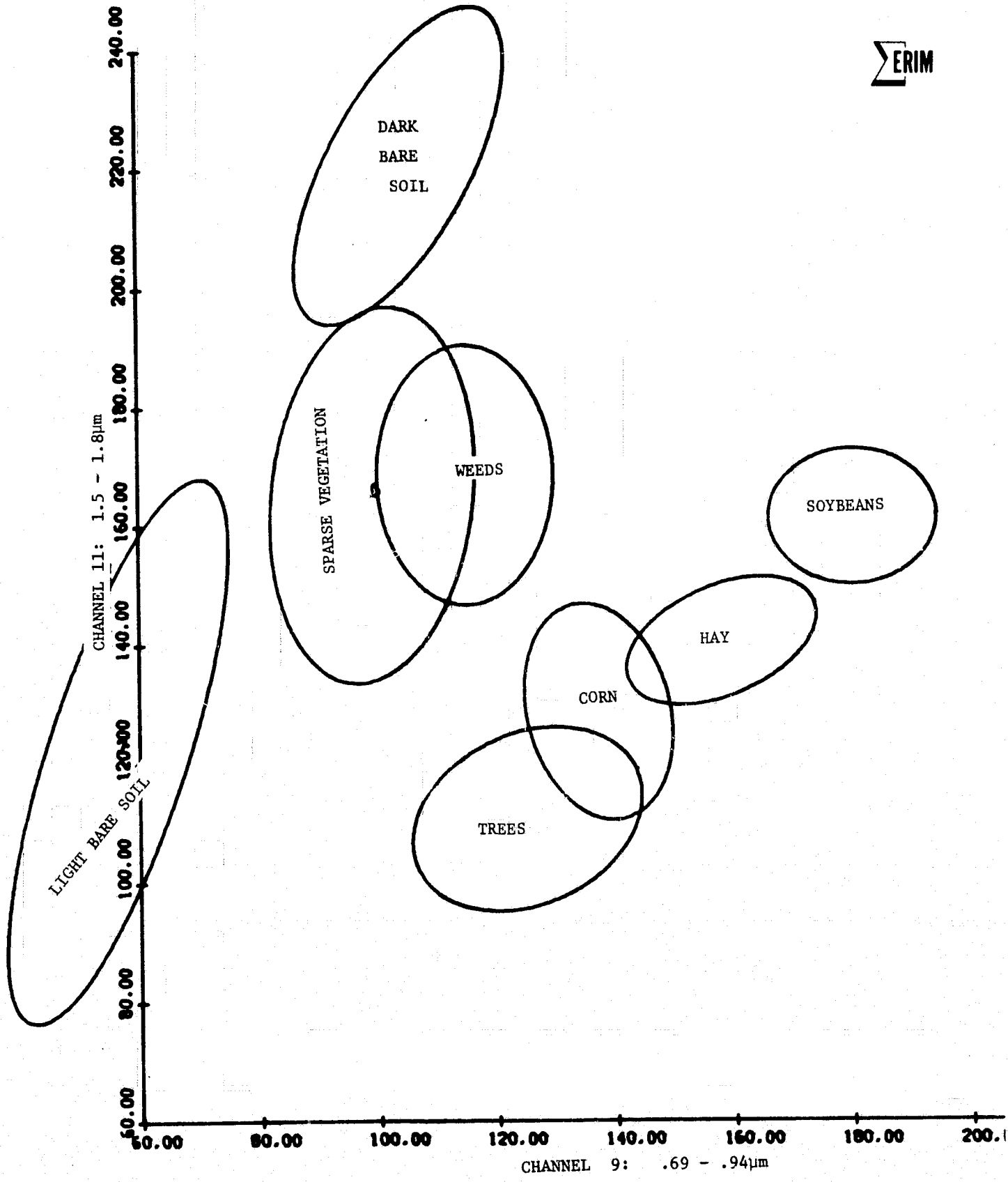

FIGURE 3.4 TWO-DIMENSIONAL SIGNATURE PLOTS FR FOR M-7 SCANNER AGRICULTURAL DATA

4

EFFECTS OF CHANNEL-TO-CHANNEL SPATIAL MISREGISTRATION ON RECOGNITION ACCURACY OF SKYLAB S-192 DATA

4.1 THE PROBLEM

The fact that Skylab S-192 data are spatially misregistered has been established. Scan-line-straightened data in particular is more severely misregistered than conic data as is described in Section 2.1.3. A significant issue to be examined here is whether this misregistration is a cause for concern with regard to the recognition accuracy achievable using these data. To address this problem two techniques were employed. The effects of channel-to-channel misregistration were examined analytically and through a simulation technique. Two experiments were designed to implement the simulation technique. One experiment concentrated on the effects of misregistration on field center pixels and a second experiment investigated the effects on border or mixture pixels. Though it was found that misregistration has an insignificant effect on the recognition accuracy of field center pixels, it was determined that the availability of these pixels was markedly reduced. That is, with the introduction of misregistration, fewer pure field center pixels exist. As a result, the classification of mixture pixels (pixels whose signals were derived from two or more ground covers) was an important concern. It was determined that the correct classification of mixture pixels deteriorated with the introduction of misregistration. Misregistration could adversely influence the false alarm rate of ground classes which adversely affects the accuracy of standard proportion estimation techniques.

4.2 THE APPROACH

In order to facilitate the analysis of the effects of channel-to-channel spatial misregistration, S-192 resolution elements may be divided into four categories as illustrated in Figure 4.1. These are: (a) pure field center pixels can be misregistered but remain field center pixels; (b) pure field center pixels can be misregistered so those channel(s) out of registration

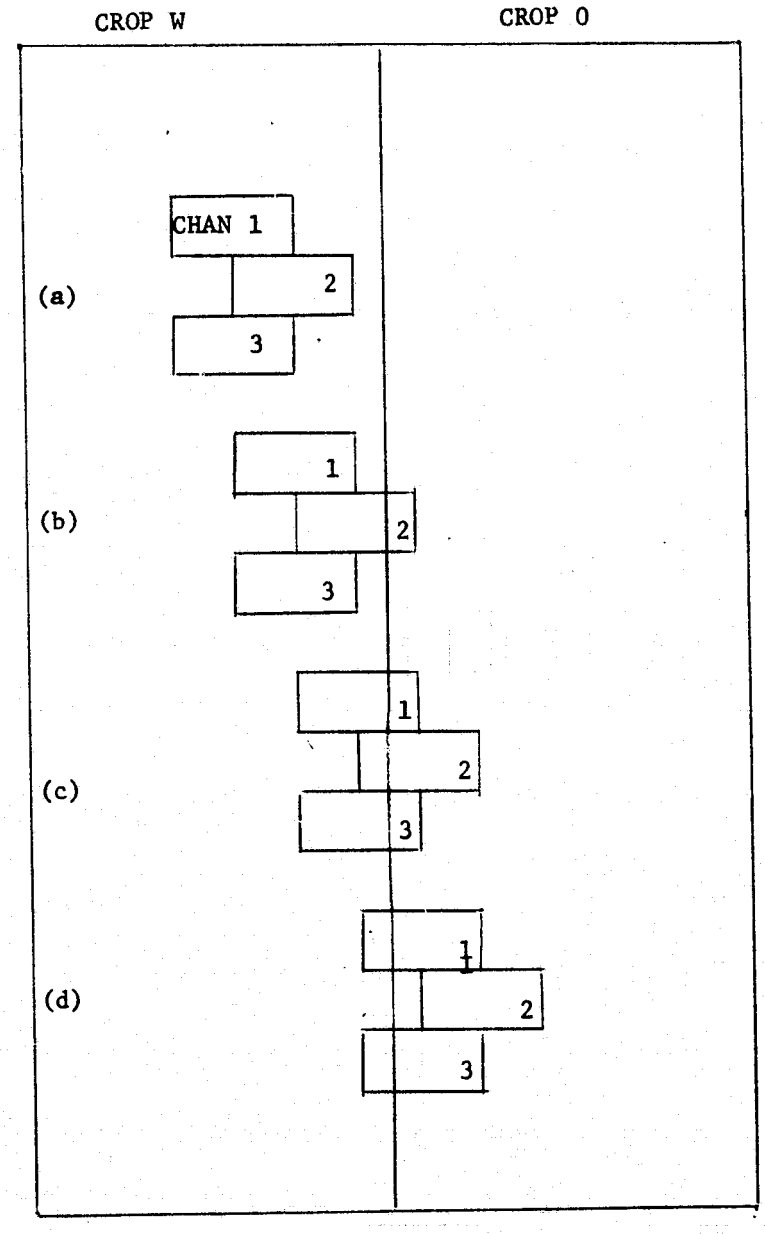

FIGURE 4.1. ILLUSTRATION OF FOUR RESOLUTION ELEMENTS MISREGISTERED ALONG THE SCAN LINE ONE-HALF PIXEL IN CHANNEL 2 OF THREE DATA CHANNELS (OFFSET IN THE VERTICAL DIRECTION FOR ILLUSTRATIVE CLARITY).

become mixtures of two or more crop types; (c) mixture pixels can be misregistered so channel(s) out of registration represent different mixture proportions; and (d) mixture pixels can be misregistered so those channel(s) out of registration become pure field center values.

In the analysis of the effects of channel-to-channel spatial misregistration, pixels falling into category (a) were examined separately from those in (b), (c) and (d). Two techniques were employed in the analysis of the effects upon pure field center pixels that are misregistered but remain field center in all channels (category (a)). The first, an analytical technique, examined a simplified data structure studying the effects of misregistration within a context of two signatures with a common covariance. The second technique employed was one based on the simulation of the effects of misregistration. A simulation was also carried out in the analysis of the effects on pixels of the above mentioned categories (b), (c) and (d).

A simulation technique was decided upon in order to quantify in some manner the effects of misregistration on a given S-192 data set. Given a signatures set from registered data, the problem was to determine in what manner the signatures would be affected by the introduction of a known degree of misregistration. Signatures were to be simulated representing not only pure field center statistics of misregistered data, but also border pixel statistics. Signatures were manipulated rather than the actual data in order to simplify the amount of processing required.

A subset of five signatures from the agricultural processing set used in Section 3 were used as the basis for the simulation. These signatures represented ground covers corn, tree, grass, bare soil and brush. The same seven bands of data previously selected were used here; these were SDOs (2, 8, 10, 12, 17, 19, 20). It was assumed for purposes of simulation that data from which the signatures were generated were perfectly registered from channel-to-channel. From these initial signatures many signatures were generated representing a variety of distributions as affected by varying degrees of misregistration. When more than one channel was misregistered in simulation

each was misregistered from the original set by the same degree. Two different sets of processing were carried out. One examined the effects of misregistration of three S-192 channels and the other was a simulation of the misregistration of a single S-192 channel.

Once a variety of misregistered distributions were simulated, several analyses were carried out. These were (1) an analysis of the effects of misregistration on the expected recognition performance matrix of misregistered field center pixels, (2) an analysis of the expected classification performance for mixtures of two crops at varying degress of misregistration, and (3) an examination of the effect of misregistration on the availability of field center pixels.

Presentation of the above analyses will first concern the effects of misregistration on field center pixels that remain field center in all channels even after misregistration and secondly the analysis of the effects of spatial misregistration on border and near border pixels will be discussed.

4.3 THE EFFECT OF MISREGISTRATION ON RECOGNITION ACCURACY OF FIELD CENTER PIXELS THAT REMAIN FIELD CENTER IN ALL CHANNELS EVEN AFTER MISREGISTRATION

The analysis of this section deals with an examination solely of field center pixels that remain field center in all bands even after misregistration.

4.3.1 RESULTS OF THE ANALYTICAL ANALYSIS OF THE EFFECTS OF MISREGISTRATION ON FIELD CENTER PIXELS

Insight was gained into what effects spatial misregistration may have on field-center recognition performance first through an analytical analysis of the problem. This analysis examined two normal distributions with common covariance for any number of channels of data. The conclusions of the analysis were intriguing. Where 'common sense' might dictate the hypothesis that misregistration would hurt field-center recognition performance, the model studied indicated that quite the opposite could be true. Under certain circumstances misregistration could actually improve results in the classification of field center pixels.

Since misregistration and correlation are highly related, the analysis examined error rate of classification as a function of correlation (ρ). It was determined that a unique maximum error rate is reached somewhere between $-1 \leq \rho \leq 1$. Figure 4.2 plots error rate ϕ as a function of correlation ρ in a conceivable manner as determined by the analysis. Misregistering data will cause correlation to tend to zero. Therefore, should the given correlation Λ between the two stated distributions lie in the range $0 \leq \Lambda \leq \rho_{crit} \leq 1$ for perfectly registered data, then by misregistering the data the expected error rate would actually decrease in value. A full presentation of the analytical analysis is presented in Appendix IX.

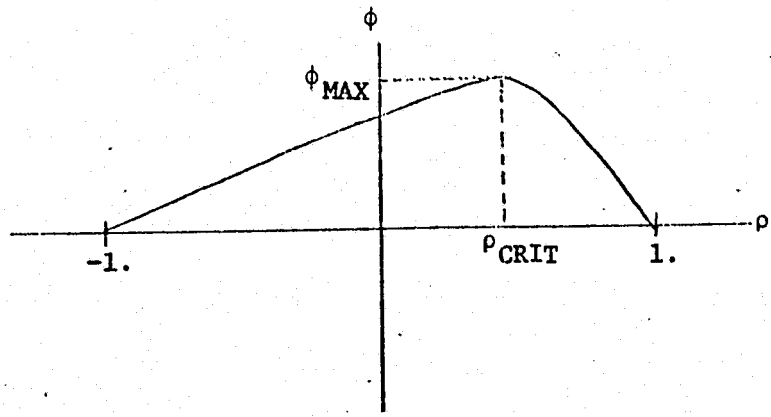

FIGURE 4.2 ERROR RATE OF RECOGNITION ϕ AS A FUNCTION OF CORRELATION ρ IN FIELD CENTERS

In order to test the hypothesis of the analytical analysis in a more realistic data processing situation where there are more than two signatures, each with a distinct covariance matrix, a simulation model was developed to empirically analyze the effects of channel-to-channel spatial misregistration on the correct classification of field center S-192 resolution elements.

4.3.2 THE FIELD CENTER RESOLUTION ELEMENT MISREGISTRATION MODEL

The simulation model presented in this section describes the effect of misregistration of field center pixels that remain field center pixels in all channels even after misregistration. The means and standard deviations of pure field center pixels are not affected by misregistration. Hence the model does not modify these statistics. Correlations are the statistics that are affected.

Analyses were made by Horwitz [8] and Coberly [9] of the correlation between ground elements studied as a function of the distance between the ground elements. Though both were studies of aircraft data, conclusions were drawn for LANDSAT size resolution elements. They determined that the correlation between LANDSAT size pixels drops exponentially as the distance between the pixels increases. In effect, two adjacent LANDSAT or S-192-sized pixels are virtually uncorrelated.

In effect a misregistered scanner channel is measuring a signal displaced from the center of focus of the registered channels. Hence the correlation between two channels which are not registered would be less than the corresponding correlation had both channels been registered. The above mentioned analyses indicate that pure field center signatures derived from misregistered data are less correlated in those channels out of registration than field center signatures derived from corresponding registered data.

The model chosen to simulate this effect is one that estimates the decorrelation as a linear function of misregistration. This estimate is a more conservative measure of the effect than the previously mentioned exponential drop measured in aircraft data. However, since S-192 resolution is not as fine as the aircraft resolution considered, this more conservative estimate was deemed more appropriate.

Given a perfectly registered distribution S_R with mean A_R and covariance C_R. For S_R with some channel or channels misregistered, it would have the same mean vector A_R but a different covariance C_M. Any term of C_M say $c_{Mi,j}$ is related to a term of C_R in the following manner.

$c_{Mij} = c_{Rij}$ for $i=j$

$c_{Mij} = c_{Rij}$ for $i \neq j$ and i and j registered with respect to one another, i.e., $\beta=1$.

$c_{Mij} = \beta c_{Rij}$ for $i \neq j$, $0 \leq \beta < 1$ and i,j misregistered with respect to one another.

where

β is dependent linearly on the degree of misregistration.

β was simply chosen to equal the degree of misregistration between two channels. For example if two channels i and j were misregistered by one-half pixel with respect to one another, then the correlation between i and j, $C_{Mi,j}$, was simulated to be one-half the measured correlation between i and j in the registered signatures.

4.3.3 THE EXPERIMENTAL DESIGN

Appendix VII describes the experiment carried out in full. For purposes of clarity the following experiment summary is presented.

Five S-192 field center signatures representing the distributions of tree, corn, grass, bare soil and brush classes were selected for use in the implementation of the experiment. Using the simulation model discussed in the previous section, signatures representing field center distributions misregistered by factors of 1/3, 1/2, 2/3 and 1 whole pixel in the SDOs 2, 12 and 17 were simulated (See Appendix I for wavelengths). These three SDOs were chosen because they were found to be the three best channels for purposes of discrimination for the given signature set. Thus we are calculating an upper bound to the errors caused by misregistration. An expected performance matrix was calculated for each of the four sets of simulated signatures along with the original signature set using the program PEC described in Appendix XI.

The same processing was carried out using the best channel for discrimination, SDO 12, as the only misregistered channel. This was an attempt to measure the sensitivity of classification results as a function of the number of channels misregistered.

4.3.4 RESULTS OF FIELD CENTER ANALYSIS

The analytical analysis described in Section 4.3.1 concluded that channel-to-channel spatial misregistration would not necessarily cause field center classification accuracy to deteriorate. However, it did not provide a measure of just how sensitive classification performance on field center pixels might be to misregistration. Therefore, the simulation technique was employed in an effort to quantitatively assess a classifier's sensitivity to misregistration. Keep in mind that both the analytical analysis and the empirical evidence gathered from aircraft data pertain only to those field center pixels that remain field center after misregistration.

Tables 4.1 and 4.2 display results calculated for simulated misregistrations of three channels and one channel, respectively. The row labelled "0 pixels" represents the expected performance of the data set as is, without misregistration. The results displayed in these tables seem to support the hypothesis that misregistration need not be harmful to the recognition performance of field center pixels that remain field center after misregistration. Note that, in both Tables 4.1 and 4.2, the total expected classification for the given signature set diminishes slightly (by 0.22%) for misregistration of up to one-half a pixel but as more misregistration is introduced, the performance improves slightly (0.44 to 1.0%) above the beginning value.

Examination of the simulation results on a crop-by-crop basis leads to further observations. First, not all the crops behaved in a like manner as misregistration was introduced. In Table 4.2 bare soil retained a somewhat constant expected performance whereas grass experienced a loss of .2% at $\beta = 1/3$ and then steadily improved from 81.1% to 84.2% at $\beta = 1$. Corn, on the other hand deteriorated up to $\beta = 1/2$ and then improved. The expected recognition of trees deteriorated up to $\beta = 2/3$. Secondly, in comparing Table 4.1 and Table 4.2 on a crop-by-crop basis, one detects more sensitivity in the misregistration of one channel in more cases than in the misregistration of 3. Most pronounced is grass which improved from 81.3 to 82.8 in Table 4.1, and from 81.3 to 84.2 in Table 4.2. Interestingly, corn deteriorated in Table 4.2 up to $\beta = 1/2$, while it improved in Table 4.1.

TABLE 4.1. EXPECTED PERFORMANCE OF S-192 SIGNATURES FOR VARYING DEGREES OF MISREGISTRATION OF SDO's 2, 12 and 17.

β Degree of Misregistration	Expected Recognition Accuracy (%)					
	Tree	Grass	Bare	Brush	Corn	Overall
0 pixels	96.5	81.3	97.9	77.2	77.9	86.16
1/3	96.3	80.3	98.2	76.8	78.2	85.96
1/2	96.1	81.1	98.1	76.0	78.4	85.94
2/3	96.2	81.8	98.1	76.0	79.0	86.22
1	96.7	82.8	98.7	76.4	78.4	86.60

TABLE 4.2. EXPECTED PERFORMANCE OF S-192 SIGNATURES FOR VARYING DEGREES OF MISREGISTRATION OF SDO 12.

β Degree of Misregistration	Expected Recognition Accuracy					
	Tree	Grass	Bare	Brush	Corn	Overall
0 pixels	96.5	81.3	97.9	77.2	77.9	86.16
1/3	95.6	81.1	97.7	78.5	76.7	85.92
1/2	95.2	81.5	97.7	79.0	76.4	85.94
2/3	95.2	82.0	97.6	79.7	76.8	86.26
1	95.7	84.2	97.7	80.9	77.3	87.16

Three conclusions can be drawn from these results: (1) as was hypothesized, misregistration is not necessarily harmful to the recognition performance of field center pixels that remain field center in all channels after misregistration, (2) though results may both decay or improve, depending on the degree of misregistration, the expected performance of the classifier was found here to vary only plus or minus one percent of the total for registered data and at most three percent on a crop-by-crop basis, and (3) the sensitivity of the classifier to misregistration did not appear to be a function of the number of channels misregistered. In fact, more change in classification was detected with only one channel misregistered than with three.

The fact that misregistration is expected to in some cases improve recognition accuracy among field center pixels should not suggest using misregistered data or actually misregistering data to improve recognition. Though the recognition of certain field center pixels may actually improve, evidence presented in the next section will indicate that other more serious problems are confronted with the introduction of misregistration. Deleterious effects can be detected among border pixels and field center pixels that are mixtures in the misregistered channels.

4.4 THE EFFECTS OF CHANNEL-TO-CHANNEL SPATIAL MISREGISTRATION ON BORDER AND NEAR BORDER PIXELS

This section deals with the category of pixels consisting of field center pixels that become mixture pixels in those channels that are misregistered as well as border or mixture pixels. Within this overall category the most deleterious effects of misregistration are encountered.

4.4.1 THE AVAILABILITY OF PURE FIELD CENTER PIXELS

Channel-to-channel spatial misregistration reduces the availability of pure field center pixels. Figure 4.3 displays several representations of three channel resolution elements. Pixel (a) is the appearance of a pixel registered in all channels. It appears as a pure field center pixel in cover type W. If this pixel were misregistered by one whole pixel in channel 2 in the right to left direction it would appear as (b). The pixel

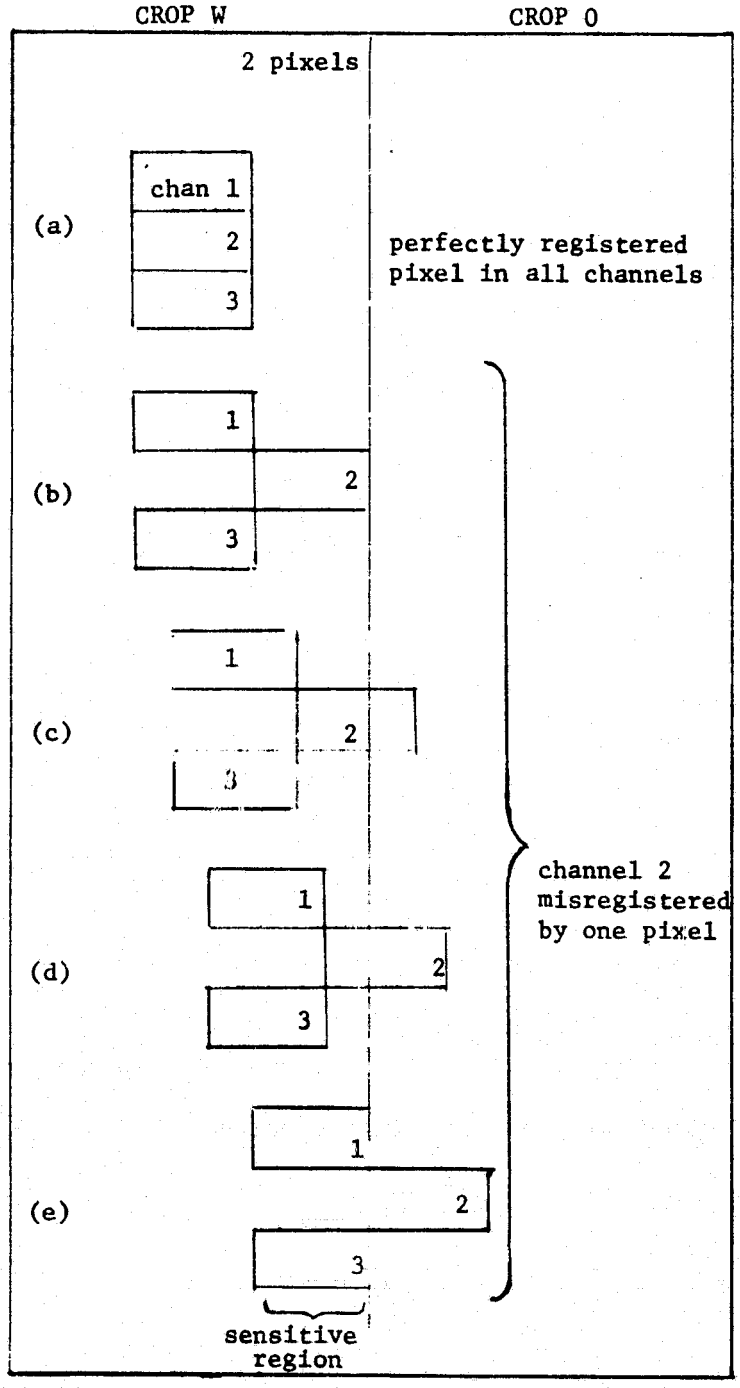

FIGURE 4.3. ILLUSTRATION OF HOW CHANNEL-TO-CHANNEL MISREGISTRATION AFFECTS AVAILABILITY OF FIELD CENTER PIXELS

TABLE 4.3. DISPLAY OF THE NUMBER OF PURE FIELD CENTER PIXELS AVAILABLE FOR VARYING DEGREES OF MISREGISTRATION

	TOTAL PIXELS INCLUDING MIXTURES	NUMBER OF FIELD CENTER PIXELS AND PERCENT OF TOTAL FOR: NO MISREGISTRATION		ONE-HALF PIXEL MISREGISTRATION		ONE-PIXEL MISREGISTRATION	
		#	%	#	%	#	%
CORN	3641	1526	41.9	1054	28.9	537	14.7
BRUSH	820	341	41.6	227	27.7	117	14.3
TREE	490	175	35.7	105	21.4	41	8.4
GRASS	2922	1250	42.8	896	30.7	491	16.8
BARE	653	222	34.0	140	21.4	55	8.4
STUBBLE	1081	391	36.2	247	22.8	100	9.3
OTHER	706	296	41.9	209	29.6	119	16.9
TOTAL	10313	4201	40.7	2873	27.9	1460	14.2

is still fully in Crop W but now channel two is detecting a signal displaced an entire pixel from the registered location. Pixels (c), (d) and (e) would all have been pure field center pixels had no misregistration been introduced. These pixels are now mixtures in channel 2 of covers W and O. In fact, pixel (e) is 100% cover O in channel 2, whereas it is 100% cover W in channels 1 and 3. This effect of misregistration causes fewer pixels to be pure field center in all channels.

Table 4.3 indicates for the given S-192 data set the availability of pure field center pixels as a function of the degree of misregistration. For a given misregistration β, any pure field center pixel within 2β of the border lies within a sensitive region. The signals detected for these pixels will be mixtures in the misregistered channels. Table 4.3 was calculated using only the larger fields (greater than 17 acres) from the S-192 Southeast Michigan agricultural test site with a program designed to count field center pixels given a set of polygon field designations. To determine how many pure field center pixels would be available for a misregistration of β, each field polygon was inset by β pixels and the available field center pixels counted with respect to the new field designation.

It is obvious from Table 4.3 that the availability of field center pixels deteriorates rapidly with increased misregistration. Column 2 indicates the number of available field center pixels with perfect misregistration. The third column indicates that with the introduction of 1/2 pixel misregistration along the scan line the total number of field center pixels diminishes by 1323 or 31.5%. Another 1/2 pixel misregistration reduces the total number of available pixels by another 34% from those available initially.

The evidence of this analysis adds great weight to the need to study the effects of misregistration on mixture pixels. Though misregistration may have no significant effect on pure field center signatures as concluded in the previous section, the diminished existence of pure field center pixels makes both the extraction of creditable field center statistics more difficult and the analysis of the effects of misregistration on mixture pixels more significant.

4.4.2 THE SIMULATION MODEL DEVELOPED FOR BORDER AND NEAR BORDER PIXELS

S-192 resolution elements lying on field boundaries are mixtures of two or more ground covers. Due to misregistration, certain channels of field center resolution elements may also represent mixtures of two or more covers. The concern was to develop a mathematical model that would enable an analyst to describe any distribution from a misregistered data set arising from mixtures of at most two crops, based on the signatures of the pure field center crops. The model developed incorporates features of the ERIM mixtures model.*

An n-channel multispectral signature for material W consists of a mean vector A_w with components a_{wi} where i=1,..,n, and a covariance matrix C_w with components $c_{wi,j}$ for each i=1,...,n and j=1,...,n.

Consider the case where the signal detected in one or more channels represents a mixture of ground cover W and some other ground cover O. The following is the model used to construct the signature of mixture pixels from the pure signatures of W and O.

Let α_w be the proportion of cover W present for each pixel and $\alpha_o=1-\alpha_w$ the proportion of cover O present for each pixel. If the pixel were of pure cover W then $\alpha_w=1$. A mean vector A_m of a mixture distribution of crop W and O consists of components:

$$A_{mi} = \alpha_{wi} A_{wi} + (1-\alpha_{wi}) A_{oi} \tag{4.1}$$

where i denotes the spectral channel.

The definition of a term $C_{mi,j}$ of the variance-covariance matrix is:

$$C_{mi,j} = \alpha_{wi} C_{wi,j} + (1-\alpha_{wi})C_{oi,j} \tag{4.2}$$

Whenever i=j the channel variance term σ^2_{mi} would be:

$$\sigma^2_{mi} = \sigma_{wi}\sigma^2_{wi} + (1-\sigma_{wi}) \sigma^2_{oi} \tag{4.3}$$

Given any two distributions then, one can approximate mixture distributions in any proportion of the two crops using Equation (4.1) and (4.2).

*The misregistration-mixtures, model discussed here was developed for NASA/JSC under [17] and current contract NAS9-14123.

With the occurrence of spatial misregistration between channels, Eq. (4.2) should not be used to estimate covariance between channels that are not in registration with respect to one another. If the pixel in question had been a field center pixel of cover W lying near the border or represents a mixture of covers W and O and if two channels, say i and j, are not in registration with respect to one another, then the following model can be used to approximate the distribution.

Let α_{wi} be the proportion of cover W present for each pixel in channel i and $\alpha_{oi} = 1-\alpha_{wi}$ the proportion of cover O present for each pixel in channel i. For the misregistered mean vector A_M, use Equation (4.1). Then for the definition of a term $C_{Mi,j}$ of the variance-covariance matrix, use:

$$c_{Mi,j} = \min(\alpha_{wi},\alpha_{wj}) * c_{wi,j} + \min(\alpha_{oi},\alpha_{oj}) * c_{oi,j} \qquad (4.4)$$

$$c_{Mi,j} = \min(\alpha_{wi},\alpha_{wj}) * c_{wi,j} + [1-\max(\alpha_{wi},\alpha_{wj})] * c_{oi,j} \qquad (4.5)$$

Whenever i = j, the variance term is given by

$$c_{Mi,i} = \alpha_{wi} * c_{wi,i} + (1-\alpha_{wi}) * c_{oi,i} \qquad (4.6)$$

Letting σ_i^2 represent the channel i variance, with appropriate subscripts we have:

$$\sigma_{Mi}^2 = \alpha_{wi}\sigma_{wi}^2 + \alpha_{oi}\sigma_{oi}^2 \qquad (4.7)$$

This expression is equivalent to the mixture variance estimation model, Eq. (4.3).

Equation (4.5) describes in full the estimated covariance between any two channels of data that are being simulated under the stated model. Diagonal terms of the variance-covariance matrix (the channel variances) are described by Eq. (4.7). Let us here consider the correlation terms between channels in an attempt to more fully describe and justify the underlying assumptions made in arriving at this simulation model.

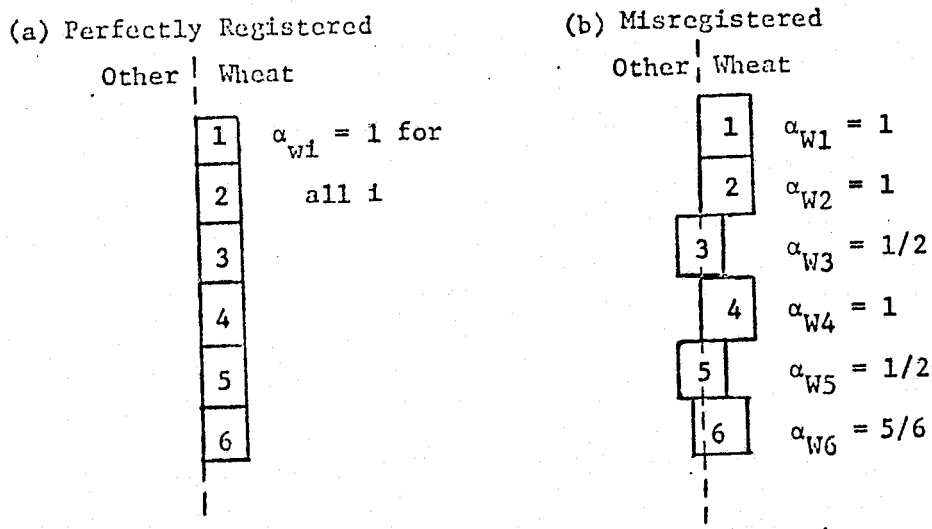

Figure 4.4. An Example of Channel Misregistration for a Single Resolution Element

Figure 4.4 displays a possible configuration of the composite signal received by six different channels while focusing on a single resolution element. Figure 4.4(a) indicates that all six channels are focused on precisely the same location, a borderline resolution element of wheat. This indicates a perfectly registered vector of signals. Figure 4.4(b) indicates a vector wherein channels 3, 5, and 6 were misregistered and actually viewing mixtures of wheat and other.

Correlation terms between channels 1, 2 and 4 remain identical in Figure 4.4(b) to their calculated value for the case shown in Figure 4.4(a). It is also easy to see that the cross correlation between channels 3 and 5 is identical to the mixture covariance estimation model: whenever $\alpha_{wi} = \alpha_{wj}$, Eq. (5) becomes:

$$c_{mi,j} = \alpha_{wi} * c_{wi,j} + \alpha_{oi} * c_{oi,j}$$

which is ERIM's mixture model [15].

However, whenever $\alpha_{wi} \neq \alpha_{wj}$ as is the case, for example, in channel 1 versus 3 or 3 vs. 6, Eq. (4.2) addresses situations not previously considered by the mixture model and assumptions made in the evaluation of these covariance terms must be fully understood.

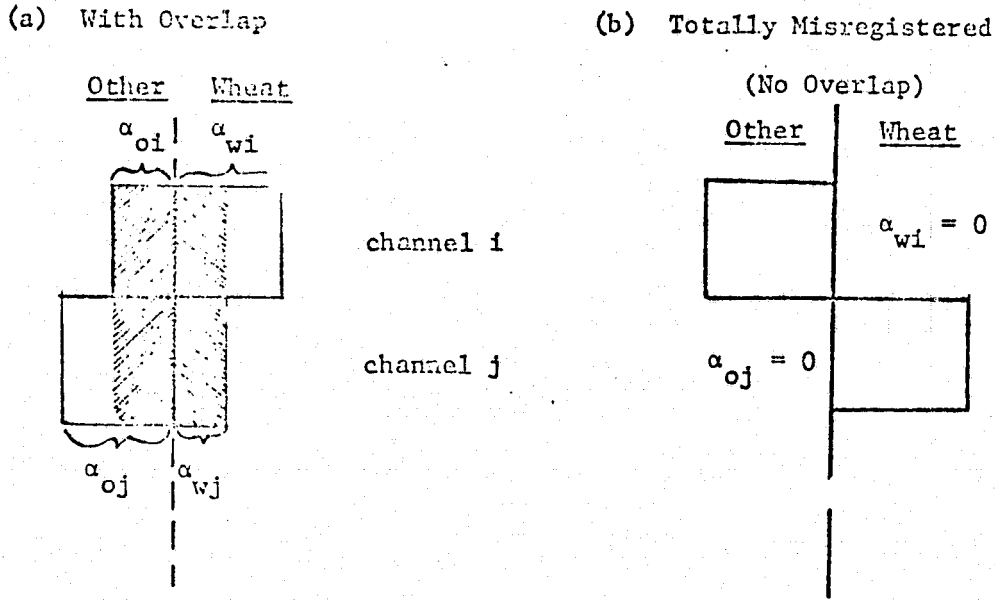

FIGURE 4.5 A MISREGISTRATION CONFIGURATION IN TWO CHANNELS FOR A SINGLE RESOLUTION ELEMENT

Eq. (4.5) is:

$$c_{mi,j} = \min(\alpha_{wi},\alpha_{wj}) * c_{wi,j} + \min(\alpha_{oi},\alpha_{oj}) * c_{oi,j}$$

Figure 4.5(a) displays what the components of Eq. (5) are estimating. Note that $\alpha_{wj} = \min(\alpha_{wi},\alpha_{wj})$ gives the proportion of overlap (area shaded) between the two channels in the wheat field. Hence $\alpha_{wj} * c_{wi,j}$ is the contribution of $c_{wi,j}$ to the constructed covariance term $c_{mi,j}$. Similarly, $\alpha_{oi} = \min(\alpha_{oi},\alpha_{oj})$ is the proportion of the other field that is common to both channels i and j (area shaded) and $\alpha_{oi} * c_{oi,j}$ is the contribution of the covariance of 'other' in channels i and j. Hence where there is no overlap, the cross correlation is assumed to be negligible and therefore zero.

The two basic assumptions made in the derivation of the covariance estimation model are (1) within the same field the correlation between two ground signals drops off rapidly as the distance between the signals increases and (2) signals from different crops are totally uncorrelated. Figure 4.5(b) illustrates the second assumption. Here the correlation $c_{Mi,j} = 0$. Also as seen in Figure 4.5 the contribution to the estimated correlation from the unshaded area is assumed zero. The only contribution is from the shaded area.

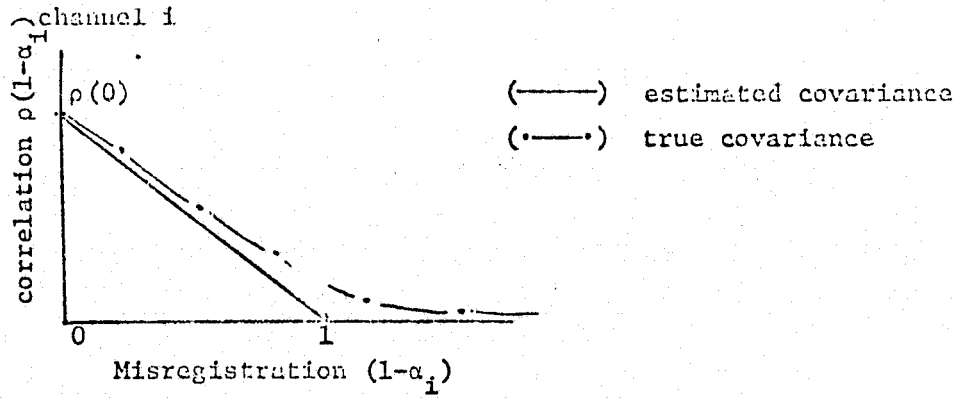

FIGURE 4.6 ILLUSTRATION OF COVARIANCE AS ESTIMATED AND TRUE COVARIANCE

Figure 4.6 illustrates a comparison between the covariance estimated by the proposed model and a hypothetical true covariance. The difference between the two curves is due to both assumption (1) above and the fact that scanner noise and atmospheric noise contributions were not considered. When there is no misregistration, $\rho(1-\alpha_i) = \rho(0)$ and the estimate is exact. As misregistration increases some error is introduced. The analytical deviation of Eq. (5), based on the assumptions mentioned above, is presented in Appendix X.

4.4.3 THE EXPERIMENT FOR MIXTURE PIXELS

Appendix VIII describes the experiment carried out in full. Fur purposes of clarity, the following experiment summary is presented.

In the analysis of the effects of channel-to-channel misregistration on mixture pixels, two types of signature simulations were required. First, signatures representing field center distributions misregistered for factors of 1/2 and 1 whole pixel in SDOs 2, 12, and 17 were calculated. Another experiment was run in parallel with only one channel, SDO 12, misregistered. The second experiment is otherwise identical to the first and anlysis of the results of both are presented in the next sections. Once field center signatures were calculated, new distributions representing mixtures of all permutations of two ground covers for varying proportions were simulated as follows. Let α_{iA} and α_{iB} be the proportions of distributions A and B in the i^{th} channel used to simulate a mixture of ground covers A and B. For perfectly registered signatures, α_{Ai} was set to 2/3, 1/3 and 0 for every channel i. However for misregistered signatures, the channels out of registration would be in different proportions. For example, if a signature was misregistered by 1/2 a pixel the proportion of cover type A would be $\alpha_A - 1/2$. Hence any field-center pixels in the registered case within 1/2 pixel of the boundary would become mixture pixels in the misregistered case. (In effect there would be fewer field center pixels). Therefore signatures representing mixtures of misregistered distributions were simulated with proportions of α_{iA} and α_{iB} in the registered channels i and $(\alpha_{jA} - \beta)$ and $(\alpha_{jB} + \beta)$ in the misregistered channels j, where β is the degree of misregistration.

Once the simulated signatures were attained, the program PEC (see Appendix XI (with a 0.001 probability of falsely rejecting a pixel from a multivariate gaussian distribution) was used to calculate the expected performance for each set of signatures representing a given misregistration case. That is, given the linear decision boundaries between the 5 field-center signatures, what will be the expected classification of mixture pixels.

Analysis consisted of the study of the expected performance curve as a function of the location of the pixel across a field boundary. The study conducted centered on the analysis of three basic problems: (1) the effect of misregistration on the classification of a mixture pixel of two ground covers; (2) the effect of misregistration on the false alarm rate of any given crop among mixtures of two other ground covers; (3) the effect of misregistration on proportion estimation; and (4) effects as a function of number of channels misregistered. These analyses are presented in the following sections.

4.4.4 INTERPRETATION OF RESULTS

In order to facilitate the discussion of the results it would be wise at this point to introduce the standard format of the graphs to be presented. These graphs were vital tools in most of the analyses carried out and it would be of invaluable aid to be fully at ease with their format.

Each figure is composed of three graphs (see Figure 4.7 as an example) with each graph displaying one of the degrees of misregistration considered (0, 1/2, or 1 pixel). The curves display the expected performance of pixels of the types labelled at the top of the graphs, as a function of the proportion present of each of the two possible crop types. In a sense one could envision, as an aid in studying these graphs, a pixel moving across a fixed field boundary and at various locations the expected probability of that pixel's classification would be calculated. Note in each of the following graphs a zone representing pure field center pixels in the registered case has been labelled as well as an an area representing mixtures of varying degrees. The width of these zones is exactly one pixel and the field boundary would appear as drawn. The right hand corner of a pixel placed on this grid would lie at the labelled mixtures proportion that it represents.

Primarily the presentation will center on the effects noted on brush and grass mixture pixels interacting with brush, grass, and corn signatures. Since corn is the major crop of interest in the scene, the analysis of the false alarm rate will revolve primarily about the false alarm rate of corn. These crops were chosen for primary consideration since corn, grass, and brush comprise almost three-fourths of the scene. The effects of misregistration analyzed through the interaction of these crops is fairly typical of the entire study; it represents neither one extreme nor the other. Some consideration will also be given to interactions between other crops.

4.4.5 DISCUSSION OF THE EFFECTS OF CHANNEL-TO-CHANNEL SPATIAL MISREGISTRATION ON BRUSH-GRASS MIXTURES

Figure 4.7 displays three graphs, one for each degree of misregistration of the three SDOs considered, plotting the expected probability of classifying brush and brush-grass mixtures as brush (the solid line) or grass (the dashed line). In Figure 4.7(a), on top, one notes that in the area designated brush, these field center pixels are for the most part classified as brush. As the mixture of brush and grass becomes predominantly grass, the performance curve increases for grass and decreases for brush. Also note in Figure 4.7(a) that at the border (1/2, 1/2), mixture pixels are in proportion one-half grass and one-half brush and are called brush or grass 70% of the time. These pixels are thus incorrectly classified 30% of the time. As misregistration is introduced (compare Figures 4.7(a), (b) and (c)), field center brush pixels are not classified as brush with as much consistency. The expected performance for those pixels most near the border deteriorates from around 78% to 42% correct for one-half pixel misregistration, and down to 15% for one pixel misregistration. The indication is that misregistration does affect the correct classification of near-border and border pixels significantly.

Figure 4.9 is a counterpart to Figure 4.7. Here misregistration is depicted from grass into brush. Again near-border grass pixel classification deteriorates, from 83% to 25% correct classification with one pixel misregistration.

Figure 4.8 displays the expected probability of classifying a brush or brush-grass pixel as corn. Even in the registered case, the corn false alarms among brush-grass pixels are significant. As misregistration is introduced, more and more corn false alarms occur among pixels that were pure field center brush pixels in the registered case. In fact those most near the border are called corn with up to 40% regularity. In view of this graph alone, one cannot dismiss the significant increase in corn false alarms introduced by misregistration of the data. Figure 4.10 acts as the counterpart for Figure 4.8 with misregistration from grass into brush. One notices that as misregistration increases more corn false alarms occur among otherwise pure grass pixels, however the rate decreases among grass-brush mixture pixels.

These observations indicate that misregistration has a significant effect on the correct classification of mixture pixels. It was also evident in these and other graphs that are not presented that the corn false alarm rate was high among mixtures of different crops [see section 4.4.7]. Several observations were also made in examining the effects of misregistration as a function of the channels misregistered. Generally, the recognition curves did not deteriorate as rapidly with only one channel misregistered. However, depending on the mixtures, some curves would deteriorate even more rapidly indicating a need for concern even though just one channel was improperly registered. The next set of curves to be presented, Figures 4.11 to 4.14 are the counterparts of Figures 4.7 through 4.10, respectively, for the simulated misregistration of only one channel

Figure 4.11 is a display of misregistration of SDO 12 from brush to grass. Near border pixels deteriorate from about 80% to 35% at the extreme of one pixel misregistration. This indicates a less rapid deterioration than in the case of Figure 4.7 where three channels were misregistered.

Figure 4.12 is a display of the corn false alarm count for one channel misregistered. In contrast to Figure 4.8 the rate is not nearly as pronounced and yet there is a marked increase in the false alarm count of corn among pixels of pure brush had the data been registered.

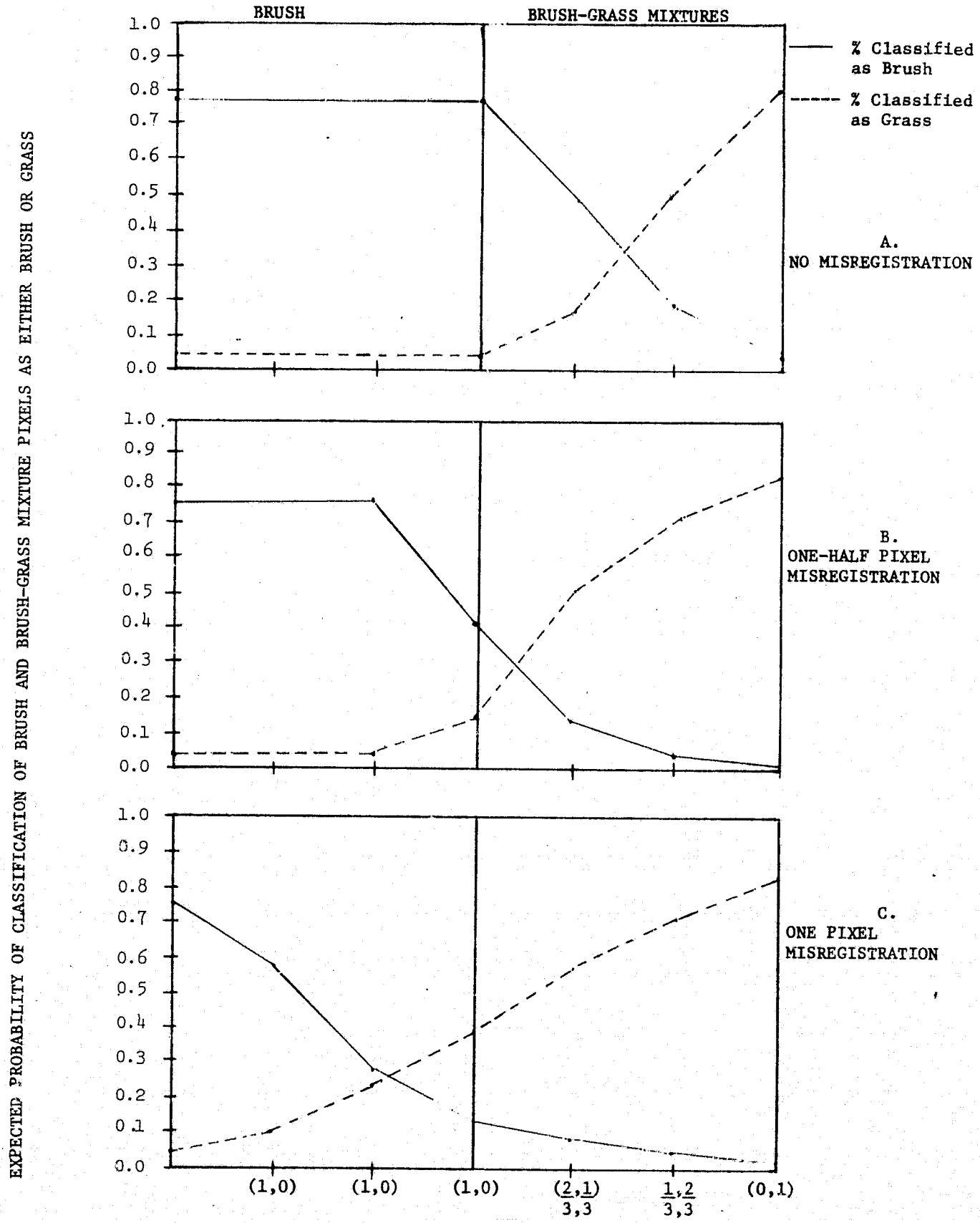

FIGURE 4.7. EXPECTED CLASSIFICATION PERFORMANCE OF BRUSH BRUSH-GRASS MIXTURE PIXELS. THREE CHANNELS MISREGISTERED.

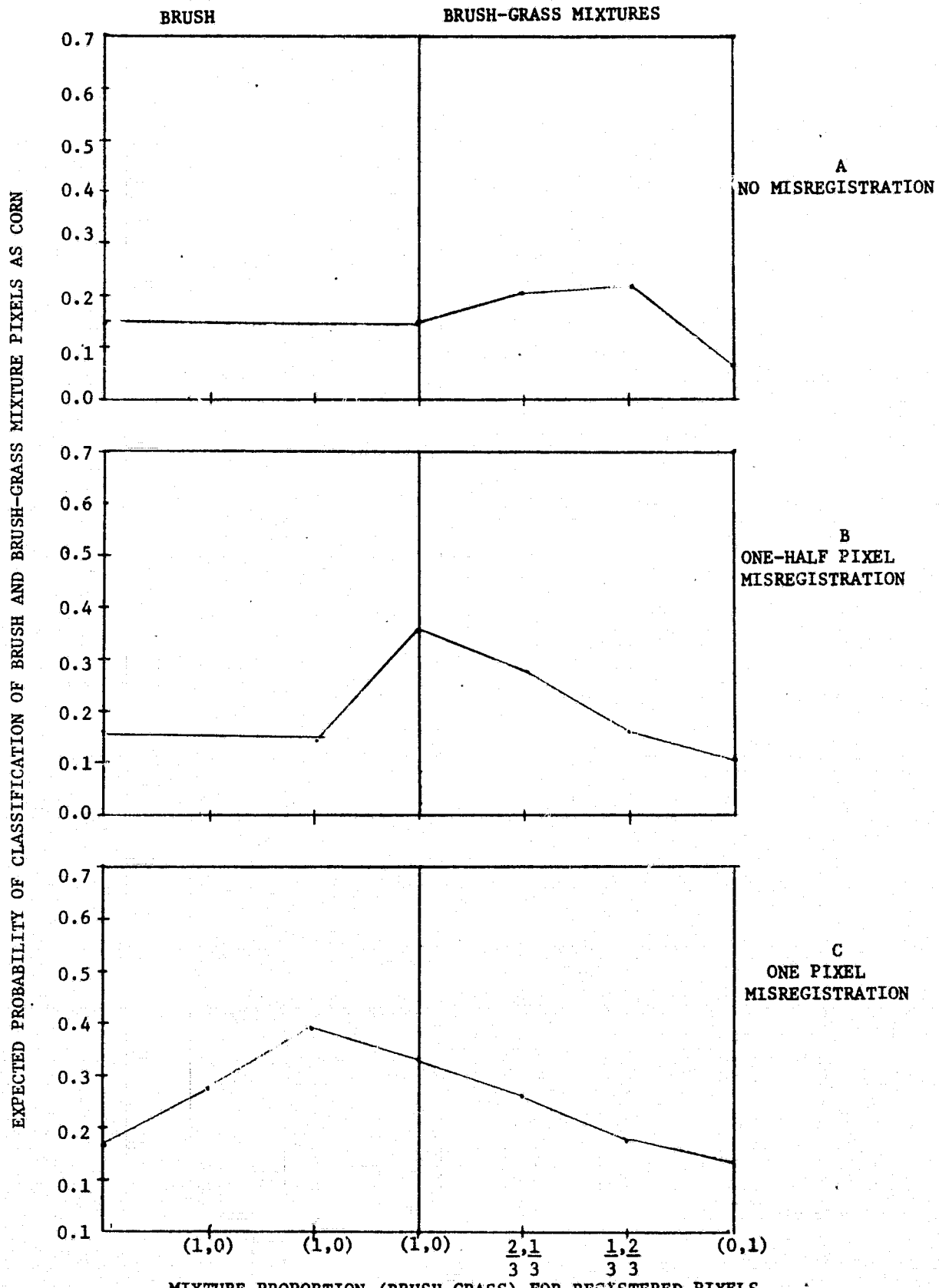

FIGURE 4.8. CORN FALSE ALARMS AMONG BRUSH AND BRUSH-GRASS MIXTURE PIXELS. THREE CHANNELS MISREGISTERED.

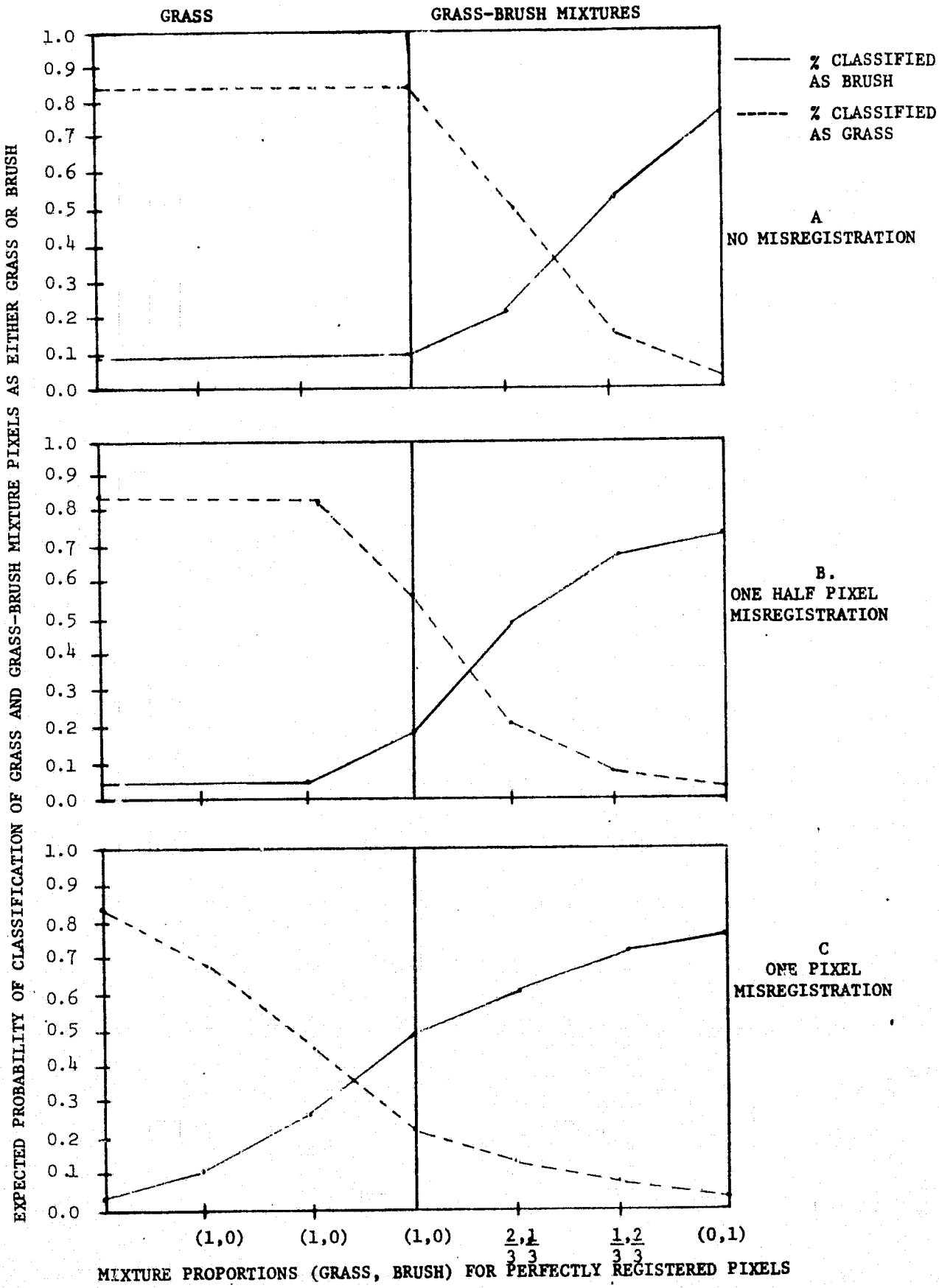

FIGURE 4.9. EXPECTED CLASSIFICATION PERFORMANCE OF GRASS, GRASS-BRUSH MIXTURE PIXELS. THREE CHANNELS MISREGISTERED.

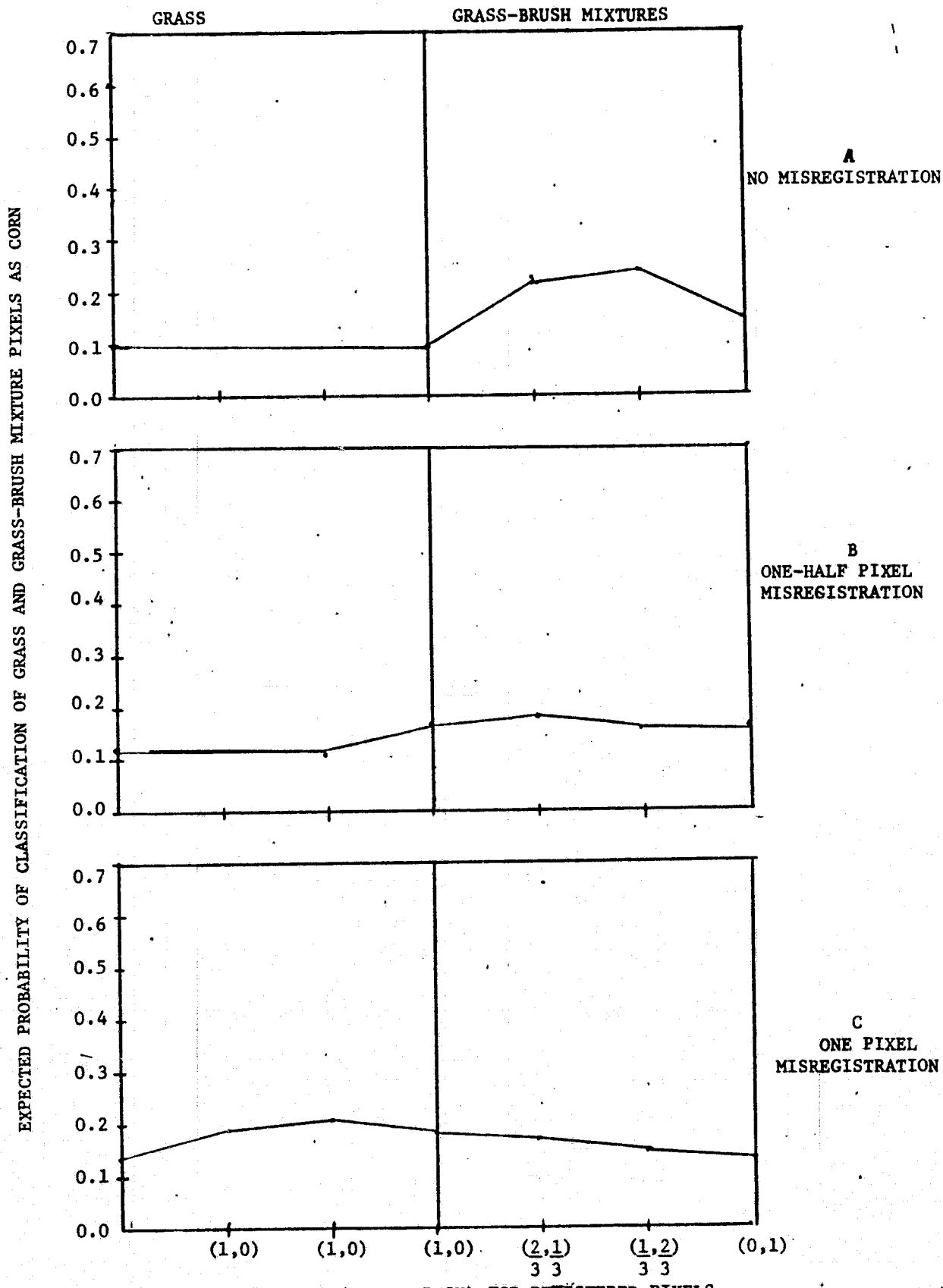

FIGURE 4.10. CORN FALSE ALARMS AMONG GRASS AND GRASS-BRUSH MIXTURE PIXELS. THREE CHANNELS MISREGISTERED

Figure 4.13 displays grass pixels misregistered into brush. Interestingly, the deterioration of the expected probability is at about the same rate as that indicated for three misregistered channels in Figure 4.9. It is especially interesting to note that the curve for brush increases at a less rapid rate for a one channel misregistration of one pixel than it does for the three channel case. The reason for this becomes clear upon examination of Figure 4.14, the display of the corn false alarm rate. Surprisingly with just one channel misregistered more corn false alarms are detected as misregistration increases than with 3 channels of misregistration. This could be explained in that SDO 12 best discriminates corn from grass-brush mixtures. Misregistration of that one channel may tend to make the mixtures look more like corn in that channel, whereas misregistration of three channels may make the mixture less like corn in SDOs 2 and 17. As a result more corn false alarms are detected among pixels misregistered in one SDO than in three. The conclusion to be drawn from this observation is most obviously that effects of misregistration should not be overlooked even though just one channel is in question.

The graphs presented to this point describe not only the effects of misregistration on the predominant scene classes, but are also typical of the kinds of observations that can be made concerning other mixture combinations. A few more graphs will be presented in the next subsection for purposes of giving the reader a broader perspective on the analysis carried out.

4.4.6 ADDITIONAL DISCUSSION OF THE EFFECTS OF CHANNEL-TO-CHANNEL MISREGISTRATION ON BORDER PIXELS

The following graphs were chosen for discussion to display various observations that were made concerning the effects of channel-to-channel spatial misregistration on the classification of S-192 data. Corn, grass, and brush have been previously discussed since they are the predominant scene classes. The examples chosen here will either (1) display a mixture for which three channels of misregistration causes much more deterioration of classification

accuracy than does one channel or (2) display an example wherein the misregistration of one channel causes a greater rate of false alarm of grass pixels than three channels.

Figure 4.15 is a display of the effect of three channels of misregistration on the classification accuracy of bare-soil brush pixels. Registered pure bare soil pixels that are nearest the border fall in expected recognition accuracy from a near 100% to 0% as misregistration is introduced. In Figure 4.15(c), near the point (1,0) it is interesting to note that only a few percent of these mixtures of misregistered bare-soil brush pixels are recognized as either bare soil or brush. Figure 4.16 indicates that a good percentage of these pixels would be misclassified as corn. Many others were called grass and a very high percentage went unclassified at a 0.001 probability of false rejection.

For one channel of misregistration (Figures 4.17 and 4.18), the expected performance of the bare-soil brush combination was not deleteriously affected. This indicates that a great deal of separation from other ground covers was maintained in spite of misregistration.

The next series of graphs (Figures 4.19 to 4.22) displays the recognition curves of mixtures of corn and bare soil. These indicate a situation for which a single channel misregistered produces a more harmful effect than three misregistered channels. Figure 4.19 (3 channels) in contrast to Figure 4.21 (1 channel) reveals similar expected performance curves for corn mixtures. However, examining Figure 4.19 as the mixtures become more like bare soil and the bare soil classification curve compensates by increasing more rapidly, than since the pixels are more like bare soil in the misregistered channels. However, examining Figure 4.19 as the mixture become more like bare soil the bare soil classification curve increases the proportion of bare soil in the mixture. However, in Figure 4.21 bare soil retains about the same classification rate regardless of the degree of misregistration of the one channel. Comparing the curves of grass false alarms among corn-bare mixtures, a remarkable increase in the false alarm rate for one channel misregistered (Figure 4.22) is noted in comparison to three channels (Figure 4.20). At the high point, one-half pixel misregistration of SDO 12 causes a 42% rate among corn-bare mixtures. At one pixel misregistration, the figures are 58% versus 38%.

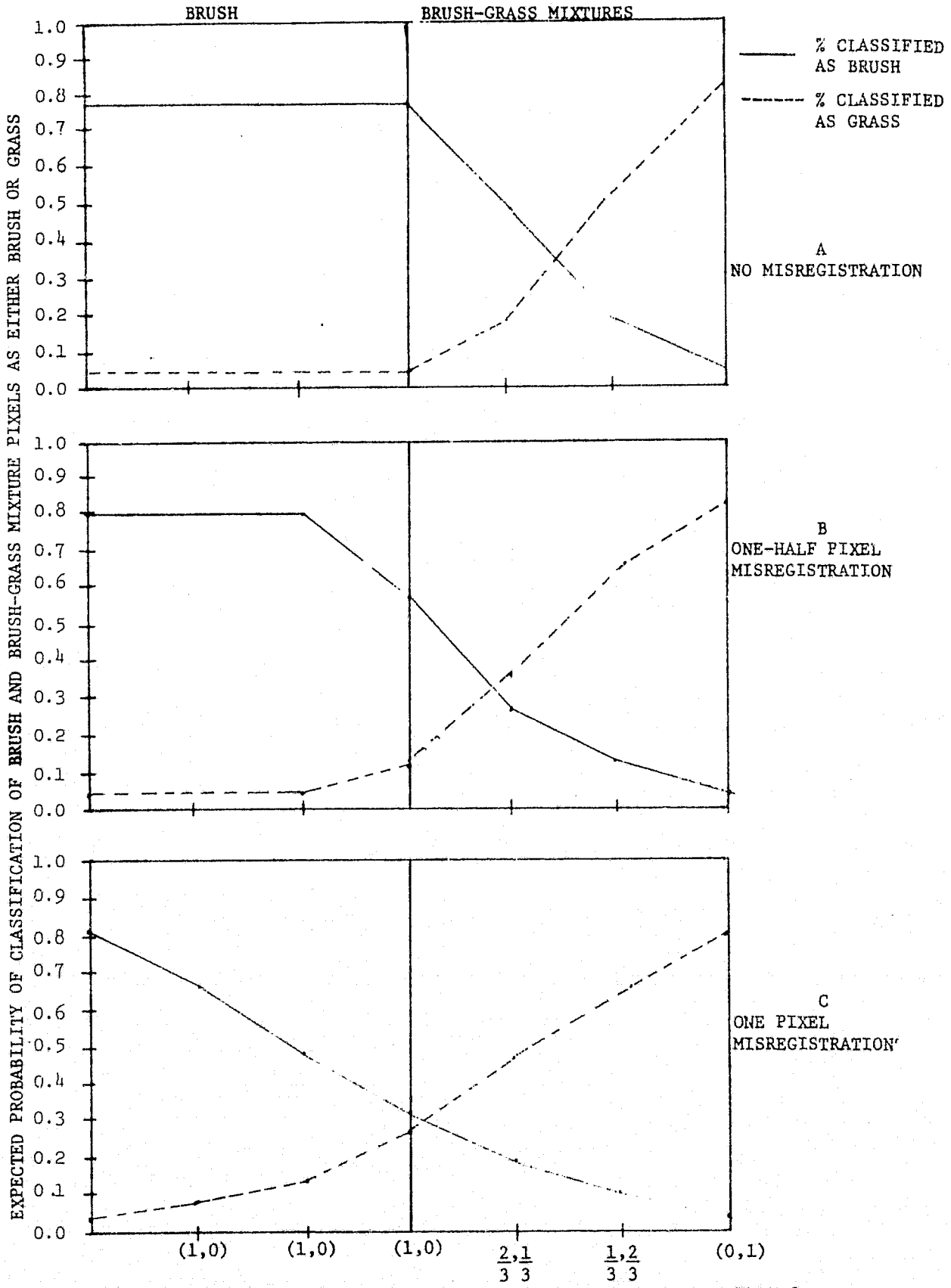

FIGURE 4.11. EXPECTED CLASSIFICATION PERFORMANCE OF BRUSH, BRUSH-GRASS MIXTURE PIXELS. ONE CHANNEL MISREGISTERED.

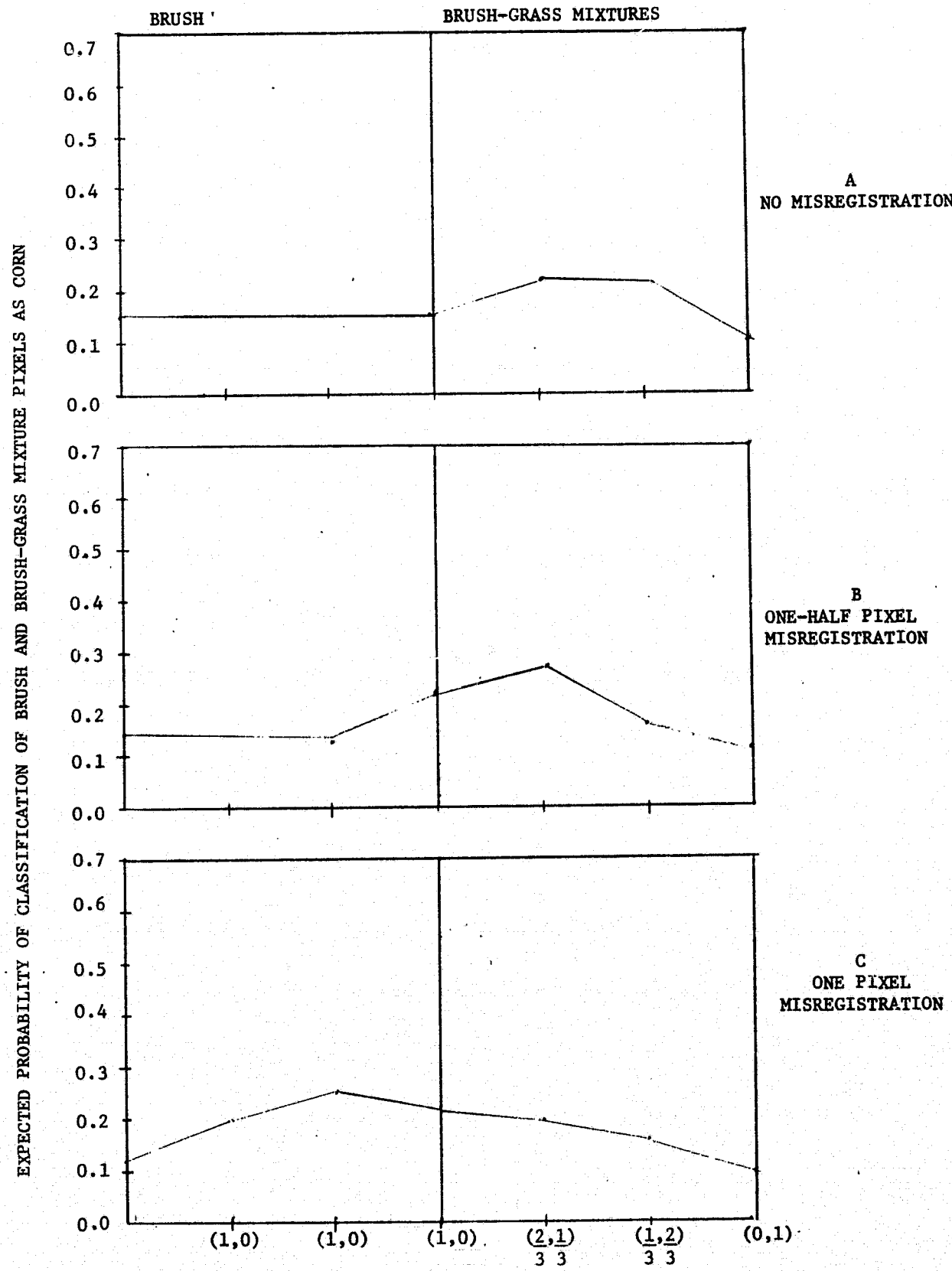

FIGURE 4.12. CORN FALSE ALARMS AMONG BRUSH AND BRUSH-GRASS MIXTURE PIXELS. ONE CHANNEL MISREGISTERED

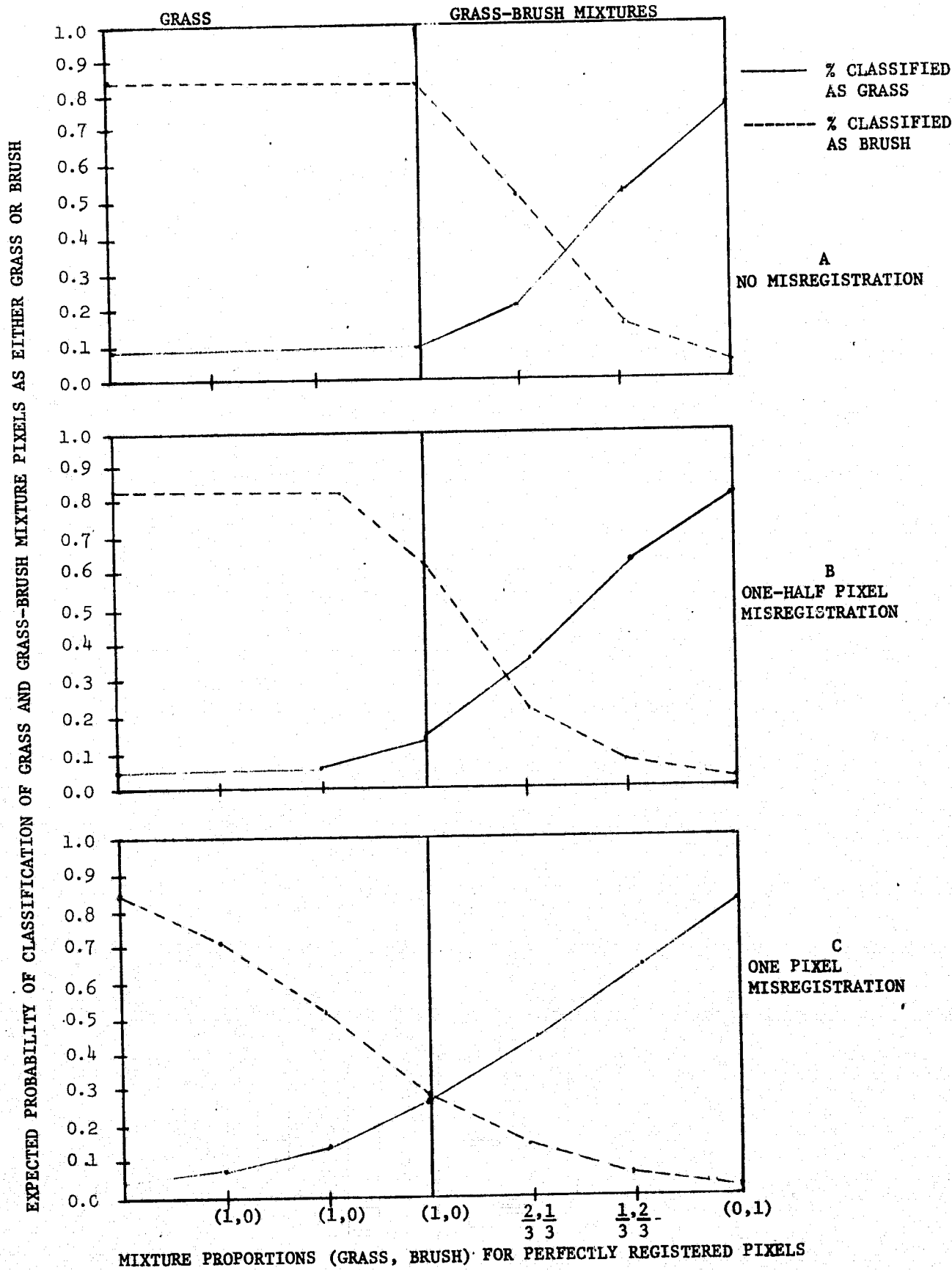

FIGURE 4.13. EXPECTED CLASSIFICATION PERFORMANCE OF GRASS, GRASS-BRUSH MIXTURE PIXELS. ONE CHANNEL MISREGISTERED.

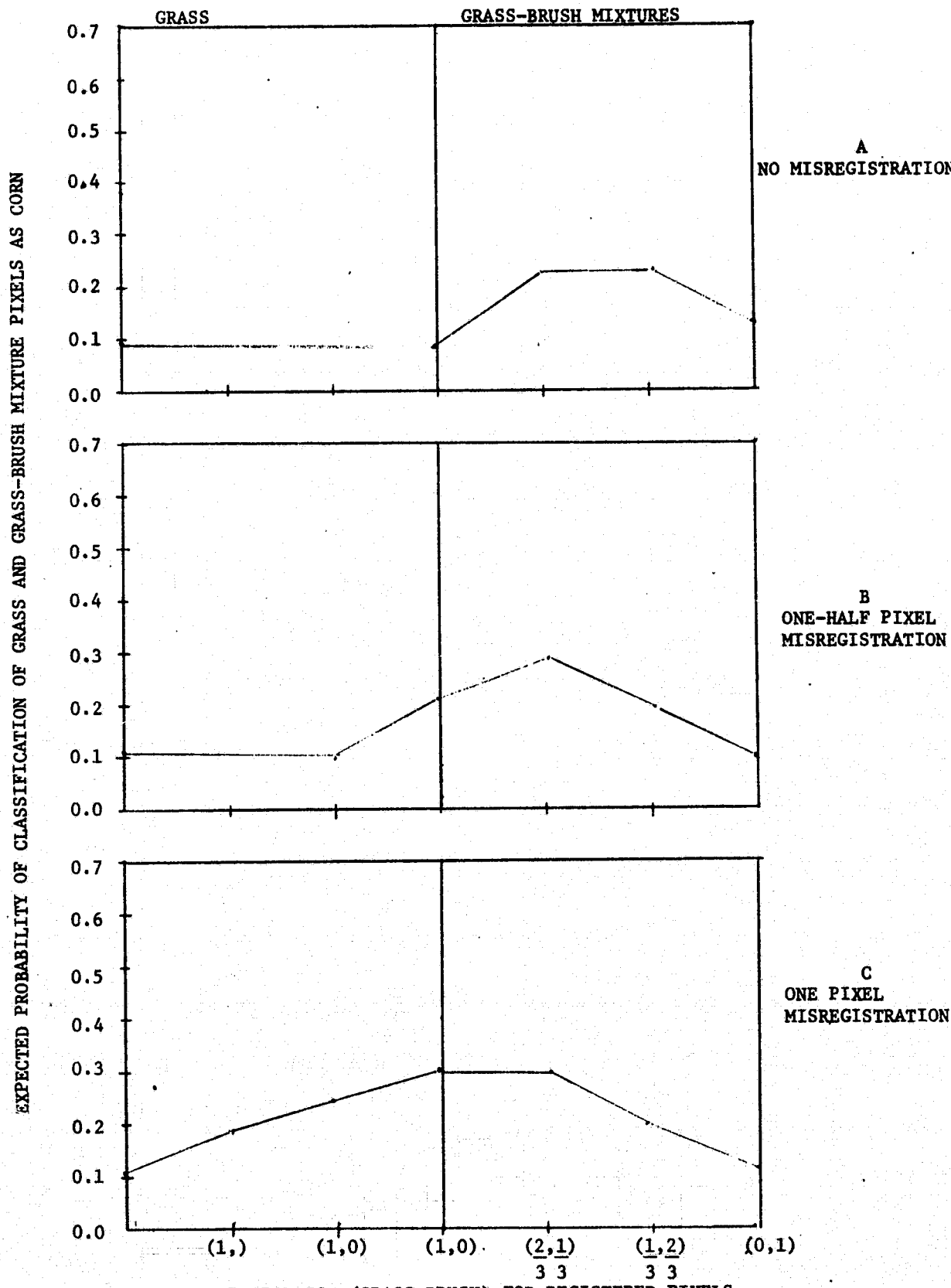

FIGURE 4.14. CORN FALSE ALARMS AMONG GRASS AND GRASS-BRUSH MIXTURE PIXELS. ONE CHANNEL MISREGISTERED.

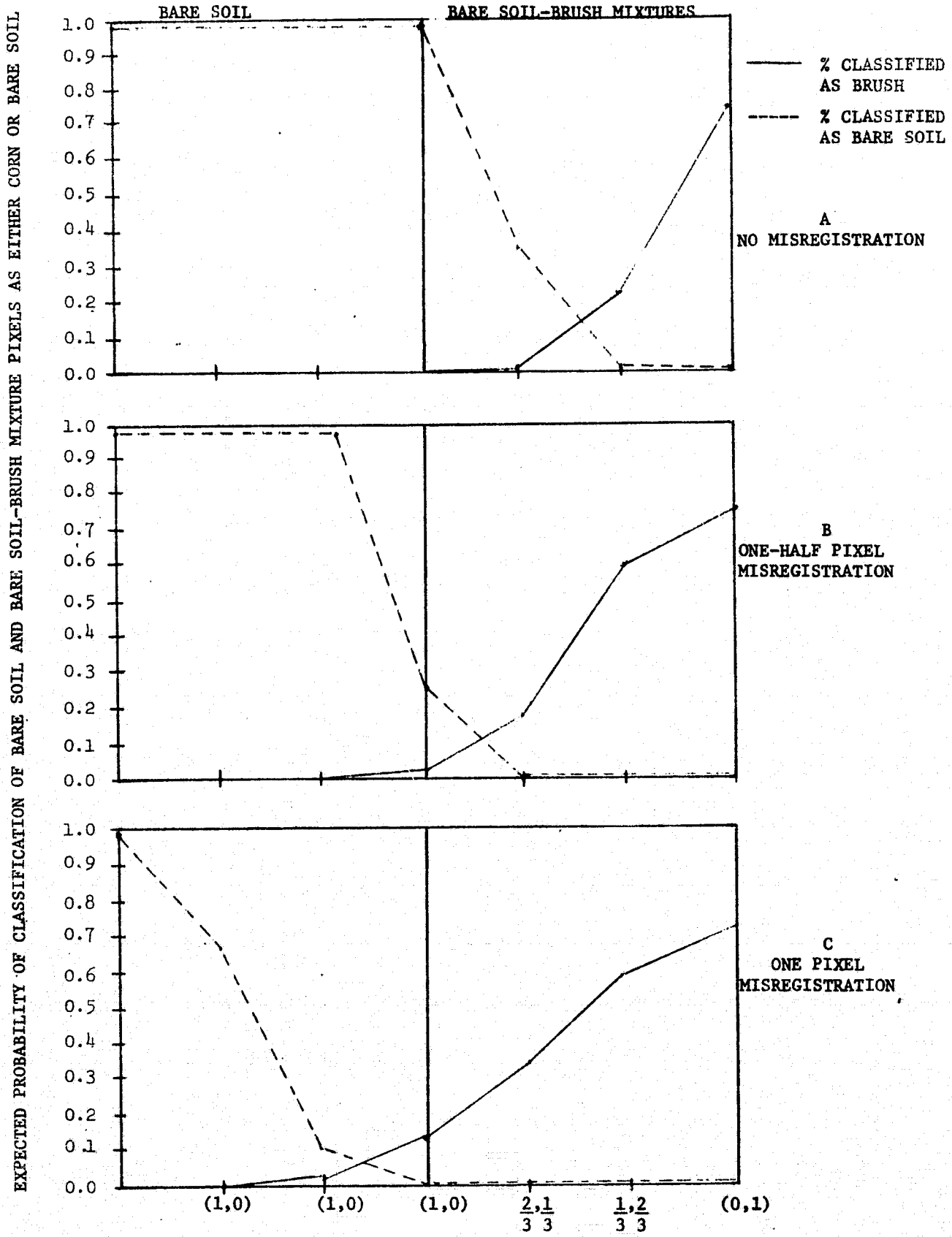

FIGURE 4.15 EXPECTED CLASSIFICATION PERFORMANCE OF BARE SOIL, BARE SOIL-BRUSH MIXTURE PIXELS. THREE CHANNELS MISREGISTERED.

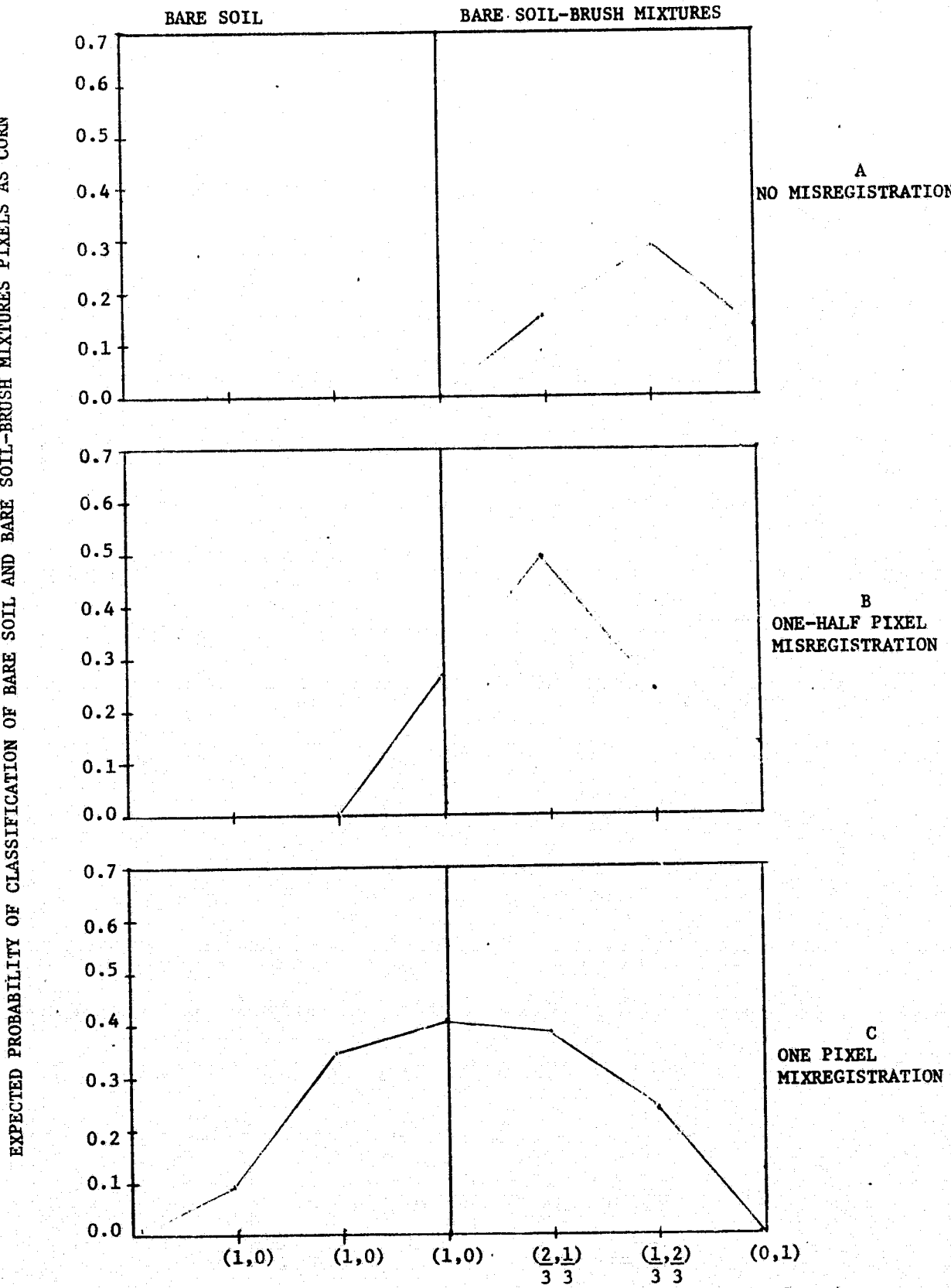

FIGURE 4.16. CORN FALSE ALARMS AMONG BARE SOIL AND BARE SOIL-BRUSH MIXTURE PIXELS. THREE CHANNELS MISREGISTERED

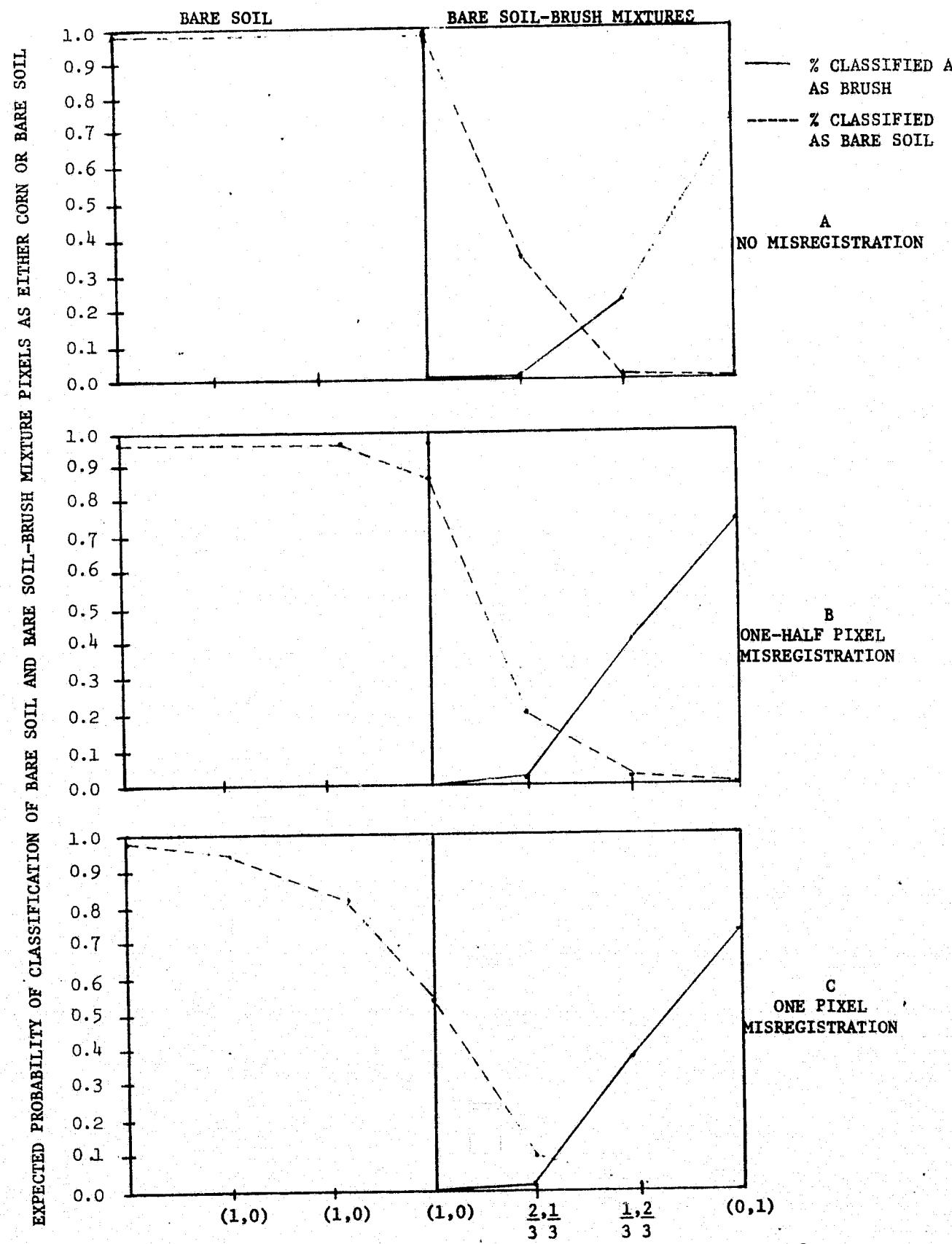

FIGURE 4,17 EXPECTED CLASSIFICATION PERFORMANCE OF BARE SOIL, BARE SOIL-BRUSH MIXTURE PIXELS ONE CHANNEL MISREGISTERED.

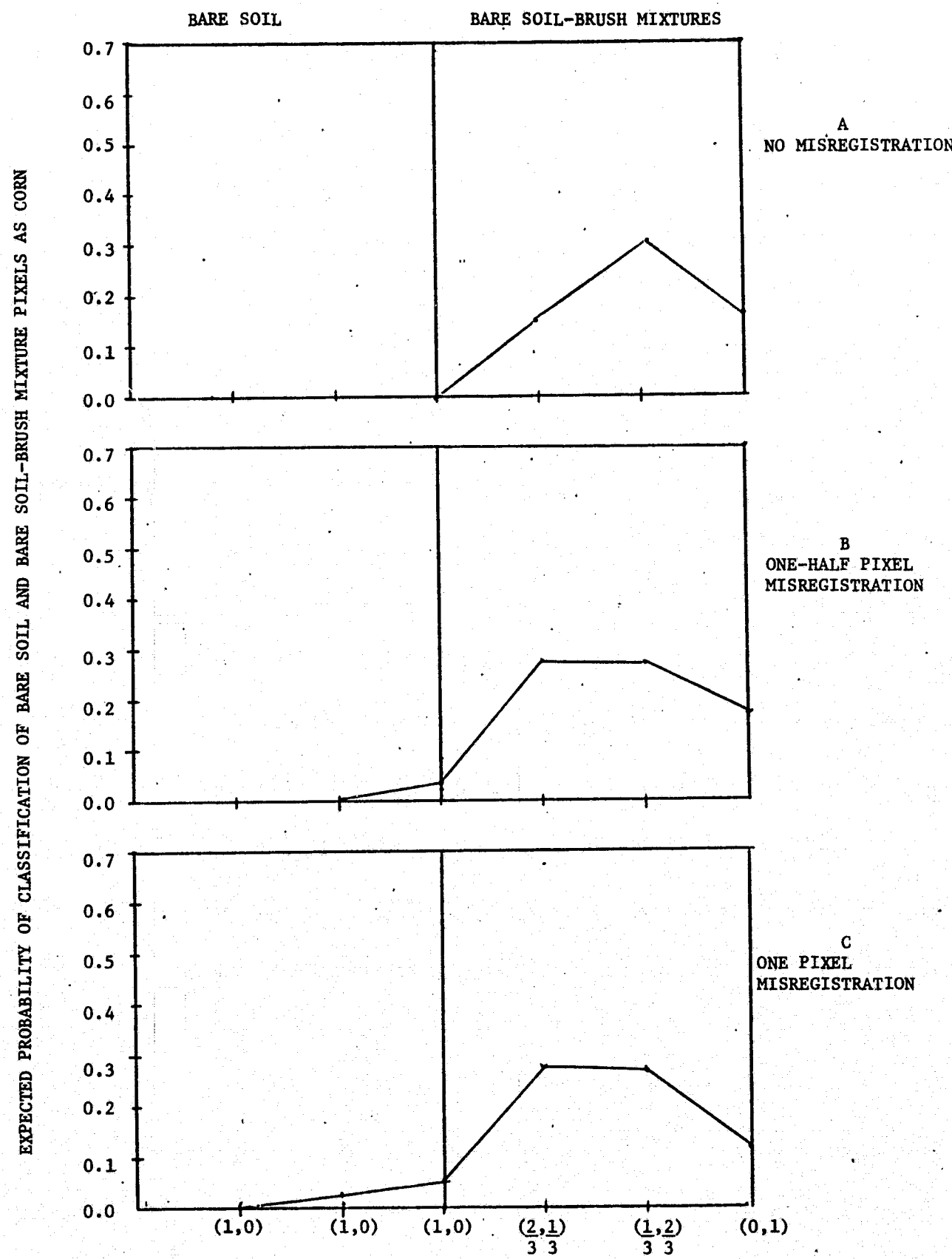

FIGURE 4.18 CORN FALSE ALARMS AMONG BARE SOIL AND BARE SOIL-BRUSH MIXTURE PIXELS. ONE CHANNEL MISREGISTERED 89

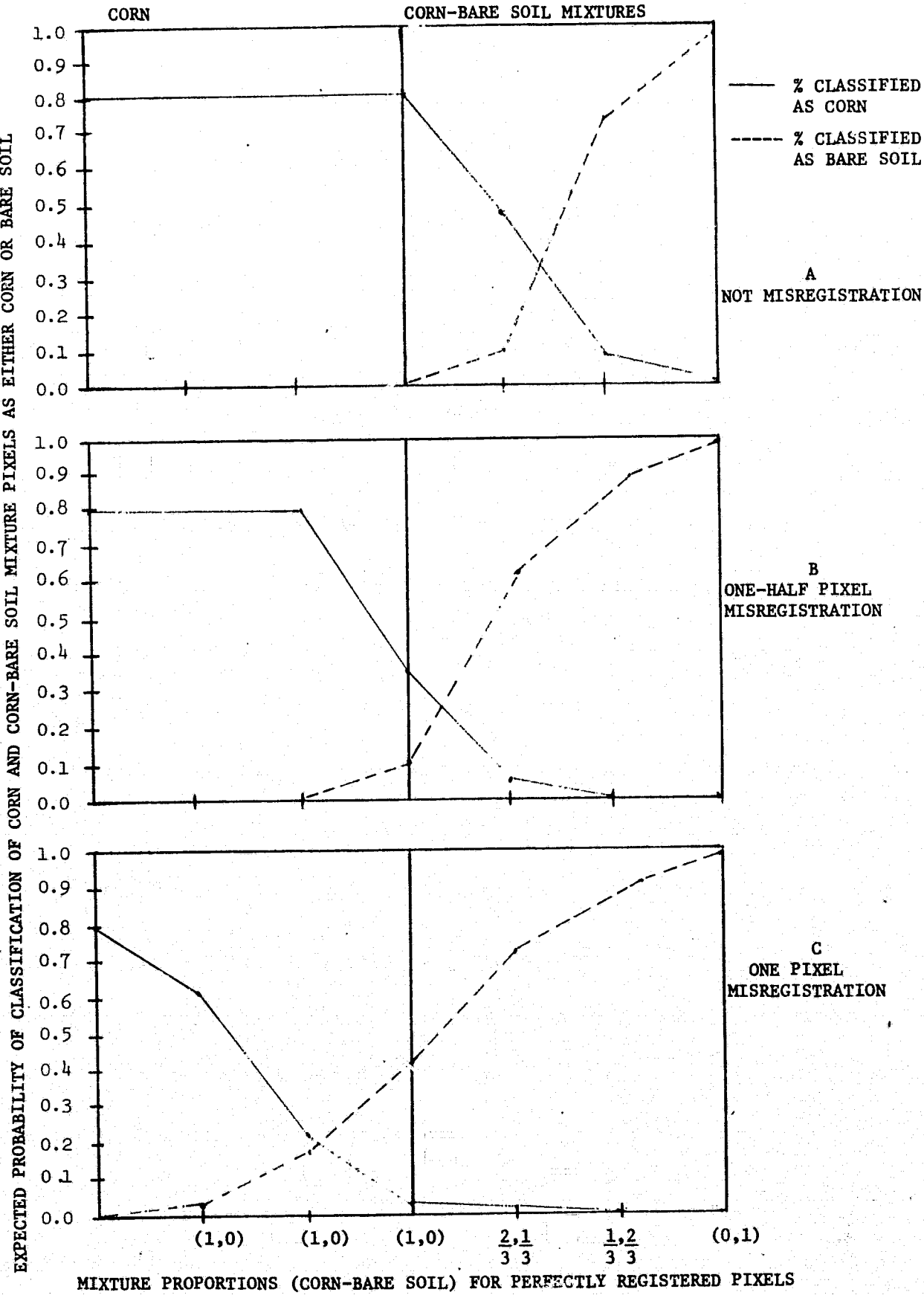

FIGURE 4.19 EXPECTED CLASSIFICATION PERFORMANCE OF CORN, CORN-BARE SOIL MIXTURE PIXELS. THREE CHANNELS MISREGISTERED

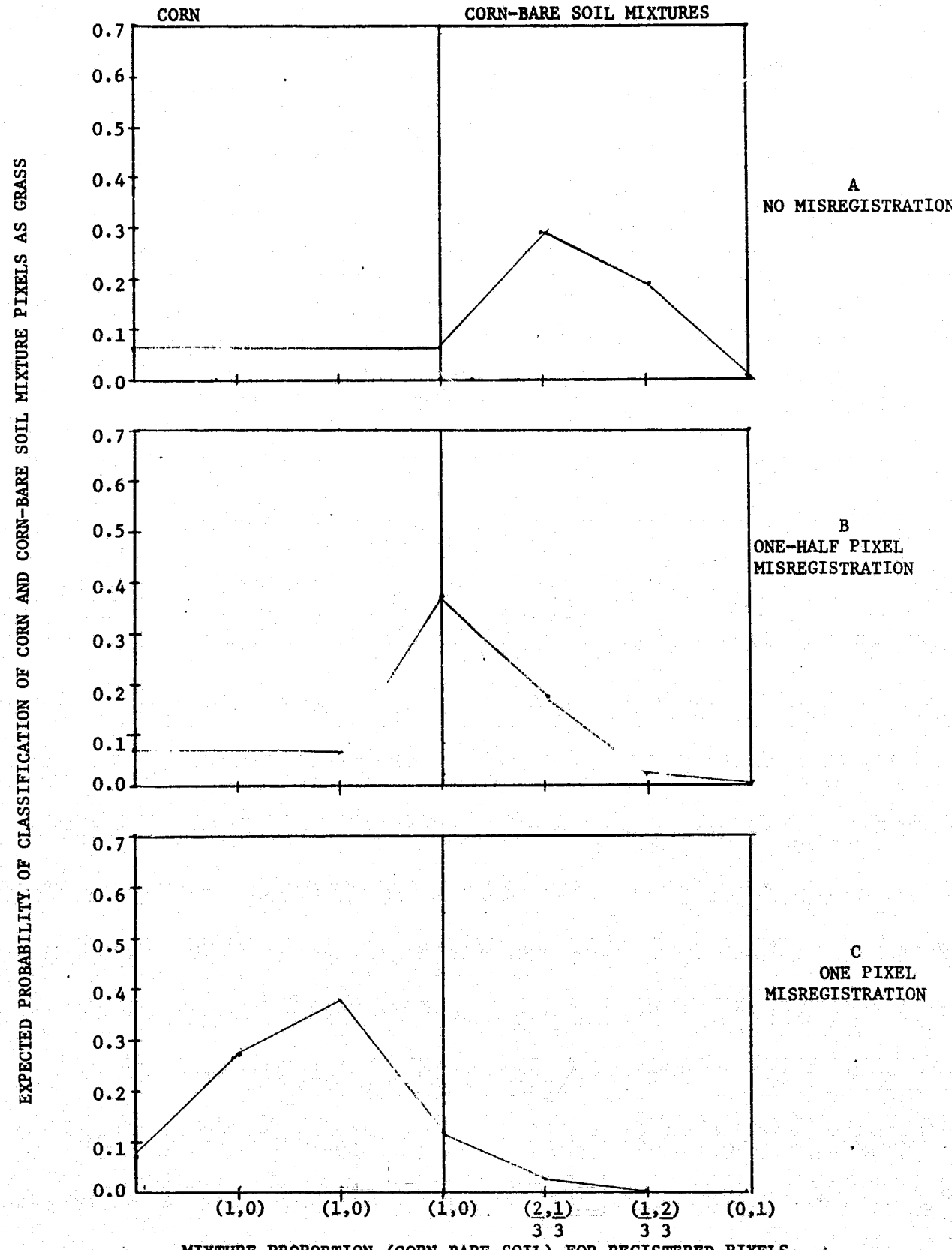

FIGURE 4.20 GRASS FALSE ALARMS AMONG CORN AND CORN-BARE SOIL MIXTURE PIXELS. THREE CHANNELS MISREGISTERED

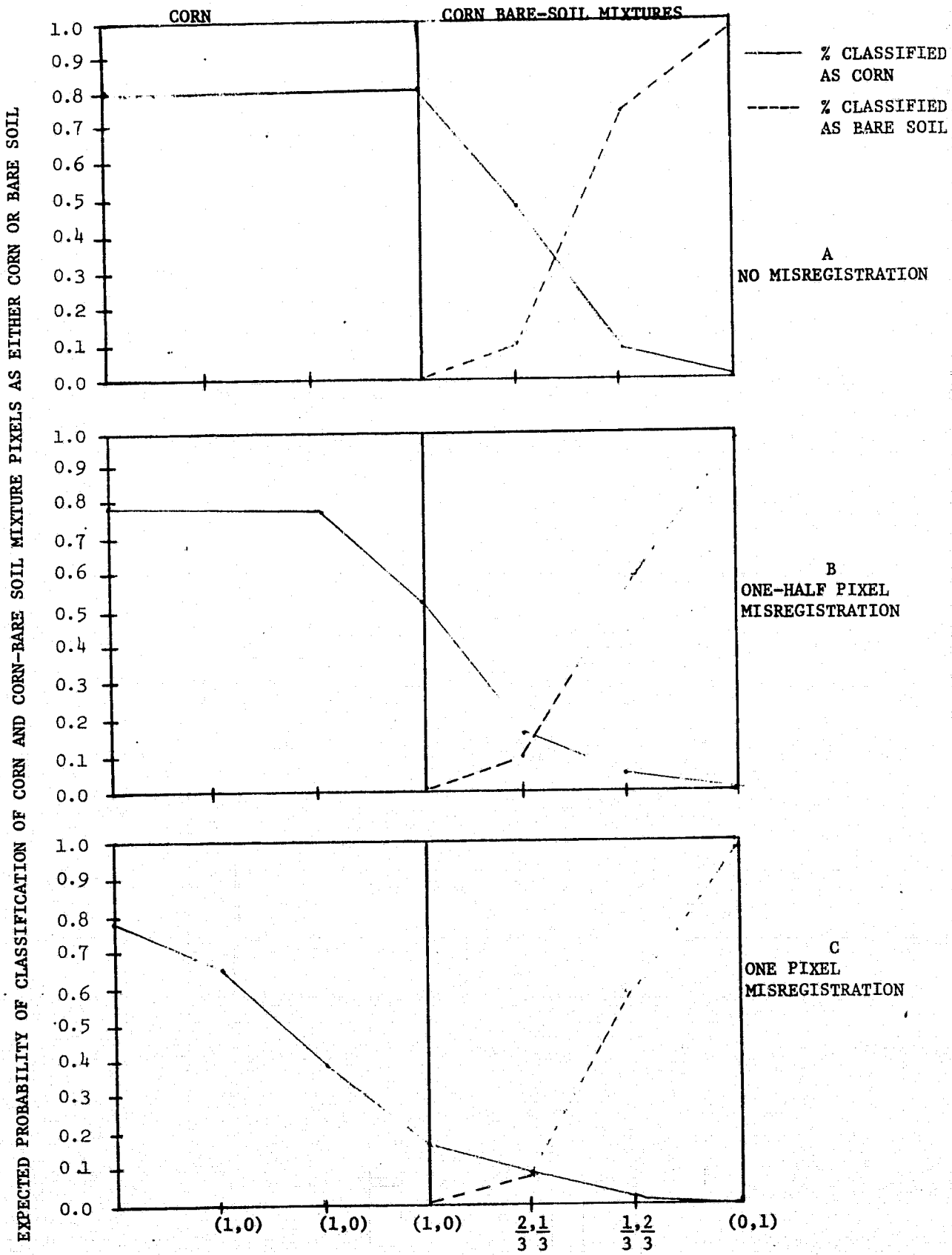

FIGURE 4.21 EXPECTED CLASSIFICATION PERFORMANCE OF CORN, CORN-BARE SOIL MIXTURE PIXELS. ONE CHANNEL MISREGISTERED.

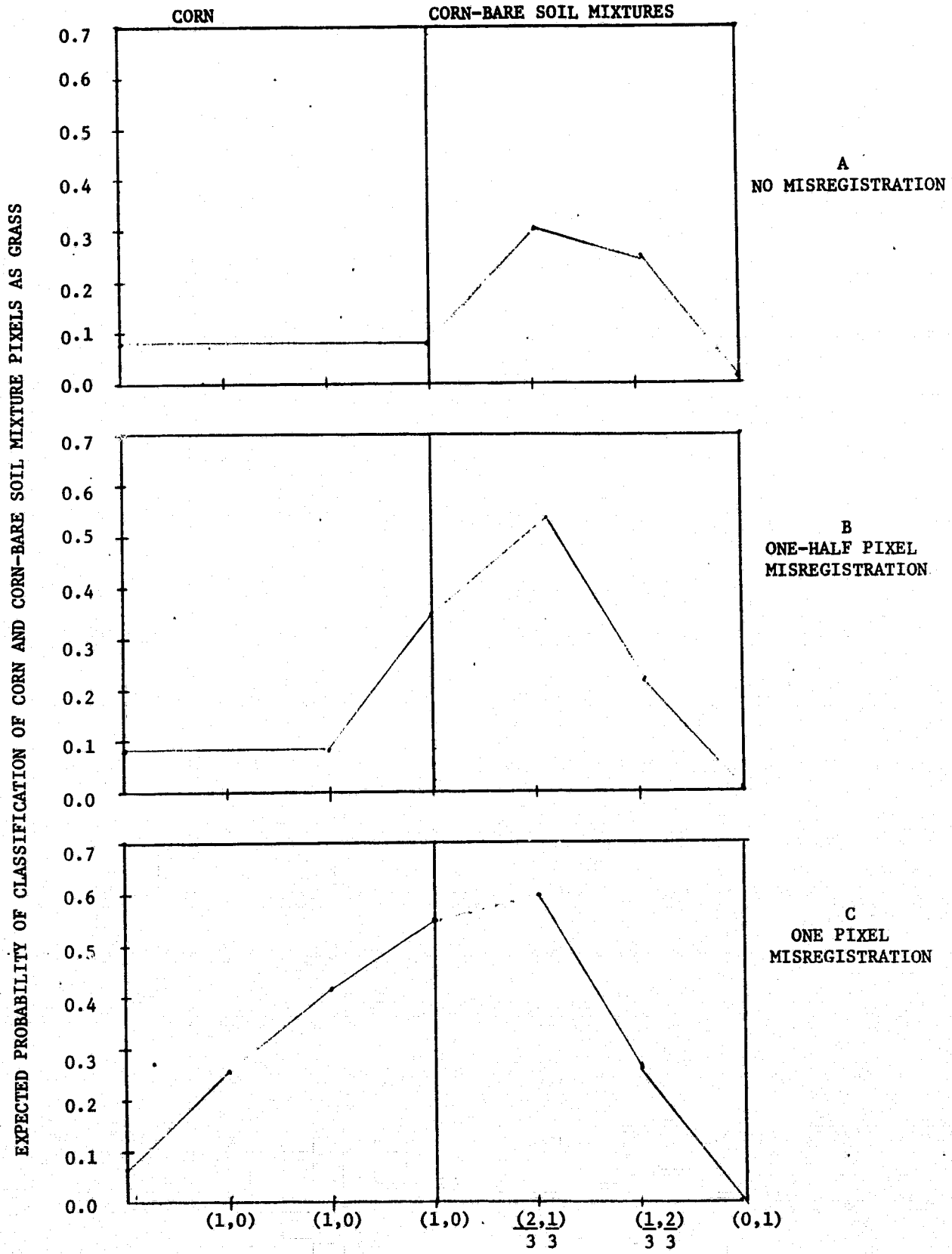

FIGURE 4.22 GRASS FALSE ALARMS AMONG CORN AND CORN-BARE SOIL MIXTURE PIXELS. ONE CHANNEL MISREGISTERED 93

4.4.7 EFFECT OF MISREGISTRATION ON STANDARD PROPORTION ESTIMATION

A question of obvious concern is to what extent proportion estimation is affected by channel-to-channel spatial misregistration. It is argued generally that errors of one kind tend to compensate for errors of another kind; that is, errors are made uniformly in all directions and over a large sample their effects will be cancelled. The surprising corn false alarm rate among registered pixels of brush-grass previously discussed already indicates that the process of proportion estimation is less than an exact science. The increased number of false alarms to be expected with the introduction of misregistration places even more reliance on compensating errors for accurate proportion estimation.

Figure 4.23 is presented to show that the errors introduced are not strictly compensatory for proportion estimation, especially when misregistration is introduced in the scene. Let us focus our attention on the estimation of the proportion of corn. Noting an increased rate of corn false alarms among brush-grass pixels, these would necessarily have to be compensated for by a decrease in the correct classification of corn or mixtures of corn-other pixels (here we use the expression correct classification in the sense that mixtures of two covers A and B are classified as either A or B). Figure 4.23 is a graph of the expected probability of "correct" classification of two ground covers as labelled as a function of the mixture proportion. The solid line indicates the amount of brush-grass correctly classified. With more misregistration there are more false alarms particularly of corn, as previously noted. However the correct classification of corn, corn-grass or corn-brush pixels does not correspondingly decrease, indicating that corn may be overestimated.

4.5 CONCLUSIONS AND RECOMMENDATIONS

Examination of the effects of spatial misregistration on S-192 scanner signals centered upon an examination of expected classification performance for certain degrees of misregistration. In the physical sense, data are affected by misregistration in that the correlation between channels not in registration with respect to one another decreases, and pure field center pixels

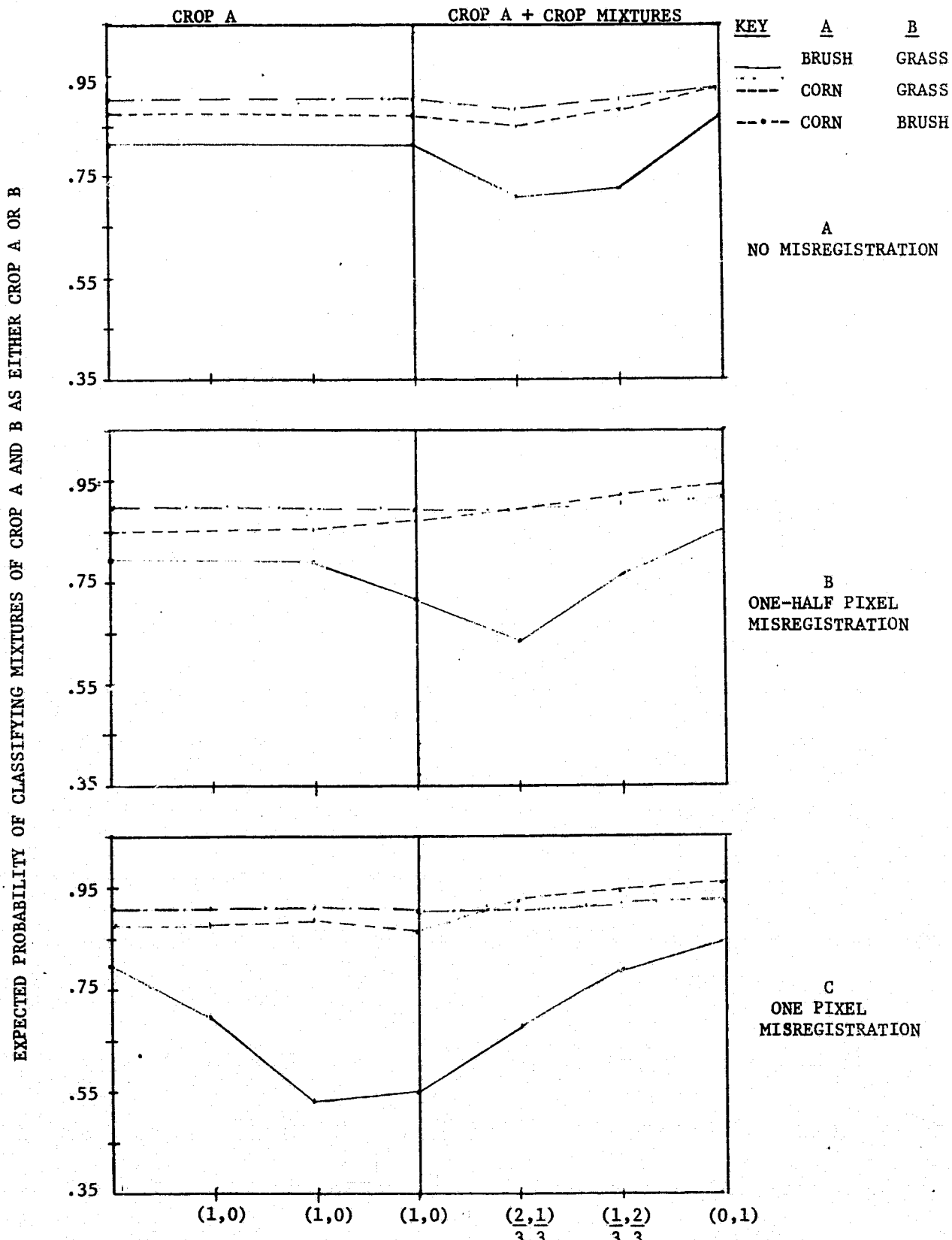

FIGURE 4.23. EXPECTED CLASSIFICATION OF MIXTURE PIXELS OF CROPS 'A' AND 'B' AS EITHER CROP AND OR CROP B

that are near borders of fields may become mixtures in those channels that are misregistered. It is due to these physical affects on the scanner signals that misregistration deleteriously affects recognition performance.

The effects on the classification of field center pixels that remain field center in all channels even after misregistration was found to be insignificant. This conclusion seemed to be independent of the number of channels misregistered.

However, misregistration had serious effects on the correct classification of border and near-border pixels. First it was determined that the availability of pure field center signatures was affected in that fewer pixels are found to be pure ground covers in all channels. This increases the number of pixels that are mixtures of two or more ground covers in some or all bands. Analysis of these mixture pixels led to the conclusions that (1) misregistration increases the error rate in the classification of S-192 data and (2) misregistration increases the false alarm rate. Increases in the false alarm rate of corn and grass were particularly noted. In terms of standard proportion estimation, the availability of fewer field center pixels, coupled with the increased rate of false alarms among mixture pixels greatly increases reliance on the compensation of errors for accurate proportion estimation. The simulation provided evidence, in one case, to indicate that errors were indeed not compensatory. The effect of misregistration as a function of the number of channels misregistered was undetermined. In some cases misregistration of three channels caused more serious effects than the misregistration of one channel. However instances were found to indicate the opposite to be true as well.

Hence, misregistration affects the processing of S-192 or any coarse spatial resolution scanner data in a manner that is not to be taken lightly. Since S-192 conic format data has already been determined to be out of registration to some degree, it would be difficult if not impossible to precisely quantify the extent to which classification accuracy has deteriorated due to the misregistration, however, it has been determined both analytically and empirically, through a simulation of the effects of misregistration, that the extent of the harm done could be significant.

As regards the processing of scan line straightened data, however, it has been shown (section 2.1.4) that the process of scan line straightening increases the misregistration in the data. Thus it is expected that the classification accuracy from processing scan line straightened data would decrease in view of the results of this section. Future scanners and data preparation algorithms and procedures must be designed to take every precaution to minimize channel-to-channel spatial misregistration in order to optimize the conditions under which scene classification and recognition processing are performed.

5
SIGNATURE EXTENSION

5.1 INTRODUCTION

Signature extension is a process by which training statistics from one scene may be modified and then used to classify features in a second scene which differs from the first in geographic location or in the measurement conditions under which the data were collected. This process may also incorporate preprocessing of the data from either or both scenes. The goal of signature extension is to minimize or to eliminate altogether the requirements for collecting ground truth and extracting training statistics for the second scene, thus reducing the costs and time delays associated with those procedures. Signature extension would then help to provide timely and cost-effective classification over extensive land areas, including remote areas for which ground truth information may not be readily available. Testing, evaluation, and further development of signature extension techniques is required to fully realize this goal.

Several signature extension algorithms* were tested on SKYLAB S-192 data collected over Southeastern Michigan. These algorithms and the testing procedure followed are discussed below.

5.2 TRAINING AREA

A portion of SKYLAB Pass 14 (5 August 1973), representing data from an area surrounding East Lansing, Michigan, was chosen for computing training statistics. The atmosphere over the area appeared to be fairly clear, although a bank of clouds was present only five miles northwest of this site. A clustering algorithm [1] was used to compile the training statistics, producing twenty-four signatures, ten of which could be associated with major features within the scene. These associations were determined with the aid of aerial photography and SKYLAB S-190A photography using both color and false color film, since no actual ground observations were performed in the East Lansing area.

---

*These algorithms were developed by ERIM for NASA/JSC under contracts NAS9-14123 and NAS9-9784.

The training statistics were extracted from S-192 data which was in conic format. Although it made the correlation between the cluster classification map and the photographic images more difficult, this data format provided better spatial registration between the spectral bands of the S-192 scanner than would have been obtained with scan-line-straightened data. The seven spectral bands used in the signatures were those chosen as the most optimum for processing the Michigan agricultural test site data, and are listed in Table 5.1.

The ten clusters identified from the training statistics for the East Lansing area appeared to be associated with features in the scene as follows: old residential - long established residential areas made up of closely spaced houses and many mature trees; green sparse vegetation - low density vegetated areas and also forests; green dense vegetation - high reflective vegetated areas such as agricultural fields and lawns (parks); concrete - high reflective areas mostly made up of segments of expressways and parking lots, or a mixture of concrete areas with other bright materials such as rooftops or high reflective soils; wet soil - wet unvegetated agricultural land, also recognized major portions of a residential district with widely spaced houses among mature trees; water - deep water which filled the instantaneous field of view of the scanner; urban - impervious materials such as parking lots and rooftops of large buildings (e.g., stores, warehouses, and factories); high reflective urban - also impervious materials, higher signal levels than urban which may be associated with real scene features or localized differences in the haze layers; dry soil - freshly graded high reflective soil such as gravel or sand; shallow water - a mixture of water and shoreline signatures. These ten signatures were those employed in the test of selected signature extension algorithms, as described in Section 5.3. The other fourteen training cluster signatures classified only a few intermittent pixels within the training area and hence were not used.

TABLE 5.1

SKYLAB S-192 CHANNELS CHOSEN FOR DATA PROCESSING
IN THE TRAINING AREA AND IN THE SIGNATURE EXTENSION AREA

S-192 BAND	WAVELENGTH (μm)	TRAINING AREA SDO #	EXTENSION AREA SDO #
3	.50 - .55	2	1
6	.654 - .734	8	7
7	.770 - .890	10	9
8	.930 - 1.050	19	19
9	1.030 - 1.190	20	20
10	1.150 - 1.280	17	17
11	1.550 - 1.730	12	11

5.3 SIGNATURE EXTENSION AREA

A second portion of SKYLAB Pass 14 (5 August 1973), representing data from a swath running from Ypsilanti, Michigan to the Detroit Metropolitan Airport, west of Detroit, was chosen for testing the signature extension algorithms. This area was located less than sixty miles downtrack from the training area. However, the atmosphere over this scene was noticeably hazy, with some occasional, but small, clouds being present as well. This scene appeared to contain nearly the same proportions of the ten selected training classes as did the training scene.

Haze would be expected to affect the scanner data in the following manner. First there would be an increased additive component of the sensed radiation due to increased path radiance. The effects of increased attenuation by the hazy atmosphere would also affect the radiation, but on balance it is expected that the resultant data values for a class viewed through a hazy atmosphere will be greater than the values for that class when viewed through a clearer atmosphere. The net effect is to reduce the signal contrast in all bands.

The data available for the signature extension area was in scan-line-straightened format, which caused a degradation in the inter-channel spatial registration within this scene relative to the training scene, which was in conic scan format. Although the same spectral bands were used to process this scene, different SDOs (Scientific Data Outputs) were chosen, when available, to maximize the registration between channels (see Table 5.1).

The various processing schemes applied to the signature extension scene are described in the subsections below.

5.3.1 LOCAL CLUSTERING RESULTS

As a prelude to testing the selected signature extension algorithms, the clustering program was run on a subset of data (around Ypsilanti proper) comprising approximately twelve percent of the signature extension area. Although more than twenty clusters were obtained (as in the signature training area), only eight major clusters emerged where each represented more than one percent of the clustered area, and these were not in an exact one-to-one correspondence with those identified in the training area.

The eight clusters selected from the signature extension area statistics appeared to be associated with features in the overall scene as follows: green sparse vegetation - low reflective vegetated areas including forests and some agricultural fields, a slightly more sparse vegetation signature than that obtained from the training area; green dense vegetation - high reflective vegetated areas such as agricultural fields, similar to the corresponding training signature, but encompassing a greater variety of features within the signature extension scene due to the differences in the local sparse vegetation cluster; old residential / urban - included parking lots and sparsely vegetated portions of old residential areas, surrendering the remainder of the old residential areas to either the local urban cluster or the local sparse vegetation cluster; water / residential - a mixture of a water signature with a residential signature: developed areas along lake or river shorelines; water - deep water which filled the instantaneous field of view of the scanner; water / vegetation - a mixture of a water signature with a vegetation signature: vegetated areas along lake or river shorelines; soil - agricultural fields with little or no vegetation and vegetated areas mostly obscured by haze adjacent to the small clouds which were present in the scene, also some concrete; urban / residential - partly vegetated urban and residential areas, mixtures of bright objects (rooftops, concrete) with vegetation. Table 5.3 lists the percentage of the signature extension scene recognized by each local cluster class when these cluster signatures were applied to the total scene.

5.3.2 RESULTS WITH UNALTERED TRAINING SIGNATURES

Since the atmosphere over the signature extension area was much hazier than that over the training area, higher signal levels would be expected and one would expect the classification of the scene using the unaltered training signatures to be biased in favor of the higher reflectance classes. In fact the testing of this arrangement confirmed that expectation, with vegetated areas being classified in favor of the dense vegetation, with water classification

TABLE 5.2

APPROXIMATE PERCENTAGE OF THE TRAINING SCENE COVERED BY EACH TRAINING CLASS

TRAINING CLUSTER #	CLUSTER IDENTIFICATION	TRAINING AREA PERCENTAGE (50250 PIXELS)
2	old residential	10.7
3	green sparse vegetation	37.2
4	green dense vegetation	14.8
6	concrete	6.2
8	wet soil	9.0
13	water	0.7
14	urban	10.8
17	high reflective urban	8.2
18	dry soil	1.2
20	shallow water	1.2
	unclassified	0.1

TABLE 5.3

APPROXIMATE PERCENTAGE OF THE SIGNATURE EXTENSION SCENE COVERED BY EACH LOCAL CLUSTER CLASS

EXTENSION CLUSTER #	CLUSTER IDENTIFICATION	EXTENSION AREA PERCENTAGE (85250 PIXELS
1	green sparse vegetation	43.4
4	green dense vegetation	19.1
6	old residential / urban	1.9
9	water / residential	0.6
11	water	0.9
14	water / vegetation	0.9
17	soil	12.7
23	urban / residential	19.5
	unclassified	1.0

biased in favor of shallow water recognition and with urban signatures dominating over residential signatures. In addition, especially hazy areas, some bright urban or residential areas, and some areas of concrete were recognized by the dry soil signature. The percentage of the signature extension scene recognized as each training class, using unaltered signatures, is listed in Table 5.4 together with the corresponding percentages recognized after applying each of the signature extension techniques discussed below.

5.3.3 RESULTS WITH DARK OBJECT ADDITIVE SIGNATURE CORRECTION

The dark object signature correction [11] assumes, channel-by-channel, that the signal levels generated by dark objects (objects of low reflectance and/or low irradiance) represent path radiance and therefore provide a means to estimate an additive correction to the mean levels of each training signature in each channel. In an attempt to avoid using correlations between spurious or anomalous low signal levels, the low end of the histogram continuum is judged to be the most appropriate reference point for the algorithm. Since spurious or anomalous gaps in the histogram continuum are also possible artifacts of any scene, this algorithm is not by any means foolproof. The algorithm also provides only an additive signature correction, whereas it is known from study of mathematical models for signature variations that a multiplicative signature correction would be desireable as well.

Table 5.5 lists the additive changes to the training signature means which were determined by the dark object signature extension algorithm. Also listed are the corresponding training signature changes resulting from the other algorithms discussed below. Note that the dark object algorithm generated larger corrections (in counts) for the shorter than for the longer wavelength bands, as might be expected from the physical cause of the differences between the training and signature extension scenes (i.e. haze).

The percentage of the signature extension scene recognized as each training class, after application of the dark object algorithm, is listed in Table 5.4. These results may be compared to the local cluster classification results

TABLE 5.4

PERCENTAGE OF THE SIGNATURE EXTENSION SCENE
CLASSIFIED AS EACH TRAINING CLASS

TRAINING CLUSTER #	CLUST CLUSTER IDENTIFICATION	UNALTERED SIGNATURES	DARK OBJECT CORRECTION	MEAN LEVEL CORRECTION	MASC
2	old residential	2.1	3.9	8.8	1.0
3	green sparse vegetation	29.3	44.3	43.2	25.3
4	green dense vegetation	31.9	20.0	8.9	25.7
6	concrete	10.0	3.6	4.4	16.3
8	wet soil	0.2	5.6	7.5	1.2
13	water	0.4	1.4	1.5	0.2
14	urban	4.6	4.9	12.3	2.7
17	high reflective urban	4.7	11.8	9.4	3.9
18	dry soil	14.7	3.2	2.5	21.3
20	shallow water	1.7	0.8	1.1	1.6
	unclassified	0.5	0.5	0.5	0.7

TABLE 5.5

SIGNATURE CORRECTIONS DETERMINED BY EACH SIGNATURE EXTENSION ALGORITHM (IN COUNTS)

S-192 BAND #	WAVELENGTH (μm)	DARK OBJECT CORRECTION (ADDITIVE)	MEAN LEVEL CORRECTION (ADDITIVE)	MASC (ADDITIVE)	MASC (MULT.)
3	.50 - .55	9	9.07	40.87	.529
6	.654 - .734	9	8.94	19.63	.741
7	.770 - .890	10	11.32	-10.16	1.195
8	.930 - 1.050	3	9.75	-11.70	1.146
9	1.030 - 1.190	5	8.12	-17.15	1.217
10	1.150 - 1.280	-1	7.48	- 8.20	1.081
11	1.550 - 1.730	0	- .15	- 1.16	.862

listed in Table 5.3, bearing in mind that some of the local cluster categories do not correspond exactly to the training cluster categories. Classification maps also were generated and were compared with aerial photography. Generally the dark object classification of the signature extension scene was judged to be a dramatic improvement over classification with unaltered training signatures, although there was evidence that the algorithm over-corrected for the differences between the training and signature extension scenes. In particular the recognition where the haze was densest was unexpectedly accurate, while in areas where the haze density was closer to the average for the scene there was a tendency to classify some urban areas as old residential areas and to classify marginal concrete areas as urban. Water recognition, however, was accurate. This tendency to misclassify bright features as darker features while correctly classifying the darkest features correlates with the effect of excluding a multiplicative signature correction for the effect of the haze.

5.3.4 RESULTS WITH MEAN LEVEL ADJUSTMENT SIGNATURE CORRECTION

The mean level adjustment algorithm [12] utilizes the correlation between averages over portions of the training scene and the signature extension scene to estimate a correction to the mean levels of each training signature in each channel an additive correction in this case. Alternatively, a purely multiplicative correction could be estimated; however in this experiment the difference between the training and signature extension scenes (hazy density) would be expected to produce a mostly additive effect. The algorithm requires that the portions of the two scenes whose averages are to be compared be of similar composition (i.e., contain similar percentages of each ground cover). Table 5.2 lists the approximate percentage present of each training class in the portion of the training scene which was averaged for this algorithm, while Table 5.3 lists the percentage for each local cluster class in the portion averaged from the signature extension scene. Although differences between local cluster categories and training cluster categories prevent a complete comparison between the data

in these tables, a general similarity between the two scenes is evident. Close inspection of the false color IR photography for these two areas revealed that some of the dissimilarities tended to balance each other, but that the signature extension scene appeared to have a slightly greater percentage, overall, of brighter features.

Since implementation of the mean level adjustment algorithm, like the dark object algorithm, provided only an additive signature correction, it might be expected to be only partially effective in general. In this particular application it was judged to be only slightly less effective than the dark object algorithm, with its results a bit more biased toward over-correction of the difference between the training and signature extension scenes. The bias toward bright features in the average over the signature extension scene apparently led to a mean level signature correction which biased the modified training signatures in favor of less bright materials.

The additive signature corrections generated by the mean level adjustment algorithm are listed in Table 5.5. Note that the corrections for the shorter wavelength bands are nearly the same, overall, as those for the longer wavelength bands. Of course the relationship between counts and radiance is not being considered here, as perhaps it should be, however the difference between the mean level adjustment classification results and the dark object results lies mostly in the treatment of the longer wavelength bands. It appears that this difference reflects the fact that the mean level adjustment results are slightly more biased in favor of darker materials and that the longer wavelength bands show more contrast between the features of the scene than do the shorter wavelength bands.

5.3.5 RESULTS WITH MASC

The Multiplicative and Additive Signature Correction (MASC) [11] employs a least squares regression to match training cluster mean signal levels with local cluster mean levels, based on the ordering and spacing of those signature means within a chosen data channel. The data channel selected for comparing the

ordering and spacing of the clusters within the two signature data sets is used to define exclusive paired matches between training clusters and local clusters. Extra clusters are discarded from the larger cluster set so that the obtainable matching between the remaining clusters is maximized. This matching is achieved by a least squares determination of appropriate multiplicative and additive coefficients in each data channel. Mathematical models of expected signature variations (changes in the atmosphere, in the illumination of the scene, and in the scanner responsivity) predict that these variations should be both multiplicative and additive, hence a proper association between clusters of the training data set and clusters of the local data set should produce a realistic signature correction from the MASC algorithm.

The MASC algorithm was implemented using the 10 Lansing area clusters and the eight test area clusters previously mentioned. Table 5.6 lists the cluster associations determined by the MASC algorithm, based on using S-192 Band #11 (1.550-1.730 μm) to order the clusters. This band was chosen for the cluster ordering because it had been determined to be the single most useful band for classifying the Michigan agricultural test site data. Note that the cluster pairings obtained are not optimum. This appears to have occurred because one band does not adequately separate all classes; a minimum of two channels would have been needed in this case to achieve an unambiguous separation of the cluster classes. Another aspect of this data set was that there was not a good one-to-one correspondence between the clusters in the training and signature extension data sets. The multiplicative and additive coefficients determined for this cluster pairing arrangement are listed in Table 5.5.

In order to facilitate a comparison between the MASC coefficients and the purely additive coefficients of the dark object and mean level adjustment algorithms, Table 5.7 has been generated. The additive coefficients listed in Table 5.7 represent the change in the signatures for the darkest material (water) and for the brightest material (dry soil) that result from applying the multiplicative and additive coefficients of MASC. These may be compared with

TABLE 5.6

TRAINING AREA AND SIGNATURE EXTENSION AREA CLUSTER ASSOCIATIONS SELECTED AND OPTIMIZED BY THE MASC ALGORITHM

Training Cluster #	Training Cluster Identification	Local Cluster #	MASC Associated Cluster
2	old residential	6	old residential / urban
3	green sparse vegetation		
4	green dense vegetation	4	green dense vegetation
6	concrete	23	urban / residential
8	wet soil	9	water / residential
13	water	11	water
14	urban		
17	high reflective urban	1	green sparse vegetation
18	dry soil	17	soil
20	shallow water	14	water / vegetation

TABLE 5.7

EQUIVALENT PURELY ADDITIVE CHANGES TO SIGNATURE MEANS OF WATER AND DRY SOIL TRAINING CLASSES

(IN COUNTS)

S-192 Band #	Wavelength (μm)	Water Training Signature		Dry Soil Training Signature	
		Unaltered Mean Value	MASC Equivalent Change	Unaltered Mean Value	MASC Equivalent Change
3	.50 - .55	55.99	14.52	79.16	3.62
6	.654 - .734	41.42	8.88	102.39	-6.94
7	.770 - .890	24.64	-5.36	79.68	5.37
8	.930 - 1.050	26.43	-7.85	93.42	1.92
9	1.030 - 1.190	25.08	-11.70	90.55	2.54
10	1.150 - 1.280	21.01	-6.49	92.24	-.70
11	1.550 - 1.730	13.66	-3.04	76.97	-11.76

the coefficients for the dark object and mean level adjustment algorithms which are listed in Table 5.5. It should be noted that the variance and covariance values of the signatures were also affected by the multiplicative coefficient in this application of MASC.

Note in Table 5.6 that the association of the concrete and high reflective urban training clusters with lower reflectance local clusters (urban / residential and green sparse vegetation, respectively) would tend to bias this MASC classification of the signature extension scene toward brighter materials. In fact such a bias was observed, with deep water areas mostly classified as shallow water, with residential areas classified as urban, and with urban areas recognized by the concrete signature. This bias in the recognition is indicated by the small positive or sometimes negative equivalent additive changes in the signature means for the longer wavelength bands, listed in Table 5.7. This result actually represented a small step backward from using the training signatures without alterations.

It appears that further algorithm development, addition of some safeguards against misassociation of clusters, and/or some intervention by the analyst are required for the MASC algorithm to realize its full potential. Some specific recommendations for improving the MASC algorithm, based on its observed performance with this data set, are discussed in Section 5.3.7.

5.3.6 RESULTS WITH ADAPTIVE PROCESSING

Adaptive processing [13] using a decision-directed Kalman filter, was also tested on the S-192 data set by generating recognition maps from local cluster signatures and from MASC signatures, but no noticeable improvement in the classification of the scene was observed. It appears that the variations in the density of the haze over the signature extension scene were sufficiently localized so that a rate of signature adaptation which would be able to correct for the haze adjacent to a small cloud would also react to local changes in the material composition of the scene, leading either to signature capture or to localized biases in the classification. It seems that in order for adaptive

processing to improve upon results obtained from conventional techniques, the signature variations should occur on a scale in time or space which is noticeably greater than the scale of localized changes in scene composition.

5.3.7 COMPARISON OF RESULTS

Of the signature extension techniques tested on this S-192 data set, the dark object correction appeared to do surprisingly well, with the mean level adjustment additive correction being a not-too-distant second best. MASC, on the other hand, did not do as well as expected, even less well than using training signatures without any alterations. Although these results run somewhat contrary to recent experiences [11] with some LANDSAT data sets, this surprise serves to bring out more clearly perhaps some of the advantages, disadvantages, and needs for improvement in these algorithms. Some specific observations in this regard are discussed below.

The surprisingly good performance of the dark object algorithm with the chosen S-192 data set may have been aided by the nature of the difference between the training scene and the signature extension scene (i.e., atmospheric haze) which might have caused a change in the signal levels which was mostly additive. This suggests that the cause of the signal change from one scene to another is a consideration in selecting an optimum signature extension algorithm for a particular application.

The mean level adjustment signature correction algorithm requires that the training scene and the signature extension scene be similar in composition of classes. Apparently, in this S-192 data set the training and signature extension scenes were sufficiently similar so that, with the differences between the two scenes being mostly additive, relatively good classification of the signature extension area was obtained. The requirement for statistical similarity between scenes, however, may be too restrictive for similar good results to be expected in other applications of the algorithm.

MASC, although in this instance, performing poorly, potentially is the most powerful of those techniques tested with this S-192 data set. It provides for both an additive and a multiplicative correction in each channel of each signature and does not require the degree of statistical similarity between scenes that is needed for the mean level adjustment algorithm. However, it does require that the clusters obtained from each of the scenes represent similar classes. The disappointing performance of the MASC algorithm used with this S-192 data set appears to have been caused by its only partial capability to identify and avoid the prejudicial effects of anomalous clusters (those without counterparts in the other cluster set). Since clustering algorithms probably cannot be expected to produce sets of signatures from two different scenes which are in a close one-to-one correspondence, some method is needed to identify non-correlating clusters and to edit them out of the cluster matching procedure which is the groundwork for calculating the signature corrections. This editing process could be aided by including more than one data channel in the cluster matching algorithm. Using more than one data channel would also help to increase accuracy in identifying the proper pairing between the clusters that remained.

Adaptive processing improves performance only when gradual changes of the measurement conditions occurs over a scene. Also, there probably is a tendency, when choosing test cases for signature extension, to select training and extension data sets over which the measurement conditions are fairly uniform, in order to better assess the performance of the non-adaptive signature extension algorithms. Such test cases might use adaptive processing as merely a way to perform a fine-tuning adjustment on the extended signatures. In the present instance, localized variations in the haze density over the signature extension scene caused too much variability for adaptation, to properly establish such a fine-tuning adjustment in time to affect the classification over the most important part of the signature extension scene (i.e., the beginning), while a more rapid rate of adaptation led to signature capture.

In summary, although the dark object signature correction appeared to do the best with this S-192 data set, it is believed that, among the signature extension algorithms tested, MASC has the most ability to improve and to grow to produce the best performance in the long run. Following original development of MASC, improvements and modifications to the basic approach are being pursued at ERIM as well as at other institutions.

6

MIXTURES AND SUBRESOLUTION ELEMENT PROCESSING

When a spatial resolution element overlaps the boundary between two or more ground classes, the radiation detected will be a mixture from the classes involved. The spatial resolution of the SKYLAB S-192 scanner is such that compared to the size of the fields or areas of the ground cover classes, the frequency of mixture pixels is fairly large. An analysis of this effect for an agricultural site is presented in 6.1 below. Further, situations arise where the classes of interest are smaller than the system's resolution. The use of conventional multispectral processing techniques on mixture pixels, will likely result in the improper classification of these pixels. If the number of mixture pixels in the data is large, processing errors can be expected to be numerous as well. In cases where the objects of interest are too small to be resolved, standard processing would be incapable of proper classification for that class.

Processing a sizable number of mixture pixels using conventional processing techniques has a major impact on the accurate estimation of proportions or acreages of classes in the scene. Such processing techniques rely on compensating errors to cancel the measureable effects of misclassifications or on some fixed bias in the estimate to produce accurate proportion estimates. That misclassification errors do not compensate is shown, in Section 6.1 below, by means of the same simulation techniques previously described in Section 4.

For the past several years ERIM has been developing special processing techniques* [14, 15, 10] to handle such situations. In this section we present the results of two studies where mixtures processing was applied to S-192 data. As previously mentioned, two processing studies had been carried out on the S-192 data: The first being for the agricultural test site, and the second being for the urban and suburban areas around Lansing, Michigan. For the agricultural area, the use of mixture processing techniques was used to try to better estimate the proportion of the classes of interest in the

*The development of these techniques has been supported by NASA/JSC under contracts NAS9-9784 and NAS9-14123.

scene. The second study utilized mixtures processing techniques to estimate the proportion of vegetative matter in an urban scene. Discussions of these studies are presented in Sections 6.3 and 6.4, respectively.

6.1 IMPACT OF MIXTURE PIXELS ON PROPORTION ESTIMATION

In assessing the impact of the standard processing of mixture pixels on proportion estimation, a first consideration is the proportion of the pixels in the scene which are mixture pixels. This information would give an indication as to the severity of the problem -- the larger the proportion of mixture pixels, the greater the likely impact on proportion estimation. Earlier in this report we addressed the problem of locating pure field center pixels and noted the substantial number of border pixels for just the larger fields in the agricultural test site.

To more directly assess the number of mixture pixels in the scene, one section (1 mile square) of the agricultural test site was selected; field boundaries for all fields were drawn on a map and the number of pure pixels and mixture pixels were counted. In the counting procedure, pixels were deemed to be field center if their edges were more than .3 pixel from a boundary in the scan (points) direction and more than .1 pixel in the along track (lines) direction, thus accounting for the effects of resolution element size and the misregistration of the bands.

Section 109, the section selected, was chosen because it had the same number of fields and about the same number of acres as the average over sections: 31 fields, 616 acres. The map displaying the fields and pixels is shown in Figure 6.1. As noted, out of a total 514 pixels, only 152 or 30% of them were pure field center pixels and the other 362 or 70% were mixture pixels. Furthermore, it seemed from the analysis that if the data had been perfectly registered, the number of mixture pixels would not have been significantly reduced. Thus it can be safely concluded that the majority of pixels being considered in this agricultural scene are mixture and not field center pixels.

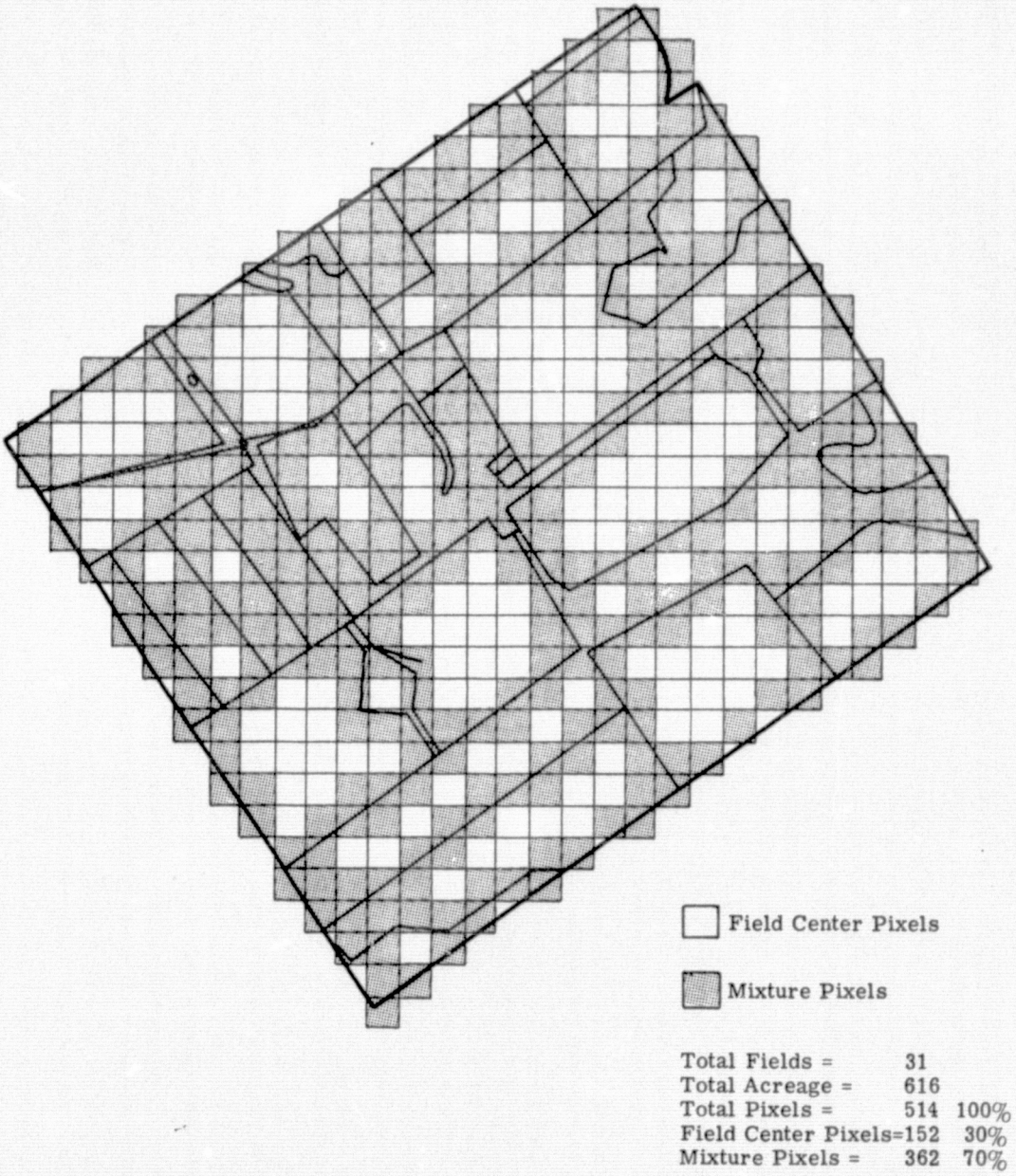

FIGURE 6.1. DISPLAY OF MIXTURE PIXELS IN LOCKE TOWNSHIP SECTION 109

This situation has major impact on the accurate estimation of proportions. The more mixture pixels in a scene that can be spuriously classified, the more the accurate estimation of proportions is dependent upon compensation of the errors. Consider for the moment a mixture pixel of two classes, say trees and grass. Using standard proportion estimation procedures, it would be hoped that such a mixture pixel would be classified as either trees or grass and that the number of times such pixels fall in either class is equal to the overall proportion of grass and trees found in all such mixtures. Should a disproportionate number of false alarms, that is detections of a third class, occur among this mixture of trees and grass, then the task of accurate proportion estimation becomes more difficult and an even greater reliance is placed on the compensation of errors.

The simulation technique used in the analysis described in Section 4 was applied to measure how prevalent a problem the false alarm rate could be in the given S-192 data set. Recall that five signatures, for corn, grass, tree, bare soil and brush, were chosen and mixtures of all possible pairs of these crops were simulated in proportions (1/3, 2/3) and (2/3, 1/3). Table 6.1 displays the expected performance for the recognition classes. Given a mixture of crops A and B, one would hope that the sum of the percentage of those mixture pixels classified as A and those classified as B would be close to 100%. The difference would be the number of false alarms detected. In examining the last column of Table 6.1, one finds that the false alarm rate is by no means insignificant. The lowest false alarm rate detected is 10% while the highest rate is 76%.

Thus it appears that the number of false alarms from mixture pixels is significant when the pixels are classified using conventional techniques. What, then, does this mean in terms of overall accurate proportion estimation?

Going back to the tree-grass example cited above, consider that a high rate of corn classifications occurs among pixels which are mixtures of trees and grass. Such false alarms would need to be compensated for by a decline in

TABLE 6.1 EXPECTED PERFORMANCE FOR RECOGNITION OF SIMULATED SKYLAB MIXTURE PIXELS BASED ON THE BEST LINEAR DECISION BOUNDARIES BETWEEN FIVE SKYLAB FIELD CENTER SIGNATURES

MIXTURE	PROPORTION	% ASSIGNED TO CLASS						% CORRECT* CLASSIFICATION	% FALSE ALARMS
		TREE	GRASS	SOIL	BRUSH	CORN	UNC		
TREE-GRASS	(1/3,2/3)	4.2	44.0	0.8	22.4	23.4	5.2	48.2	51.8
	(2/3,1/3)	31.6	10.2	0.4	24.6	21.2	12.0	41.8	58.2
TREE-SOIL	(1/3,2/3)	4.6	8.8	56.6	0.0	12.2	17.8	61.2	38.8
	(2/3,1/3)	47.2	6.6	8.2	0.6	13.0	24.4	55.4	44.6
TREE-BRUSH	(1/3,2/3)	6.0	4.4	0.0	67.8	16.8	5.0	73.8	26.2
	(2/3,1/3)	32.4	3.6	0.0	37.6	15.6	10.8	70.0	30.0
TREE-CORN	(1/3,2/3)	9.6	5.0	0.0	27.6	52.8	5.0	62.4	37.6
	(2/3,1/3)	39.0	2.2	0.0	26.2	25.2	7.4	74.2	25.8
GRASS-SOIL	(1/3,2/3)	0.8	27.0	63.0	0.0	2.6	6.6	90.0	10.0
	(2/3,1/3)	1.2	69.8	15.4	1.2	7.0	5.4	85.2	14.8
GRASS-BRUSH	(1/3,2/3)	0.6	20.2	0.0	51.2	23.4	4.6	71.4	28.6
	(2/3,1/3)	1.6	50.2	0.0	22.4	22.2	3.6	72.6	27.4
GRASS-CORN	(1/3,2/3)	1.6	29.0	0.2	10.6	55.6	3.0	84.6	15.4
	(2/3,1/3)	1.4	60.2	0.4	7.6	28.0	2.4	88.2	11.8
SOIL-BRUSH	(1/3,2/3)	8.6	28.0	1.0	23.0	31.0	8.4	24.0	76.0
	(2/3,1/3)	7.2	28.6	32.8	1.4	16.2	13.8	34.2	65.8
SOIL-CORN	(1/3,2/3)	4.8	31.2	4.6	1.6	50.2	7.6	54.8	45.2
	(2/3,1/3)	3.4	22.6	48.8	0.0	13.0	12.2	61.8	38.2
BRUSH-CORN	(1/3,2/3)	1.6	8.8	0.0	32.4	54.2	3.0	86.6	13.4
	(2/3,1/3)	1.2	6.8	0.0	59.6	28.6	3.8	88.2	11.8
FINAL ESTIMATION OF PROPORTION BY CLASS** (CORRECT = 100%)		52%	118%	58%	104%	128%	40%		

* Assigned to one of the two classed considered.
** Assuming all above mixtures equally likely.

the classification rate of pure corn pixels and/or by offsetting false alarms of other classes among corn and corn-mixture pixels. This then triggers a chain-reaction of other compensations within other classes. The odds of this all happening so that the errors do indeed compensate, would seem to be very slight.

In referring back to Table 6.1, the bottom line shows strikingly that, for this data set, the errors would not compensate. Tree and bare soil classes are grossly underestimated while corn is significantly overestimated among mixture pixels.

It is clear, then, that significant numbers of mixture pixels, when processed by conventional means, will yield significant numbers of false alarms. Further, the odds that significant numbers of false alarms will compensate one with another so that estimation of proportions of classes may be accurately accomplished using classification counts from conventional classifiers seems rather small. To complete this study, an investigation of whether there is a fixed, estimable bias in the proportion estimates is needed.

6.2 BRIEF DESCRIPTION OF THE MIXTURE PROCESSOR

For the example discussed in the previous section, the task of accurately estimating proportions of classes in a scene where a significant portion of the pixels are mixture pixels could not be done by using conventional classification processing techniques. In the following sections we discuss the application of a specialized processor, here called the mixtures processor, which allows for the fact that pixels may contain mixtures of different ground covers, and is capable of analyzing the proportions of the classes present in each pixel.

Before proceeding further, a short explanation of the manner in which the mixtures processor is applied is in order.

It is obvious that a pixel may be purely or almost purely of one ground class, or it may be a mixture of several ground classes. Thus the algorithm used, as its first stage, determines the several likeliest possibilities. First, the most probable single signature for a pixel, and the attendant chi-square value are determined. (The chi-square value is a measure of the likelihood that the pixel is a member of the signature distribution being considered.) Next, the likeliest mixture of two classes is calculated and the

proportion of each class in the pixel, and an associated chi-square value is calculated. The pixel may be further analyzed as a mixture of three and four classes. For reasons of processing time and computer space requirements, for the agricultural test site part of this study we limited the consideration to either pure or two-class mixture pixels. This is not an unrealistic restriction for this case when one considers the scan swath over the ground: For an agricultural area like the current data set, most mixture pixels will occur at field boundaries so that the vast majority of such pixels will be mixtures of two ground classes. Figure 6.1 also provides an illustration of this situation.

The data are then processed through a second stage where a pixel is determined to be a pure pixel if the chi-square value for the likeliest pure case is less than some threshold τ_1. If it is not pure according to this test, then the chi-square value for the two-class mixture case is compared to a second threshold τ_2. If it is less than τ_2, the pixel is determined to be the mixture indicated; otherwise, further tests with τ_3, τ_4, etc. are conducted when three and four class cases are considered. If the pixel fails all the tests, it is considered to be from a class or classes not included in the signature set. Currently the thresholds τ_1, τ_2, etc., are chosen empirically so as to minimize the error of the proportion estimate over some training area of known proportion.

The chief factor affecting the performance of the mixtures processor is the geometrical configuration of the signatures used to define the ground cover classes. The signatures can be defined as hyperellipses in an n-dimensional orthogonal space where n is the number of bands or SDOs. A simplex is a hypervolume defined by m vertices, where a signature mean defines each vertex. A pure pixel would be one which is located near a signature mean, while a mixture pixel would be one which was located between several of the signatures. Further, if for a given set of signatures, the simplex they define is not convex; e.g., one signature being a linear combination of some other signatures, then the simplex is said to be degenerate. For such a simplex, a non-unique answer is mathematically possible and as a result such simplexes should not be used for processing.

6.3 APPLICATION OF MIXTURES PROCESSOR TO AN AGRICULTURAL SCENE

The initial step in implementing the mixtures processor is to define a signature set. It is important that the signatures used be sufficiently distant one from the other; that is, the simplex formed by the set of signatures cannot be degenerate, otherwise the algorithm breaks down. For this reason it is wise to limit the number of signatures used. Also, since the processing time goes as $m(m+1)/2$ (for m signatures), there is a second reason to keep the size of the set as small as possible.

For the agricultural test site the set of 15 signatures used for the classification had the following composition:

CORN	4 Signatures
TREES	2 Signatures
BRUSH	1 Signature
GRASSES, WEEDS, ETC.	5 Signatures
BARE SOIL	1 Signature
SOYBEANS	1 Signature
ALFALFA	1 Signature

Since soybeans and alfalfa are very minor ground covers in the test site, we excluded them from this study. An analysis of the tree and brush signatures showed the two tree signatures to be very disparate, but the brush and one of the tree signatures were found to be very similar spectrally -- overlapping some 75%. The brush signature, representing primarily areas of scrub forest, was therefore combined with the one tree signature. As for the corn signatures, the two signatures with most of the corn points were found to be very different; since corn is a major cover, both these signatures were selected for use. The bare soil signature also was included.

The grasses were represented by 5 diverse signatures. Since combining several signatures into one resultant signature with a large spread would have decreased the inter-signature distances in the simplex, we endeavored to choose just one signature. An examination of 2-dimensional scatter plots

of all the signatures indicated that one grass signature seemed to be more toward the exterior of the total signature simplex than any of the other grass signatures. That cluster probably represents the grass subclass which had the highest percentage ground cover and thus the lushest condition of the grass object class. This grass signature was selected to represent grass with the hope that pixels from pasture or weed fields would be called a mixture of grass and bare soil.

The signature set described above was applied to a small 550 pixel section of the data. Subsequent analysis showed that very little of the data were being called out as grass, and as a result the error rate was substantial. It seemed that the initial choice of a grass signature was a poor one. Accordingly, a different grass signature was selected, this one being from the grass cluster containing the greatest number of grass pixels.

The test data subset was again processed through the mixtures classifier. The results were somewhat better, but the total error in the proportion estimation for the test data subset was still slightly inferior to the error rate achieved using the normal, i.e., linear maximum likelihood, classifier. It was further noted that the chi-square thresholds chosen, which minimized the total error of the proportion estimate, resulted in 73% of the pixels being counted as "pure" and only 18% of the pixels being assessed as mixtures. Many more mixture pixels had been anticipated.

One hypothesis that might explain these results is that the conventional classification had been done using 15 signatures -- the mixtures approach used only six. It seems that it would be necessary to further pack the signature simplex with other grass signatures so as to increase the grass classification rate. Such a procedure would increase the grass classification, but it would further decrease the number of pixels processed as mixtures.

That few pixels were called out as mixture pixels seems to be another result of the poor signal range discussed in Section 2. The signature set is such that not only are the means relatively close together, but also the

individual distributions are very broad so that pixels which are mixtures of separate classes are themselves very near the center of some distribution so that they would be classified as being from that distribution. Figure 6.2 illustrates the point, and the reader is referred back to Figures 3.1 and 3.2 for further illustrations of this point using the S-192 data. Because of these results, no further mixtures processing was performed on the agricultural test site data.

6.4 APPLICATION OF MIXTURE PROCESSOR TO URBAN AREA

As a second exercise, the mixtures processor was used to classify two small portions of data from the urban area of Lansing, Michigan, using signatures acquired by clustering the data. This portion of the data and the training methods used were specified in Section 5.1 of this report.

For this exercise, we were interested in determining the amount of vegetative material, or alternatively of impervious materials, in an urban area. Such information is of use to geographers, and urban planners and impacts local urban climatology, etc. In this case it was expected that most of the classes of interest would be smaller than the resolution size of the scanner. In other words, it was expected that each pixel would be a mixture of two, three or even more classes.

Initially, five of the signatures from the set were identified as being classes of interest for this problem: green vegetation, concrete, other impervious (rooftops, asphalt etc.), bare soil, and water (there is a river which runs through the city). This signature set was analyzed using program GEOM. This program calculates a measure of separateness (in a probability sense) for each signature mean in the simplex. The measure calculated is roughly the distance in standard deviations between the signature mean and the hyperplane through the other signature means. If the distance for a given signature is small, then the simplex is liable to be degenerate and the mixtures algorithm will not work well. The results, Table 6.2, show that the simplex of these five classes is degenerate -- concrete, other impervious

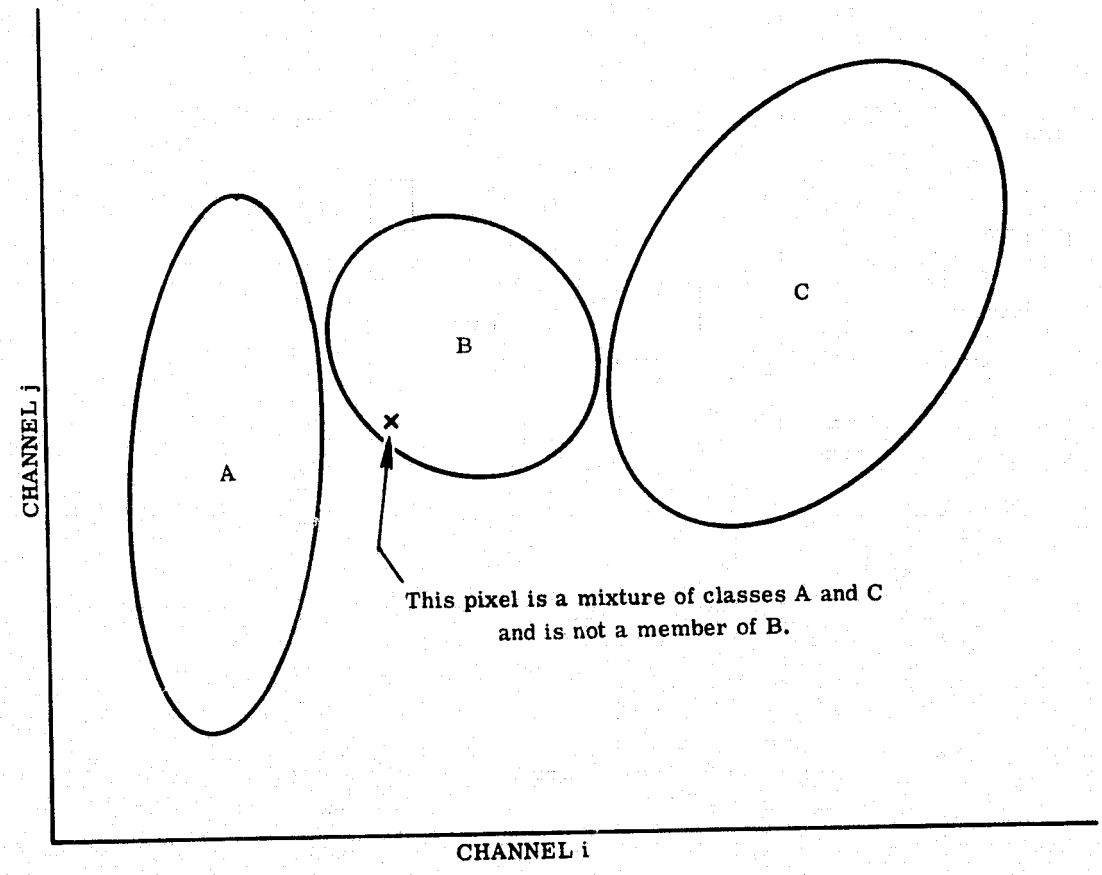

FIGURE 6.2. ILLUSTRATION OF A MIXTURE PIXEL IN A THREE SIGNATURE SIMPLEX

and bare soil each overlap with the simplex formed by the other four signatures. Additionally the other two distances are small.

TABLE 6.2
GEOM RESULTS FOR AN URBAN 5 SIGNATURE SIMPLEX

CLASS	GEOM DISTANCE
Green Vegetation	2.98
Concrete	0.28
Water	1.99
Other Impervious	0.26
Bare Soil	0.58

Investigating further, we tried all 4-tuples to see if some of these simplexes would not be degenerate. All were degenerate. Next all triplets of signatures were tried and here several of the combinations yielded non-degenerate simplexes. From these results the triplet of concrete, other impervious and green vegetation was chosen for the processing effort, since it seemed that these classes would be the most prominent in the scene. The GEOM results for this triplet are given in Table 6.3 below.

TABLE 6.3
GEOM RESULTS FOR FINAL URBAN SIMPLEX

CLASS	GEOM DISTANCE
Green Vegetation	6.06
Concrete	3.0
Other Impervious	4.5

The fact that simplexes with more than three signatures were degenerate indicates that only two out of seven channels were important for separating these classes -- the other five being redundant. This follows since for the

spectrally disparate classes involved, a non-degenerate simplex existed only for some triplets of the signature set, and each triplet in turn defines only a plane (2-space). Thus there are only two independent channels for this problem.

The mixtures processor described in the previous section was implemented to process the data, using the three signatures mentioned above. It was noticed that, for most of the pixels, low chi-square values were being calculated for the best one-at-a-time case -- i.e., that it was most probable that the pixel was pure. The rest of the pixels were deemed most likely to be mixtures of a pair of classes. Only a few pixels were deemed to be mixtures of the three classes. The results were also poor, with the other impervious signature overestimated and the vegetation greatly underestimated.

6.5 CONCLUSIONS

It was concluded from the results of both studies that the lack of adequate dynamic range, as demonstrated here by the size of the simplex in relation to the size of the class distributions, precluded the possibility for most of the pixels to be processed as mixture pixels since the pixels were associated with higher probabilities of being pure. The mixtures processor discussed in this section cannot be expected to yield good results under these circumstances.

7

CONCLUSIONS AND RECOMMENDATIONS

In preparation for the processing and analysis of SKYLAB S-192 data, a fairly detailed examination of the data was undertaken, investigating in each SDO (Scientific Data Output) signal-to-noise characteristics and dynamic range. Aircraft scanner data gathered over the agricultural site the morning of S-192 data collection were examined also and used as a basis for comparison. The results of the examination of S-192 data quality were essentially in keeping with the published S-192 performance evaluations [4]. Conclusions reached were that four of the spectral bands were sufficiently noisy so as not be of use in classification processing and that the remaining bands all had a very limited range of values in relation to the noise content of the data. Also examined was the spatial registration of the scanner data. The SDO-to-SDO misregistration in conic data was measured and shown to be greater than one pixel in some instances. More importantly, further analysis showed that the effect of scan-line-straightening was to compound and increase the misregistration of the S-192 data: a maximum misregistration of 2.2 pixels was calculated. Not only is the misregistration of scan-line-straightened data not easily correctable but the additional misregistration seriously reduces the number of pure pixels available for training.

Analytical and simulation studies were performed to investigate the effects of misregistration on classification accuracy. The results showed that, for pixels which imaged more than one ground class in one or more channels, the error rate was substantial and increased as the degree of misregistration increased. Also shown was that while the correct classification rate for pure (one class) pixels did not change significantly as misregistration increased, the number of such pure pixels markedly decreased as misregistration increased. Because of the increased, uncorrectable misregistration in scan-line-straightened data, the recognition processing for this contract was carried out with conic data. Using the conic data, we were able to substantially correct for misregistration by selecting a set of 13 SDOs (one for each band) and shifting some relative to others such that the maximum misregistration was one third of a pixel.

In preparation for recognition processing of the agricultural test site using conventional techniques, a set of training statistics was extracted and the utility of the 13 spectral bands for recognition processing this area was determined. Using a computer algorithm which computed the average pairwise probability of misclassification, the 13 bands were rank ordered with the result that the four bands previously identified as having poor signal quality were adjudged to be among the worst bands. The two best bands, by far, were 1.55-1.73 m (SDO 12) and 0.93-1.05 m (SDO 19). The result of classifying the agricultural site using conventional techniques and the 7 best bands were somewhat disappointing, with accuracies of field center pixels on the order of 70%, with confusion noted among in a triad of corn, trees and brush. The classification of the data was affected by a combination of the limited signal range in the data and the apparent spectral similarity of many of the ground classes. The latter effect was attributed to the contrast reducing effect of atmospheric haze and the fact that, at the time of year the data was collected, there was a large range of conditions for several classes (e.g., some of the corn had tasseled and some had not) leading therefore to added spectral similarity among classes. Errors in the proportion estimation were also affected by the large number of mixture pixels in the scene. A brief study indicated that more than 70% of the scene was composed of such mixture pixels. In general a disproportionate number of such pixels were classified as corn, resulting in a substantial overestimation of corn in the scene.

The utility of signature extension techniques for S-192 data was tested using the Lansing and Ypsilanti sites for training and test, respectively. Several signature extension techniques were utilized to process data for the signature extension test site located some 70 miles from the signature extension training area. The test area was chosen particularly because a layer haze covering this site was very evident in the S-190B imagery; thus, this was a test under very different atmospheric conditions as well as a test over distance. Training statistics were gathered using an unsupervised clustering technique and clusters for urban, residential, vegetation, water, concrete, bare soil and sparse vegetation were generated. A classification attempt without

the use of signature extension techniques resulted in poor accuracy while the use of signature extension techniques improved classification accuracy. The best results were obtained using the dark object algorithm. In a qualitative sense these results matched those obtained using local clusters (i.e., clusters generated at the signature extension site).

Further classification was carried out on both training sites previously mentioned using the unresolved object or mixtures classifier. Such a classifier would seem to be well suited to a data set where more than 70% of the pixels were mixture pixels. The results of using this approach on both sites was unsatisfactory, due apparently to the previously mentioned limited signal range, contrast and spectral discriminability of the data. Thus, no general conclusions were drawn with regard to the utility of the mixtures classifier on S-192 data.

Results of this investigation indicate that deficiencies in the S-192 data will tend to limit its ultimate utility and that to minimize deleterious effects of channel-to-channel misregistration the further use of S-192 data in conic format is recommended. Furthermore, the design of future multispectral scanner and data processing systems should take into account the experience gained in processing and analyzing S-192 data. To this end, two recommendations are made. First, finer spatial resolution should be considered for future sensors; this would alleviate the problems caused by having a large proportion of mixture pixels in the scene and the attendant problem of having so few pure pixels on which to base training statistics. The second recommendation is that future systems provide a means to adjust scanner gain and offset parameters to better match the radiance characteristics of individual scenes and thus make fuller use of the available scanner dynamic range. For spacecraft scanners the long atmospheric path traversed by the ground-reflected radiation has the effect of adding a sizeable constant radiance (path radiance) while also attenuating the radiation resulting in reduced contrast in the data. If future scanners are designed with appropriate offset and gain capabilities

(indeed, is there a need to set the zero response of a band equal to a zero radiance level in that band or rather should it be set close to a zero reflectance level) it is safe to say that higher contrast, more useful data, would result. As for making specific recommendations regarding spatial and radiometric parameters of future scanner systems, such work was beyond the scope and context of this investigation. These are very complex areas and need to be properly and fully addressed in order to derive more definitive recommendations for future spacecraft multispectral scanners.

APPENDIX I

S-192 SCANNER CHARACTERISTICS

A. SPECTRAL CHARACTERISTICS

BAND	SDO s	λ (μm)
1	22	.41-.45
2	18	.45-.50
3	1,2	.50-.55
4	3.4	.54-.60
5	5,6	.60-.65
6	7,8	.66-.73
7	9,10	.77-.89
8	19	.93-1.05
9	20	1.03-1.19
10	17	1.15-1.28
11	11,12	1.55-1.73
12	13,14	2.10-2.34
13	15,16,21	10.2-12.5

B. OPTICAL CHARACTERISTICS

Instantaneous Field of View	0.182 mrad
Scan Rate	94.79 revs/sec.
No. of Samples/Scanline/detection:	
Low Sample Rate Bands	1240
High Sample Rate Bands	2480
Analog to digital Conversion	8 bits/value
Cone Angle	5°32'
Portion of Scan Viewing the ground	116.25°
Scan Swath	72.4 km
Altitude at time of data collection	441,429 m

APPENDIX II

M-7 SCANNER CHARACTERISTICS [6]

A. SPECTRAL CHARACTERISTICS FOR MISSION 85M, AUGUST, 1973

BAND	λ (μm)
1	.41-.48
2	.46-.49
3	.48-.52
4	.50-.54
5	.52-.57
6	.55-.60
7	.58-.64
8	.62-.70
9	.67-.94
10	1.0-1.4
11	1.5-1.8
12	9.3-11.7

B. OPTICAL CHARACTERISTICS

Resolution	
Spectrometer (bands 1-9)	2.0 x 2.0 mrad
Near IR (Bands 10,11)	2.0 x 4.0 mrad
Thermal (9.3-11.7 μm)	3.3 x 3.3 mrad
Scan Rate	60 scans/sec.
Along track velocity	2.75 ft/scan
Analog to Digital Conversion	9 bits/value
Altitude at time of data collection	2000 ft
Portion of Scan Viewing Ground	90°
Scan Swath	4000 ft.

APPENDIX III

SOUTHEAST MICHIGAN TEST SITE GROUND TRUTH

The Southeast Michigan Test site consists of three rural townships, LeRoy, Locke and White Oak, in Ingham County. The location of the test site is given in the map, Figure III.1. Michigan State University provided ground truth for the three townships. The acreages and number of fields of each ground cover class are given in Tables III.1-III.3. Designations are grouped as follows.

CORN	-	corn
SOYBEANS	-	soybeans
TREES	-	trees, brush, woods
GRASS	-	grasses, sudan grass, clover, weeds, pasture, short grass, tall weeds
STUBBLE	-	stubble, cut grass, cut oats, cut wheat, cut beans
SOIL	-	soil, bare soil
ALFALFA	-	alfalfa

		SYMBOL
OTHER	-	D - barley F - lettuce H - hay I - onions J - orchard N - beans O - oats W - wheat X - homesteads, buildings, towns, freeway Y - water, lakes, swamp ? - unknown, crop?, illegible

CLOUD COVER - Indicates that the section was cloud covered in the high altitude photography which served as a source for "ground truth".

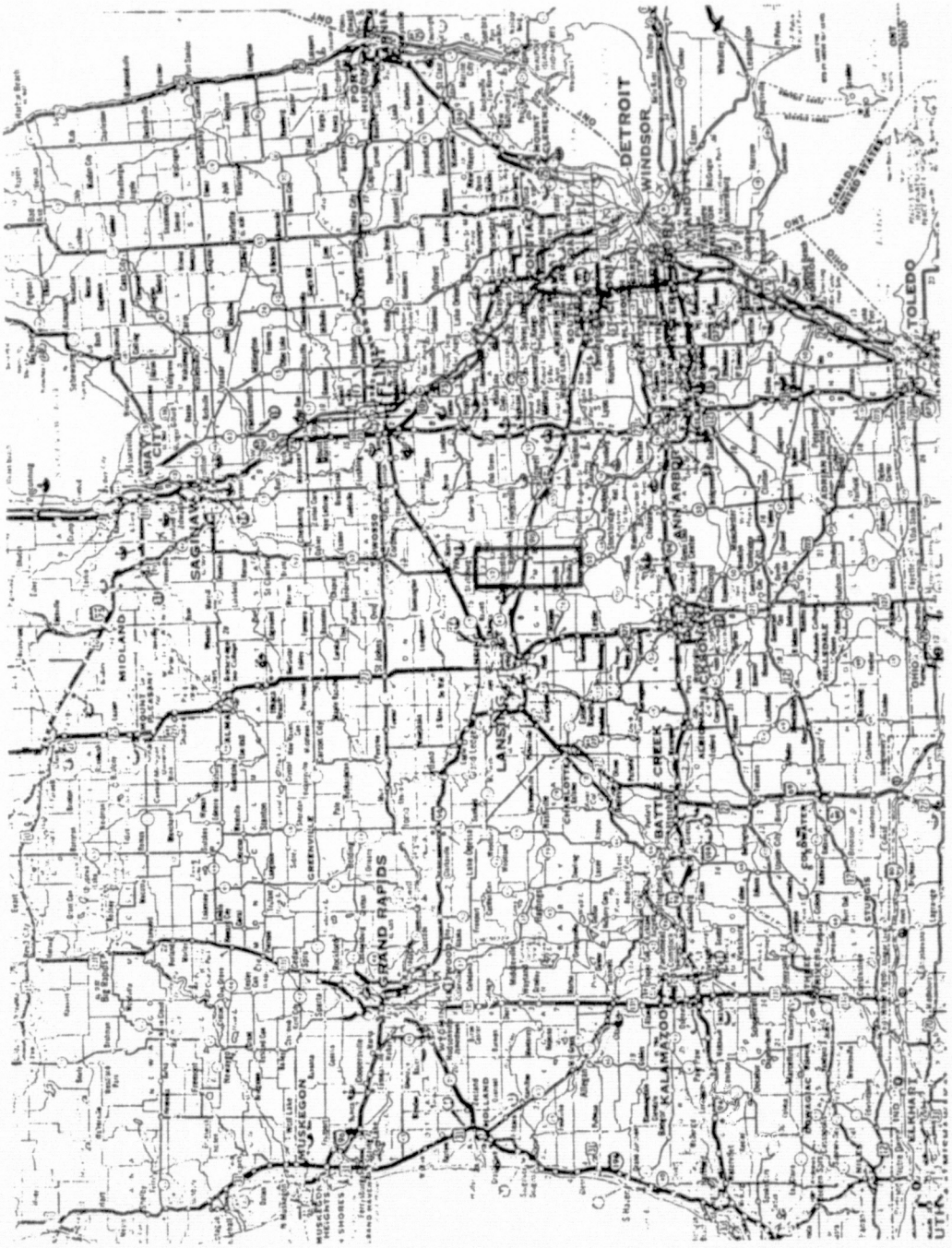

FIGURE III.1. LOCATION OF S-192 TEST SITE ON EXCERPT OF ROAD MAP OF SOUTHERN LOWER MICHIGAN

TABLE III.1. GROUND TRUTH FOR LOCKE TOWNSHIP, INGHAM COUNTY, MICHIGAN
GIVEN IN ACRES AND NUMBER OF FIELDS

LOCKE SECTIONS = 30

SECTION	CORN		SOYBEAN		TREES		GRASS		STUBBLE		SOIL		ALFALFA		OTHER		TOTAL		SYMBOL
	#	ACRE	#	ACRE	#	ACRE	#	ACRE	#	ACRE	#	ACRE	#	ACRE	#	ACRE	#	ACRE	FOR OTHER
2	8	170.5	3	42.2	6	177.7	17	206.5	1	7.0	4	21.1	1	11.1			40	636.1	
3	9	192.0	2	32.8	4	108.3	15	297.9	4	65.5	3	24.0	4	58.5	2	19.9	43	798.9	X,θ
4	8	136.3	4	78.4	11	141.4	10	261.3	4	59.8	3	66.1			3	42.7	43	786.0	X,θ,N
5	8	259.6	1	23.4	4	272.0	3	72.6	4	58.6	5	92.4					25	778.6	
6	14	253.9	1	18.8	4	71.4	7	96.7	10	123.4	3	31.0			2	10.6	41	605.8	X,W
7	5	60.7			1	59.7	10	259.4	4	49.1	5	53.3	1	18.1	1	5.8	27	506.1	Y
8	11	231.1	4	37.4	6	204.2	3	28.1	9	106.4	5	28.7					38	635.9	
9	11	269.3	2	62.6	3	63.1	9	137.7	2	13.4	2	34.6			2	35.7	31	616.4	?
10	4	81.3	1	25.1	6	145.0	14	270.8	4	95.9			1	17.0	1	7.0	31	642.1	θ
11	5	62.7			8	101.3	11	409.5	2	11.8	3	43.9			2	10.5	31	639.7	H,Y
14					3	139.2	17	366.8	3	121.7							23	627.7	
15	1	52.0			1	101.2	6	432.5	1	76.1							9	661.8	
16	9	186.7	4	81.8	2	38.6	7	237.3	1	13.5	4	41.7					27	599.6	
17	16	187.8	1	26.9	5	124.6	15	183.7	3	34.6	4	28.2	1	19.9	1	12.3	46	618.0	N
18	10	113.0	4	45.5	7	117.5	8	57.3	4	52.3	5	45.6	1	29.8	1	7.6	40	486.6	N
19	3	46.7			6	99.5	15	218.9	6	52.6	4	18.8	1	20.5	1	12.8	36	469.8	θ
20	8	126.8			1	94.8	13	185.4	9	120.8	6	51.6	2	35.7			39	615.1	
21	3	54.4			4	61.4	5	302.5	2	41.6	2	137.5			1	18.8	17	616.2	H
22	3	192.5			7	143.4	5	320.2									15	656.1	
23	11	332.9	3	46.2	5	66.8	3	55.0	2	84.3	1	49.2					25	634.4	
26	9	266.9			4	68.5	3	72.5	2	68.0	1	25.1	3	124.6	2	17.0	24	642.6	X
27	6	135.0	1	8.2	6	65.5	13	336.2	2	74.9	2	18.1			1	5.3	31	643.2	W
28	11	223.6	1	32.2	3	31.6	7	91.3	7	132.3	7	137.8	1	8.2			37	657.0	
29	11	191.1			9	110.1	11	199.1	3	25.1	6	92.6					40	618.0	
30	7	129.5	1	36.9	4	107.1	5	70.8	2	10.5	5	70.2	1	15.8	1	4.7	26	445.5	X
31	7	76.8	5	55.6	6	74.3	2	167.3	5	33.9	3	24.6	1	10.0	2	21.0	31	463.5	H,θ
32	8	149.1	1	8.2	5	203.7	5	74.3	5	95.4	5	45.6			3	55.0	32	631.3	2N,H
33	8	266.1	2	23.4	3	35.8	8	163.2	3	86.6	2	27.0			1	17.0	27	619.1	θ
34	6	269.0	1	13.5	5	53.8	6	99.4	2	73.7	3	122.4					23	631.8	
35	3	123.4			7	114.6	10	264.5	5	85.6	3	26.9			2	14.1	30	629.1	2H
TOTAL	223	4840.7	42	699.1	146	3196.1	263	5938.7	111	1874.4	96	1358.0	18	369.2	29	317.8	928	18594.0	
AVE.	7.4	161.4	1.4	23.3	4.7	106.5	8.8	198.9	3.7	62.5	3.2	45.3	.6	12.3	1.0	10.6	30.9	619.8	

TABLE III.2. GROUND TRUTH FOR LEROY TOWNSHIP. INGHAM COUNTY, MICHIGAN
GIVEN IN ACRES AND NUMBER OF FIELDS.

LEROY: SECTIONS = 29

SECTION	CORN		SOYBEAN		TREES		GRASS		STUBBLE		SOIL		ALFALFA		OTHER		TOTAL		SYMBOL
	#	ACRE	#	ACRE	#	ACRE	#	ACRE	#	ACRE	#	ACRE	#	ACRE	#	ACRE	#	ACRE	FOR OTHER
2	1	41.6			5	193.1	6	269.1	2	22.8	4	13.5			1	8.2	19	548.3	Y
3	3	105.4	1	14.0	4	83.7	3	148.6	4	104.8	2	65.5	2	29.2			19	551.2	
4	4	50.9	1	71.3	4	180.4	4	180.1	3	14.6	2	11.1	3	41.0	1	8.8	22	558.2	Y
5	8	203.0			3	160.4	4	52.9	3	104.7	2	19.3					20	540.3	
6	7	205.2	1	6.5	3	45.7	4	66.7	1	18.8	2	35.7			2	21.7	20	400.3	X
7	7	97.2	3	69.7	3	33.9	4	67.4	6	114.7	3	32.1			3	62.6	29	477.6	2N,X
8	7	278.6			4	104.1	7	159.6	1	21.6	3	50.4			3	29.9	25	644.2	2X,Y
9	8	300.7	3	33.3	5	84.2	1	14.0	4	73.7	1	27.5			3	109.4	25	642.8	X,Y,θ
10	9	217.1			4	32.8	4	96.5	5	65.4	8	97.1	5	96.5	1	42.1	36	647.5	X
11	5	82.5			4	51.0	9	226.7	5	51.0	3	23.9	2	48.0	1	157.4	29	640.5	X
14	6	136.1			8	80.0	12	280.5			8	81.1	2	10.3	3	38.0	39	626.0	2X,θ
15	8	231.0			3	62.8	7	159.6	4	35.8	5	27.0	4	61.2	2	47.1	33	624.5	2X
16	7	373.4	2	31.7	5	69.6	4	62.8	4	70.3	1	10.3					23	618.1	
17	10	355.8	1	11.5	2	32.9	12	159.2	2	23.1					2	61.5	29	644.0	θ
18	6	54.6	2	17.8	6	54.1	5	207.1	4	73.1	5	35.2	2	19.5			30	461.4	
19	9	152.8	3	42.7	2	75.4	8	108.2	2	62.8	2	12.6	1	19.6	1	24.2	28	498.3	N
20	5	364.7			5	42.3	7	64.3	4	86.4	3	25.3	4	36.3	2	30.0	30	649.3	θ,X
21	3	269.1			1	194.8	3	53.7	2	73.2	1	25.4			2	28.8	12	645.0	2θ
22	6	200.4	2	59.3	4	98.5	5	133.8	3	78.9			1	69.1			21	640.0	
23	8	256.3			3	70.8	11	155.0	4	60.5	3	91.7	1	10.3			30	644.6	
26	6	300.0	1	14.9	3	189.5	8	84.2			6	59.7					24	648.3	
27	7	212.3	3	26.4	3	16.2	12	148.2	2	39.7	7	95.4	4	72.7	1	20.1	39	631.0	N
28	12	221.8	2	57.6	6	127.3	8	141.1	2	20.1	7	54.2	2	20.8			39	642.9	
29	12	230.1	4	91.4	3	55.9	9	170.4	2	25.3	3	63.3			1	9.8	34	646.2	θ
30	11	201.8	1	14.4	2	41.9	7	127.8	5	51.6	7	64.3	3	20.1	1	10.3	37	532.2	θ
31	5	183.8	1	23.6	3	99.6	5	72.1	2	22.6	4	89.9	1	36.8	1	19.0	22	547.4	D
32	9	243.8	2	23.1	3	51.9	6	95.7	4	87.4	1	2.9			5	148.2	30	653.0	N,2θ,B,H
33	11	239.6	6	72.6	3	103.6	6	60.7	8	102.1	3	17.2	2	8.6	2	16.1	41	620.5	N,X
34																			Cloud Cover
35	8	374.2	1	17.3	3	87.0	4	79.7	1	11.5	4	47.3	1	29.3			22	646.3	
TOTAL	208	6183.8	40	699.1	107	2523.4	185	3645.7	89	1516.5	100	1178.9	40	629.3	38	893.2	807	17269.9	
AVE.	7.2	213.2	1.4	24.1	3.4	87.0	6.4	125.7	3.1	52.3	3.4	40.7	1.4	21.7	1.3	30.8	27.8	595.5	

TABLE III.3. GROUND TRUTH FOR WHITE OAK TOWNSHIP INGHAM COUNTY, MICHIGAN
GIVEN IN ACRES AND NUMBER OF FIELDS

WHITE OAK: SECTION = 29

SECTION	CORN		SOYBEAN		TREES		GRASS		STUBBLE		SOIL		ALFALFA		OTHER		TOTAL		SYMBOL
	#	ACRE	#	ACRE	#	ACRE	#	ACRE	#	ACRE	#	ACRE	#	ACRE	#	ACRE	#	ACRE	FOR OTHER
2	9	205.1			6	38.0	12	350.0	2	29.9	6	49.5	2	66.8			37	739.3	
3	14	319.9	1	38.6	3	110.0	11	118.8			8	99.7	1	5.7	1	4.1	39	696.8	X
4	7	208.6	2	19.7	9	99.7	8	160.7	5	146.1	4	32.2	1	17.3	1	8.7	37	693.0	N
5	5	103.1	4	100.2	2	120.9	10	137.1	10	125.3					1	106.0	32	692.6	N
6	18	222.1	5	59.3	4	69.7	3	21.7	7	86.6	9	119.6	1	21.9	1	6.9	48	607.8	θ
7	6	139.4	1	26.5	4	189.4	3	45.0	3	39.7	5	35.2	2	81.9	1	19.7	25	576.8	θ
8	5	178.0	2	27.0	6	94.3	6	214.8	1	28.8	3	21.2			5	79.0	28	643.1	H,4N
9	8	293.3	2	47.8	6	73.0	4	42.9	2	38.0	5	94.0			3	57.1	30	646.1	X,2H
10	7	235.5			5	141.1	5	88.0	1	11.5	4	32.1	3	109.3	3	10.8	28	628.3	3X
11	2	72.6			4	292.8	5	224.6			2	61.7	1	7.5			14	659.2	
14	3	91.0			6	156.0	12	337.7	2	36.8	1	25.4					24	646.9	
15	9	267.5			4	69.1	3	65.6	1	88.7	6	119.8	1	4.1	2	13.9	26	628.7	θ,X
16	12	307.5	3	18.9	8	89.4	9	172.3	1	19.0	3	28.2					36	635.3	
17	8	159.5	2	43.2	5	150.5	5	55.4	6	62.1	9	74.8			6	91.0	41	636.5	?,5H
18	11	247.3			9	99.7	5	74.3	4	76.7	3	55.9	1	11.0	2	22.4	35	587.3	θ,X
19	8	201.3	1	39.8	4	76.5	3	45.4	4	128.9	1	29.3	1	45.5	1	2.9	23	569.6	X
20	8	207.3	2	89.2	6	100.2	9	168.7	4	28.3	2	6.8			3	42.0	34	642.5	N,X,J
21	7	192.4	2	24.7	9	80.7	6	236.8	4	36.3					2	70.9	30	641.8	N,θ
22	12	233.4	2	71.9	5	30.5	7	78.3	6	121.6	5	100.7	1	7.5			38	643.9	
23	2	29.5			2	90.5	8	196.8	2	30.5	3	88.8			8	196.4	25	632.5	Y,I,5F
26	2	62.7	1	7.5	4	347.9	9	192.8	1	16.2	1	1.8			2	11.0	20	639.9	2Y
27	11	149.9	2	29.9	6	130.5	12	161.9	8	83.5	8	59.3	1	8.7	4	12.1	52	635.8	θ,3X
28	5	110.0	1	26.5	7	137.7	4	176.8	6	93.2	6	71.2	3	36.0			32	651.4	
29	4	277.7			1	46.1	6	206.8	4	39.1	2	35.2	1	12.6	2	31.1	20	648.6	H,X
30	8	153.3			7	107.7	12	127.7	5	59.3	5	47.1	2	32.8	5	58.5	44	586.4	3H,2X
31																			Cloud Cover
32	12	242.5			3	52.4	6	131.0	4	39.1	4	23.7	7	127.8	1	4.1	37	620.6	X
33	9	139.2	1	15.5	9	135.4	7	143.3	7	82.8	3	37.4	1	4.6	5	76.0	42	634.2	?,W,X,2H
34	11	199.5			9	142.3	11	157.7	10	99.1	3	13.3	1	4.6	3	21.9	48	638.4	θ,2X
35	7	184.3	1	6.9	7	146.2	7	141.6	4	72.6			4	72.5	1	11.5	31	635.6	J
TOTAL	230	5433.4	35	693.1	160	3418.2	208	4274.5	114	1719.7	111	1363.9	35	678.1	63	958.0	956	18538.9	
AVE.	7.9	187.4	1.2	23.9	5.5	117.9	7.2	147.4	3.9	59.3	3.8	47.0	1.2	23.4	2.2	33.0	33.0	639.3	

If a field was listed as 1/2 one crop and 1/2 another, it was treated as if it were 2 separate fields; but if it was listed as woods pasture or weeds and brush, it was placed under the category first mentioned. However, weedy soybeans were called soybeans. Since fields with dual crop identification were arbitrarily classified by the first designation, there may be a bias in the results. This bias is likely to be significant only for the GRASS and TREES categories.

Table III.4 totals the information from the previous tables. The percentage of fields belonging to each ground cover class do not differ significantly between townships. However, the percentage of the total acreage is significantly different for corn and grass. Corn covers 35.8 percent of Leroy Township but only 26.0 percent of Locke while grass ranges from 21.1 percent in Leroy to 31.9 percent in Locke Township. The major ground cover classes, in order of decreasing importance according to the percent found in the test site, are listed below:

Corn	30.3%
Grass	25.5%
Woods	16.8%
Stubble	9.4%
Bare Soil	7.2%

All other ground covers represent less than 5% of the total acreage of the area.

TABLE III.4. PERCENTAGE TOTALS OF ACREAGES AND NUMBER OF FIELDS FOR VARIOUS GROUND COVER CLASSES FOR EACH OF THE THREE TOWNSHIPS AND FOR THE ENTIRE TEST SITE.

	LOCKE			LEROY			WHITE OAK			TOTALS		
	% OF TOTAL FIELDS	% OF TOTAL ACREAGE	AVERAGE ACREAGE	% OF TOTAL FIELDS	% OF TOTAL ACREAGE	AVERAGE ACREAGE	% OF TOTAL FIELDS	% OF TOTAL ACREAGE	AVERAGE ACREAGE	% OF TOTAL FIELDS	% OF TOTAL ACREAGE	AVERAGE ACREAGE
CORN	24.0	26.0	21.7	25.8	35.8	29.7	24.0	29.3	23.6	24.6	30.3	24.9
SOYBEAN	4.5	3.8	16.6	5.0	4.0	17.5	3.7	3.7	19.8	4.3	3.8	17.8
TREES	15.7	17.2	21.9	13.3	14.6	23.6	16.7	18.4	21.4	15.3	16.8	22.1
GRASS	28.3	31.9	22.6	22.9	21.1	19.7	21.8	23.1	20.6	24.4	25.5	21.1
STUBBLE	12.0	10.1	16.9	11.0	8.8	17.0	11.9	9.3	15.1	11.7	9.4	16.3
SOIL	10.3	7.3	14.1	12.4	6.8	11.8	11.6	7.4	12.3	11.4	7.2	12.7
ALFALFA	1.9	2.0	20.5	5.0	3.6	15.7	3.7	3.7	19.4	3.5	3.1	18.0
OTHER	3.1	1.7	11.0	4.7	5.2	23.5	6.6	5.2	15.2	4.8	4.0	16.7
TOTAL			21.4			20.0			19.4			20.2

APPENDIX IV
DERIVATION OF CROSS-CORRELATION FOR MISREGISTRATION STUDY

The following is a procedure for determining the amount of misregistration between two correlated data channels. By reconstructing the continuous waveform over a lengthy interval in both channels, the cross-correlation function of the two waveforms can be determined. Let f(t) and g(t) denote the reconstructed waveforms in the two channels over the interval [A,C]. The cross-correlation function $r(t_o)$ is defined as

$$r(t_o) = \int_A^C f(t)g(t + t_o)\, dt$$

The amount of misregistration between the two channels can be estimated as the value of the parameter t_o which maximizes the cross-correlation. The continuous waveforms can be reconstructed from the sample values by making assumptions which allow the use of Shannon's sampling theorem. The sampled data is converted into continuous form to allow the misregistration to be estimated to within a fraction of a pixel rather than in whole pixel increments. The length of the interval [A,C] must be long in comparison to the range of the parameter values t_o. This condition is required to minimize the effect of inaccuracies which will occur near the endpoints of the interval.

Shannon's sampling theorem indicates that a continuous signal y(t), bandlimited to B(radians/sec), can be exactly reconstructed from samples taken with a sampling interval $\tau = \pi/B$. The sampling rate is equal to twice the highest frequency component contained in the signal. The original signal y(t) can be expressed in terms of the sample values $y(m\tau)$ as

$$y(t) = \sum_{m=-\infty}^{\infty} B\, y(m\,) \frac{\sin B(t - m\tau)}{B(t - m\tau)}$$

Assume that the two continuous data channels f(t) and g(t) are bandlimited to B and that the sampling interval τ is equal to /B. Let the vample values

of these two waveforms over the interval [A,C] be denoted as $f(k\tau)$ and $g(i\tau)$ $i, k = 1, \ldots, N$. The cross-correlation $r(t_o)$ can be expressed in terms of the samples as

$$r(t_o) = \sum_{i,k=1}^{N} f(k\tau)g(i\tau) \int_A^C \frac{\sin B(t - k\tau)}{B(t - k\tau)} \frac{\sin B(t + t_o - i\tau)}{B(t + t_o - i\tau)}$$

Using a variation of Parseval's Theorem, the integral can be evaluated by extending the limits of integration to positive and negative infinity, and $r(t_o)$ can be expressed as

$$r(t_o) = B\pi \sum_{i,k=1}^{N} f(k)g(i) \frac{\sin B(k\tau - i\tau + t_o)}{B(k\tau - i\tau + t_o)}$$

or, since $B\tau = \pi$

$$r(t_o) = B\pi \sum_{i,k=1}^{N} f(k)g(i) \frac{\sin \pi(k - i + t_o/\tau)}{\pi(k - i + t_o/\tau)}$$

This relationship can be expressed in terms of a fraction of a sampling interval (or fraction of a pixel) by defining a variable $\Delta = t_o/\tau$. Then

$$r(\Delta) = B\pi \sum_{i,k=1}^{N} f(k)g(i) \frac{\sin \pi(k - i + \Delta)}{\pi(k - i + \Delta)}$$

Neglecting the constant factor $B\pi$ and expressing $f(k\tau)$ and $g(i\tau)$ as f_k and g_i, respectively, the function $d(\Delta)$ must be evaluated, where

$$d(\Delta) = \sum_{i,k=1}^{N} f_k g_i \frac{\sin \pi(k - i + \Delta)}{\pi(k - i + \Delta)}$$

which can be simplified as

$$d(\Delta) = \sum_{j=-(N-1)}^{(N-1)} \left[\sum_{j-k=j} f_k \, g_i \right] \frac{\sin \pi(\Delta - j)}{\pi(\Delta - j)}$$

For large N, the variable j need not extend over the entire range because of the insignificant contribution of the high magnitude terms. To reduce the effects of noise, the function $d(\Delta)$ should be determined for several scan lines and averaged.

Initial tests of this algorithm indicated that the misregistration estimate was being biased by the DC (average) component of the signal in each channel To remove this bias, the algorithm was modified to subtract out the mean value of each channel before computing the cross-correlation. In essence, this means that the cross-correlation between the AC (varying) components of the signals was then computed and this modification removed the bias that had been noted.

APPENDIX V
DIGITIZATION AND PREPROCESSING OF M-7 DATA

The data set selected for processing was Run 2 which was collected over Flight line 1 of the intensive study site at an altitude of 2000 feet. The time of data collection was 1100 hours EDT, approximately the same time as SKYLAB overpass.

First the analog tape was duplicated to remove relative skew (misregistration) between channels, and the tape was reviewed in regard to data quality. The scan rate was checked and found to be 60 cycles per second as per specifications. The relative ground speed of the aircraft was checked and found to be approximately 2.75 feet/scan or 98 knots. Each data channel was checked. The only problem found was in the thermal channel, track 12, where the offset was very noisy, with variations in the cold plate signal of as much as 15% of the total dynamic range.

As mentioned above, the data were gathered at an altitude of 2000 feet. This means that the ground size of each resolution element is very small compared to the size of ground objects of interest; or conversely, that each ground object of interest would contain an enormous number of resolution elements. For example, the spectrometer on the M-7 scanner exhibits a resolution of two milliradians, resulting in a resolution element of four feet by four feet. A typical 15 acre agricultural field would be scanned by as many as 40,875 resolution elements.

Accordingly, it was felt that we could take advantage of the gross redundancy in the data by means of spatial filtering to improve the signal to noise ratio of the data, and decrease considerably the number of pixels to be processed, thus decreasing processing time and costs. Naturally, some information, such as the ability to more precisely locate boundaries between two areas or detect fine-scale structure in the data, would be lost in using such filtering. For this data set, it was felt that such drawbacks would not hurt the analysis effort. Accordingly, it was decided to filter along each

scan line using an appropriate low pass analog filter and sampling once every 20 milliradians. In addition digital smoothing over 9 scan lines was used at each scan point. The result was one digitized "average" datapoint from every 10 x 9 rectangle of data points in the original analog tape. This represents an increase in signal to noise of 9.5:1 and a large decrease in the volume of data output. In addition, this sampling scheme allowed the data to be digitized eight times faster than it could have been done had we digitized every point in the scan line. In all, some 40,000 analog data scan lines (representing approximately 21 miles on the ground) were digitized. Each digitized scan line consisted of 85 points of ground scene, and an additional 55 points of calibration information.

After digitizing, the data were again checked for any unusual problems (noise, skew between channels, dropouts, etc.); none were found. The data were then dynamically clamped to the zero signal reference source (cold plate for the thermal channel and dark level for the other channels), i.e., processed to reduce any changes in the offset of each channel by calculating for each scan line the average values of the reference area for each of the channels, then subtracting these values from all points in the scan line.

The preprocessing stage was completed by application of the average signal versus angle data transformation [16]. In this method, for each channel, the average signal at each discrete scan angle (pixel) is calculated and the resulting function analyzed. The average signal function in all channels was quadratic in form. The data were corrected by dividing the data values by the corresponding value of the correction function.

The output data were then used in the training and classification stages described in the text.

APPENDIX VI
FIELD LOCATION IN S-192 DATA

As a first step in identifying individual fields, graymaps were generated for several of the bands which displayed good contrast and homogeneous areas, however, it was not possible to accurately locate individual fields. Even geographic features such as roads are not defined clearly enough to be of use in matching the ground information to the graymaps.

Since fields could not be located by inspection of graymaps, a semi-automatic procedure employed which made use of an x-y coordinate digitizer which efficiently digitizes the coordinates of points where a cursor has been momentarily positioned. All points of interest, section corners, field corners, etc., were located on large scale photography. Points digitized for Skylab processing were located on black and white enlargements of imagery acquired by the U-2 overflights in mid-August, 1973.

To transform the photographic (x,y) coordinates into (scan line, and scan point) coordinates, control points which could be found with confidence on the graymaps as well as on the photographs were used. Being unable to find such obvious control points as roads or road intersections, bodies of water were used for control points. Comparison of a signature for a deep water lake and a general vegetative signature indicated a large separation of signals in SDO's 17 and 19. Therefore a two-channel classification for water was performed; all points so classified were indicated on a scan-line-straightened graymap. These points were compared to U-2 and S-190A false color IR imagery to ascertain their precise place in the scene and finally were located on the enlarged U-2 photographs.

A transformation was calculated using the control points and regression techniques. The digitized points were then mapped from the photography (x,y) coordinates to scan line, scan point coordinates for scan-line-straightened data. The best-fit regression for the Skylab conversion yielded a first order equation with no cross terms.

These coordinates were then converted to conic data coordinates. The appropriate transformation was calculated by again defining a set of control points and by using the inverse of the scan line straightening transformation equations as given in the EREP Users Handbook, coupled with regression techniques to accurately calculate the constants in the equations. The equations we used were:

$$\text{CONIC POINT} = A\left[\frac{N}{\theta}\sin^{-1}\left[\frac{P\pi\theta}{180\cdot N}\right] + \left[\frac{N+2}{2}\right]\right] + B$$

where

P = [STRAIGHT POINT - 517.8-0.5]

N = 1239 Points/Conic Scan Line

$\theta = 116.25^{o}$ Field of Scan

A & B are constants estimated from regression techniques.

Similarly, for scan lines:

$$\text{CONIC LINE} = C + D \cdot \text{STRAIGHT LINE} - E\cdot R\cos\left[\frac{(\text{CONIC POINT} * 2 - 2 - N)\theta}{2N}\right]$$

with

R = Radius of the scan circle projected on the Earth

$R \approx 608$ pixels

and C,D, and E are constants estimated from regression techniques. To perform the regression, 18 points were located on both conic and straightened graymaps. The regression fit was very good and further, all 5 coefficients seemed to be sensible, a reflection of the physical reality.

With the field coordinates converted, the ground information was merged with the conic data. Graymaps of two conic data channels and the ground information channels were overlayed for comparison and the conversion was deemed very satisfactory.

APPENDIX VII

DESIGN OF THE EXPERIMENT TO ASSIST IN THE ANALYSIS OF THE EFFECTS OF CHANNEL-TO-CHANNEL SPATIAL MISREGISTRATION OF S-192 DATA ON "FIELD-CENTER" PIXELS

An integral part in the evaluation of the effects of misregistration of S-192 data is an investigation of the effects on field center pixels that remain field center in all channels even after misregistration. The following outlines the experiment designed to assist in this analysis. Since the analysis was based on a simulation of the effects of misregistration, the base signatures were extracted from the corrected conical S-192 data set which was assumed for purposes of simulation to be perfectly registered from channel-to-channel.

Step 1. Choose a signature set.

Five S-192 field center signatures were chosen representing the predominant scene classes: corn, tree, grass, brush, and bare soil. A subset of seven S-192 SDOs were used (SDOs 2, 8, 10, 12, 17, 19, 20).

Step 2. Choose a subset of n channels to misregister in simulation

There were two phases to this step in the experiment. Initially three channels, SDOs 2, 12, and 17 were chosen to be misregistered. These three SDOs were chosen because they were found to be the three best channels for purposes of discrimination in the least-probability-of-misclassification sense. Next, in a parallel experiment, only SDO 12 was misregistered. It had been determined to be the best single SDO for purposes of discrimination.

Step 3. Choose varying degrees of misregistration to simulate.

Each of the channels described in step 2 were misregistered in simulation by fixed amounts of 1/3, 1/2, 2/3 and 1 full pixel.

Step 4. Run a Computer Program to calculate simulated field-center signatures for each degree of misregistration determined in Step 3.

The simulation model used is described in section 4.3.2. A computer program was written to implement the algorithm simulating the effects of channel-to-channel spatial misregistration of field center pixels. This program was run to produce four sets of signatures with three misregistered channels and four sets of signatures with one channel misregistered. Each set represented a different degree of misregistration.

Step 5. Calculate an expected performance matrix for each set of signatures. The program PEC was used to calculate these matrices. PEC is fully described in Appendix XI. The program was run for each set of signatures simulating effects of misregistration along with the original "registered" signatures,

Step 6. Analyze the results in light of the analytical expectations. The performance matrices were analyzed as is described in Section 4.3.4.

APPENDIX VIII

DESIGN OF THE EXPERIMENT TO ASSIST IN THE ANALYSIS OF THE EFFECTS OF CHANNEL-TO-CHANNEL SPATIAL MISREGISTRATION OF S-192 DATA ON "BORDER" OR "MIXTURE" PIXELS

The following experiment was implemented to determine the effects of misregistration on mixture pixels. Since the analysis was based on a simulation of the effects of misregistration, the base signatures were extracted from the corrected conical S-192 data set which was assumed for purposes of simulation to be perfectly registered from channel-to-channel. The analysis carried out pertains only to those pixels that are mixture pixels in some channel(s) after misregistration.

Step 1. Choose a signature set.

Five S-192 field center signatures were chosen representing the predominant scene classes: corn, tree, grass, brush, and bare soil. A subset of seven S-192 SDO's (2, 8, 10, 12, 17, 19, 20) were used.

Step 2. Choose a subset of n channels to misregister in simulation.

There were two phases to this step in the experiment. First three channels, SDOs 2, 12, and 17, were used. These three SDOs were chosen because they were found to be the three best channels for purposes of discrimination in the least-probability-of-misclassification sense. Next, a single SDO, 12, was used. It had been determined to be the best SDO for purposes of discrimination.

Step 3. Choose varying degrees of misregistration to simulate.

Each of the channels described in Step 2 were misregistered in simulation by fixed amounts of 1/2 and 1 full pixel in the east to west direction.

Step 4. Run a computer program to calculate simulated field center signatures for each degree of misregistration determined in Step 3.

The simulation model used is described in section 4.4.2. A computer program was written to implement the algorithm simulating the effects of channel-to-channel spatial misregistration on field center pixels. This program was run to produce six sets of signatures, three for each parameter setting of channels to be misregistered.

Step 5. Choose varying proportions of mixtures of two ground covers to simulate.

A distribution of mixtures of two ground covers A and B were to be simulated in proportion of 2/3 A and 1/3 B, 1/3 A and 2/3 B.

Step 6. Simulate mixture distributions in the proportions chosen in Step 5 for all possible pairs of registered field center signatures chosen in Step 1.

The program discussed in step 4 was optionally run to simulate these mixture distributions in the proportions described in Step 5. These mixtures represented the actual distributions expected to be found in the S-192 data set under the assumptions of the model used.

Step 7. Simulate mixture distributions in the proportions chosen in Step 5 for all possible pairs of misregistered field center signatures for each misregistration chosen in Step 3.

For one-half pixel misregistration, twelve distributions were simulated for each of the field-center misregistered distributions calculated in Step 4. For one pixel misregistration, twenty signatures were simulated for each of the base signatures. The difference in the number of simulations lay in the fact that, for a greater degree of misregistration, more field center pixels would be mixtures in the misregistered channels. Hence more distributions were simulated in order to better represent the situation.

Step 8. Calculate an expected performance matrix for each degree of misregistration.

Using the program PEC, three performance matrices were calculated, one for each misregistration of 0, 1/2 and 1 full pixel. Program PEC is described in Appendix XI. The field center signatures simulated in Step 4 were used as recognition classes. Linear decision boundaries were determined based on these signatures. Then the signatures simulated in Step 7 were used as the scene classes and expected performance probabilities

were calculated for each of the simulated distributions.

Step 9. Plot the results.

Graphs were generated displaying the probability of classification of a ground cover as a function of the mixture and misregistration.

Step 10. Analyze the results.

The plots were analyzed as a described in Section 4.4.5.

APPENDIX IX

A SIMPLE ANALYTICAL MODEL TO STUDY THE EFFECTS OF MISREGISTRATION ON FIELD CENTER CLASSIFICATION ACCURACY

Insight has been gained into what effects spatial misregistration may have on field-center classification accuracy through an analytical analysis of the problem. Consider two normal distributions in n channels, $N_A(\mu_A, R)$ and $N_B(\mu_B, R)$, with a common covariance R. The probability of a type-one error* using the linear decision rule is

$$\Phi[1/2(\mu^t R^{-1}\mu)^{\frac{1}{2}}] \qquad \text{(IX-1)}$$

where

$$\Phi(x) = \frac{1}{\sqrt{2\pi}} \int_x^\infty e^{-\frac{1}{2}y^2}\, dy \qquad \text{(IX-2)}$$

and $\mu = \mu_A - \mu_B$, the channel to channel mean difference.

Studies have indicated that misregistration from channel to channel, or time period to time period in the case of multitemporal analysis, causes resultant signatures to be less correlated. This analysis, therefore, attempts to examine the error rate Φ as a function of correlation ρ

$$\text{Let } R = \begin{pmatrix} \sigma_1^2 & \rho\sigma_1\sigma_2 \\ \rho\sigma_1\sigma_2 & \sigma_2^2 \end{pmatrix} \quad ; \quad \text{then } R^{-1} = \frac{1}{\sigma_1^2\sigma_2^2(1-\rho^2)} \begin{pmatrix} \sigma_2^2 & -\rho\sigma_1\sigma_2 \\ -\rho\sigma_1\sigma_2 & \sigma_1^2 \end{pmatrix} \qquad \text{(IX-3)}$$

*Under the assumption of common covariance, type-two error is equivalent to to type-one error.

Also, let $f(\rho) = \mu^t R^{-1} \mu$ for $-1 \leq \rho \leq 1$ (IX-4)

and $g(\rho) = 1/2 f(\rho)^{1/2}$

$f(\rho) \to \infty$ at $\rho = \pm 1$

Similarly $g(\rho) \to \infty$ at $\rho = \pm 1$, which implies $x \to \infty$ at $\rho = \pm 1$. Φ can be expressed as a function of ρ through $f(\rho)$ and/or $g(\rho)$:

$$\Phi(x) = \Phi[1/2\ f(\rho)^{1/2}] = \Phi[g(\rho)].$$

Substituting $x = \infty$ into Eq. IV-2 we have $I(\infty) = 0$. We have established therefore, that the error rate Φ is minimized for correlation $\rho = \pm 1$. Let us now examine the behavior of the function Φ for $-1 < \rho < 1$.

Although restricting ourselves to two channels we note that the following analysis can be generalized for ρ_{ij}, the correlation between any pair of channels i and j.

Let us now calculate the first derivative of $f(\rho)$:

$$f(\rho) = \mu^t R^{-1} \mu$$

$$\frac{df(\rho)}{d(\rho)} = \mu^t \frac{d\, R^{-1}}{d\rho} \mu \qquad \text{(IX-5)}$$

We can simplify the calculation of $\frac{d\, R^{-1}}{d\rho}$ by noting the following relationship between $\frac{dR^{-1}}{d\rho}$ and $\frac{dR}{d\rho}$:

$$\frac{d}{d\rho} (RR^{-1}) = \frac{d}{d\rho} (I) = 0 = (\frac{dR}{d\rho})\, R^{-1} + R\, (\frac{dR^{-1}}{d\rho})$$

Solving for $\frac{dR^{-1}}{d\rho}$ we find:

$$\frac{dR^{-1}}{d\rho} = - R^{-1} (\frac{dR}{d\rho})\, R^{-1} \qquad \text{(IX-6)}$$

Substituting Eq. IX-6 into Eq. IX-5 and solving:

$$\frac{df(\rho)}{d\rho} = -\mu^t R^{-1} \frac{dR}{d} R^{-1}\mu$$

Noting that $\mu^t R^{-1} = [(R^{-1})^t \mu]^t$ and $(R^{-1})^t = R^{-1}$

$$\frac{df(\rho)}{d\rho} = -(R^{-1}\mu)^t \frac{dR}{d} (R^{-1}\mu) \qquad \text{(IX-7)}$$

Eq IX-7 is an expression for the first derivative of $f(\rho)$ in terms of the derivative of R. Now let us examine if, for $-1 < \rho < 1$, critical values of $f(\rho)$ exist. Individually examining the components of equation (IX-6) determine the following expression for two channels.

$$R^{-1}\mu = \frac{1}{\sigma_1^2\sigma_1^2 (1-\rho^2)} \begin{pmatrix} \sigma_2^2\mu_1 & -\rho\sigma_1\sigma_2\mu_2 \\ \sigma_1^2\mu_2 & -\rho\sigma_1\sigma_2\mu_1 \end{pmatrix} \equiv c_1 \begin{pmatrix} a_1 \\ a_2 \end{pmatrix} \qquad \text{(IX-8)}$$

$$\frac{dR}{d\rho} = \sigma_1\sigma_2 \begin{pmatrix} 0 & 1 \\ 1 & 0 \end{pmatrix} = c_2 \begin{pmatrix} 0 & 1 \\ 1 & 0 \end{pmatrix} \qquad \text{(IX-9)}$$

now substituting IX-8 and IX-9 intoIX-7:

$$\frac{df(\rho)}{d\rho} = -c_1(a_1, a_2)\, c_2 \begin{pmatrix} 0 & 1 \\ 1 & 0 \end{pmatrix} c_1 \begin{pmatrix} a_1 \\ a_2 \end{pmatrix}; \quad \text{let } b = -c_2 c_1^2 \qquad \text{(IX-10)}$$

$$\frac{df(\rho)}{d\rho} = b(a_1 a_2) \begin{pmatrix} a_2 \\ a_1 \end{pmatrix} = 2ba_1a_2 \; ; \; b > 0 \qquad \text{(IX-11)}$$

For $\frac{df(\rho)}{d\rho} = 0$, either a_1 or a_2 one of the two rows of R^{-1}, must equal zero. Since $\Phi(x) \geq 0$ and continuous, and has minima defined at $\rho = \pm 1$, then Φ is maximized at

$$\rho_C = \frac{\mu_1\sigma_2}{\mu_2\sigma_1} \text{ or } \frac{\mu_2\sigma_1}{\mu_1\sigma_2} \text{ for } -1 \leq \rho \leq 1.$$

Before examining the implications of this result, let us determine whether this result can be generalized.

Eqs. IX-5 to IX-7 can be generalized by letting $\rho \equiv \rho_{ij}$ and $\frac{dR}{d\rho} \equiv \frac{\partial R}{\partial \rho_{ij}}$ for any pair of channels i and j.

Hence:

$$f(\rho_{ij}) = \mu^t R^{-1} \mu$$

and

$$\frac{\partial f(\rho_{ij})}{\partial \rho} = \mu^t \frac{\partial R^{-1}}{\partial \rho_{ij}} \mu$$

Examining a three-dimensional case,

$$R = \begin{pmatrix} \sigma_1^2 & \rho_{12}\sigma_1\sigma_2 & \rho_{13}\sigma_1\sigma_3 \\ \rho_{12}\sigma_1\sigma_2 & \sigma_2^2 & \rho_{23}\sigma_2\sigma_3 \\ \rho_{13}\sigma_1\sigma_3 & \rho_{23}\sigma_2\sigma_3 & \sigma_3^2 \end{pmatrix}$$

Therefore:

$$\frac{\partial R}{\partial \rho_{12}} = \begin{pmatrix} 0 & 1 & 0 \\ 1 & 0 & 0 \\ 0 & 0 & 0 \end{pmatrix} ; \quad \frac{\partial R}{\partial \rho_{13}} = \begin{pmatrix} 0 & 0 & 1 \\ 0 & 0 & 0 \\ 1 & 0 & 0 \end{pmatrix} ; \quad \frac{\partial R}{\partial \rho_{23}} = \begin{pmatrix} 0 & 0 & 0 \\ 0 & 0 & 1 \\ 0 & 1 & 0 \end{pmatrix}$$

Following the same line of reasoning as in two dimensions [Eq. IX-10 and IX-11 we find that

$$\frac{\partial f(\rho_{12})}{\partial \rho_{12}} = 0 \text{ when either the 1st or 2nd row of } R^{-1}\mu \text{ is zero;}$$

similarly for $f(\rho_{23})$ and $f(\rho_{13})$.

We can now generalize to conclude

$$\frac{\partial f(\rho_{i,j})}{\partial \rho_{i,j}} = 0 \text{ at some } \rho_{ci,j} \text{ in the interval defined by } -1 < \rho_{ij} < 1$$

for any pair of channels i, j. The point $\rho_{ci,j}$ can be calculated exactly by setting the i^{th} or j^{th} row of $R^{-1}\mu$ equal to zero and solving for $\rho_{i,j}$. The function f is a function of many variables, $f(\rho_{12},\rho_{13},\ldots,\rho_{ij},\ldots)$ for all i,j. We have determined that (1) the function Φ is minimized along its boundary in the interval $-1 \leq \rho \leq 1$ and (2) the function f has a critical point at $\rho_{ci,j}$ with respect to each variable $\rho_{i,j}$ for all i and j and these critical points must be maxima. Under these conditions we can conclude that the function Φ reaches a maximum on the interval $-1 < \rho_{ij} < 1$.

Let us now examine the implications of this analysis graphically for two channels of data:

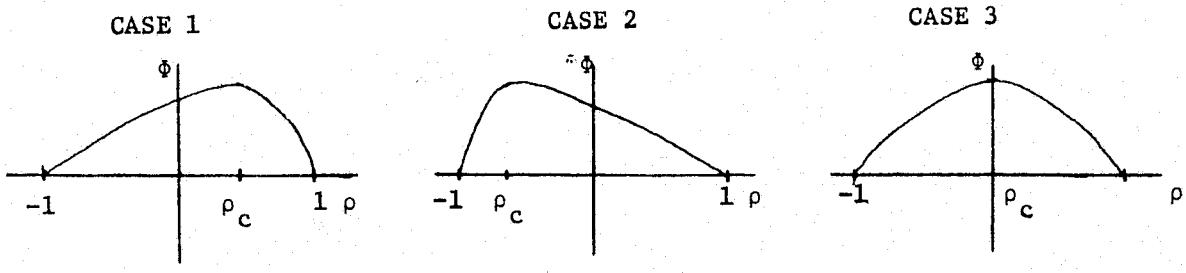

FIGURE IX-1 ERROR RATE OF RECOGNITION Φ, AS A FUNCTION OF CORRELATION ρ IN FIELD CENTERS

Figure IX-1 displays possible curves mapping the error rate Φ in field centers as a function of ρ. A maximum error occurs at ρ_c. Φ is minimized at $\rho = \pm 1$ and intercepts the y axis at $\rho=0$, $f(0) = f(0) = \dfrac{\mu_1^2 \sigma_2^2 + \mu_2^2 \sigma_1^2}{\sigma_1^2 \sigma_2^2}$.

ρ_c occurs at $\rho_c = \dfrac{\mu_1\sigma_2}{\mu_2\sigma_1}$ or $\dfrac{\mu_2\sigma_1}{\mu_1\sigma_2}$.

Let ρ_r be the correlation of a registered data set in two channels and let ρ_m be the correlation of the same data set but misregistered to varying degrees. Keep in mind that misregistering data will cause the correlation to decrease. Let us examine each case depicted in Figure IX-1 separately.

CASE 1

(1) if $0 \leq \rho_c \leq \rho_r \leq 1$, then misregistering the data set would cause the error rate to increase until $\rho_m = \rho_c$, then it would restore accuracy somewhat until $\rho_m = 0$.

(2) if $0 \leq \rho_r \leq \rho_c \leq 1$, then misregistration would actually improve results.

(3) if $-1 \leq \rho_r \leq 0$, then misregistration would cause the error rate to increase.

(4) if $\rho_c \approx 1$, misregistration would always improve field center results.

CASE 2

(1) if $-1 \leq \rho_r \leq \rho_c < 0$, this behaves as case 1 step (1).

(2) if $-1 \leq \rho_c \leq \rho_r \leq 0$, see case 1, step (2).

(3) if $0 \leq \rho_r \leq 1$, see case 1 step (3).

(4) if $\rho_c \approx -1$, see case 1, step (4)

CASE 3

In this case misregistration would always cause the error rate to increase.

APPENDIX X

DERIVATION OF CORRELATION ESTIMATION MODEL FOR TWO CHANNELS MISREGISTERED WITH RESPECT TO ONE ANOTHER

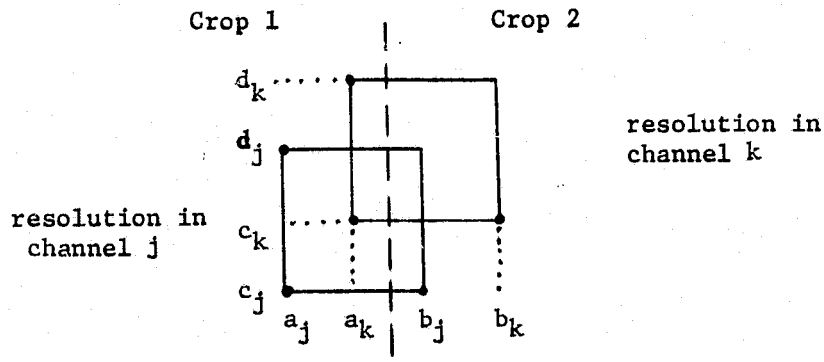

FIGURE X-1. CONFIGURATION OF BOUNDARY RESOLUTION ELEMENTS OF TWO CHANNELS OF DATA MISREGISTERED WITH RESPECT TO ONE ANOTHER

In the derivation of the covariance estimation model, we restrict ourselves to two channels of data and two crop types. Figure X-1 illustrates a possible configuration of boundary elements for two channels misregistered with respect to one another. It is the cross-correlation between two such channels that we are interested in calculating.

Let $S_{ij}(\alpha,\beta)$ be the signal per unit area from ground coordinate (α,β) for the i^{th} crop, j^{th} channel. This signal is assumed to originate from a stationary random process, with statistics:

$$E[S_{ij}(\alpha,\beta)] = A_{ij}$$

$$E\{[S_{ij}(\alpha_1,\beta_1) - A_{ij}]\,[S_{hk}(\alpha_2,\beta_2) - A_{hk}]\}$$

$$= \delta(i,h)\, r_{ijk}\,(\alpha_1-\alpha_2,\beta_1-\beta_2)$$

$\delta(i,h)$ is Kronicker's Delta Function. If $i \neq h$, i.e. two different crops, correlation is assumed to be zero.

$r_{ijk}(\alpha_1-\alpha_2,\beta_1-\beta_2)$ is the correlation function and is dependent on the distance between the locations on the ground.

The assumption made is that the correlation between two pixels drops rapidly as the distance between two pixels increases. The correlation between two adjacent pixels is assumed to be zero.

The scanner signal in the j^{th} channel is the sum over the resolution area of all signals $S_{ij}(\alpha,\beta)$:

$$x_j = \int_{a_j}^{0} d\alpha \int_{c_j}^{d_j} d\beta S_{1j}(\alpha,\beta) + \int_{0}^{b_j} d\alpha \int_{c_j}^{d_j} d\beta\, S_{2j}(\alpha,\beta)$$

with statistics:

$$E(x_j) = \int_{a_j}^{0} d\alpha \int_{c_j}^{d_j} d\beta a_{1j} + \int_{0}^{b_j} d\alpha \int_{c_j}^{d_j} d\beta a_{2j}$$

$$x_j - E(x_j) = \int_{a_j}^{0} d\alpha \int_{c_j}^{d_j} d\beta [S_{1j}(\alpha,\beta) - A_{1j}] + \int_{0}^{b_j} d\alpha \int_{c_j}^{d_j} d\beta [S_{2j}(\alpha,\beta) - A_{2j}]$$

the correlation between channels j and k is:

$$R_{jk} = E\left\{[x_j - E(x_j)]\,[x_k - E(x_k)]\right\}$$

$$= E\left\{\left[\int_{a_j}^{0} d\alpha_1 \int_{c_j}^{d_j} d\beta_1 [S_{1j}(\alpha_1,\beta_1) - A_{1j}] + \int_{0}^{b_j} d\alpha_2 \int_{c_j}^{d_j} d\beta_2 [S_{2j}(\alpha_2,\beta_2) - A_{2j}]\right]\right.$$

$$\left. * \left[\int_{a_k}^{0} d\alpha_1 \int_{c_k}^{d_k} d\beta_1 [S_{1k}(\alpha_1,\beta_1) - A_{1k}] + \int_{0}^{b_k} d\alpha_2 \int_{c_k}^{d_k} d\beta [S_{2k}(\alpha_2,\beta_2) - A_{2k}]\right]\right\}$$

multiplying this expression out we note that cross terms drop out due to Kronecker's Delta:

$$R_{jk} \int_{a_j}^{0} d\alpha_1 \int_{c_j}^{d_j} d\beta_1 \int_{a_k}^{0} d\alpha_2 \int_{c_k}^{d_k} d\beta_2 \; r_{1jk}(\alpha_1-\alpha_2,\ \beta_1-\beta_2)$$

$$+ \int_{0}^{b_j} d\alpha_1 \int_{c_j}^{d_j} d\beta_1 \int_{0}^{b_k} d\alpha_2 \int_{c_k}^{d_k} d\beta_2 \; r_{2jk}\ (\alpha_1-\alpha_2,\ \beta_1-\beta_2)$$

To simplify the algebra let $c_j=c_k$ and $d_j=d_k$. This means that only misregistration in one direction is considered. We will generalize later to two directions. Using this assumption along with the identity*

$$R_{jk} = \int_{a_j}^{0} d\alpha_1 \int_{a_k}^{0} d\alpha_2 (d-c) \int_{-(d-c)}^{d-c} r_{1jk}(\alpha_1-\alpha_2,\beta) \left(1 - \frac{|\beta|}{d-c}\right) d\beta$$

$$+ \int_{0}^{b_j} d\alpha_1 \int_{0}^{b_k} d\alpha_2 (d-c) \int_{-(d-c)}^{d-c} r_{2jk}(\alpha_1-\alpha_2,\beta) \left(1 - \frac{|\beta|}{d-c}\right) d\beta$$

$$\text{let } F_{1jk} = (d-c) \int_{-(d-c)}^{d-c} r_{ijk}\ (\alpha_1-\alpha_2,\beta) \left(\frac{1-|\beta|}{d-c}\right) d\beta$$

and similarly

$$F_{2jk} = (d-c) \int_{-(d-c)}^{d-c} r_{2jk}\ (\alpha_1-\alpha_2,\beta) \left(1-\frac{|\beta|}{d-c}\right) d\beta$$

---

* Simplified using the identity

$$\int_{A}^{B} \int_{A}^{B} F(u-v)\ du\ dv = (B-A) \int_{-(B-A)}^{B-A} F(x)\ \ 1- \frac{|x|}{B-A}\ \ dx$$

substituting we have:

$$R_{jk} = \int_{a_j}^{0} d\alpha_1 \int_{a_k}^{0} d\alpha_2 \, F_{1jk}(\alpha_1-\alpha_2) + \int_{0}^{b_j} d\alpha_1 \int_{0}^{b_k} d\alpha_2 F_{2jk}(\alpha_1-\alpha_2) \qquad \text{(X-1)}$$

now examine each component of R_{jk} assuming that $a_j \leq a_k$ (the same argument applies otherwise).

$$\int_{a_j}^{0} d\alpha_1 \int_{a_k}^{0} d\alpha_2 \, F_{1jk}\,(\alpha_1-\alpha_2)$$

$$= \int_{a_j}^{a_k} d\alpha_1 \int_{a_k}^{0} d\alpha_2 \, F_{1jk}\,(\alpha_2-\alpha_1) + \int_{a_k}^{0} d\alpha_1 \int_{a_k}^{0} d\alpha_2 \, F_{1jk}\,(\alpha_2-\alpha_1)$$

$$= \int_{a_j}^{a_k} d\alpha_1 \int_{a_k}^{0} d\alpha_2 \, F_{1jk}\,(\alpha_2-\alpha_1) + (-a_k) \int_{a_k}^{-a_k} F_{1jk}(\alpha) \left(1-\frac{|\alpha|}{-a_k}\right) d\alpha \qquad \text{(X-2)}$$

The contribution to the estimated covariance from any non-overlapping region is assumed to be zero. The left component of Eq. X-2 determines this contribution, hence it can be eliminated. Thus the left hand term of R_{jk} is:

$$\approx (-a_k) \int_{a_k}^{-a_k} F_{1jk}(\alpha) \left(1-\frac{|\alpha|}{-a_k}\right) d\alpha \qquad \text{(X-3)}$$

Similarly for $b_j < b_k$ we find:

$$\int_{0}^{b_j} d\alpha_1 \int_{0}^{b_k} d\alpha_2 \, F_{2jk}\,(\alpha_1-\alpha_2) \approx (b_j) \int_{-b_j}^{b_j} F_{2jk} \left(1-\frac{|\alpha|}{b_j}\right) d\alpha \qquad \text{(X-4)}$$

substituting Eqs. X-3 and X-4 into Eq. X-1 we have:

$$R_{jk} \approx (-a_k) \int_{a_k}^{-a_k} F_{1jk}(\alpha) \left(1-\frac{|\beta|}{-a_k}\right) d\alpha + (b_j) \int F_{2jk} \left(1-\frac{|\alpha|}{b_j}\right) d\alpha \qquad \text{(X-5)}$$

If the pixels being examined were pure crop 2 pixels, the expression evaluated for R_{jk} would be the covariance R_{2jk} between channels j and k in crop 2. In order to simplify the expression for a border pixel we need to evaluate it in the field center case.

For crop 2, $a_k = 0$ and let $b_j = b_k = b$, hence

$$R_{jk} = R_{2jk} = 0 + \int_0^b d\alpha_1 \int_0^b d\alpha_2 \, F_{2jk} \, (\alpha_1 - \alpha_2)$$

simplifying:

$$R_{2jk} = b \int_{-b}^{b} F_{2jk} \, (\alpha) \left(1-\frac{|\alpha|}{b}\right) d\alpha \qquad \text{(X-6)}$$

Similarly for crop 1, $b_j = 0$, and let $a_j = a_k = a$

$$R_{1jk} = a \int_{-a}^{a} F_{1jk} \, (\alpha) \left(1-\frac{|\alpha|}{a}\right) d\alpha \qquad \text{(X-7)}$$

We know have R_{2jk} and R_{1jk}, the covariance terms for channels j and k for crops two and one.

For a mixed pixel, we mak[illegible] two observations.

(1) The covariance of two points on the ground drops very rapidly as a function of the distance between them then:

(2) To substitute Eqns. (X-6) and (X-7) into Eq. (X-5) we need to normalize by dividing respective terms by a and b, the widths of the respective pixels.

Having made these observations we can conclude for a boundary pixel, the covariance R_{jk} can be calculated using the expression

$$R_{jk} = \frac{a_k}{a} R_{1jk} + \frac{b_j}{b} R_{2jk} \qquad \text{(X-8)}$$

Eq. X-8 was derived under the assumption that misregistration was in only one direction. The simulation model described in section 4.4.2 is based on this assumption. The analogy of Eq. X-8 with misregistration in two directions is a trivial extension of Eq. X-8 and is determined to be:

$$R_{jk} = \left(\frac{d_k - c_j}{ac}\right) a_k R_{1jk} + \left(\frac{d_k - c_j}{ad}\right) b_j R_{2jk} \qquad \text{(X-9)}$$

where $c = d_k - c_k$ and $d = d_j - c_j$ are the heights of each resolution element. We note that in our case the widths of the respective pixels are the same size, hence a=b. Therefore $\frac{a_k}{a}$ is the proportion of overlap in crop 1, and $\frac{b_j}{b}$ is the proportion of overlap in crop 2.

APPENDIX XI
DESCRIPTION OF PROGRAM PEC

PEC is a program written in the MAD language under UMESS for the IBM 7094. PEC will compute the expected performance matrix for the ERIM linear rule classifier on a given set of signatures and classifier parameters by using a Monte-Carlo technique. The matrix gives the probability that pixels from each given signature distribution will be classified into each given recognition class based on the best linear decision boundaries between recognition classes. The classifier works as follows. Between each pair of signatures A and B, a boundary is found to separate those pixels which might be classified as A from those classified as B. This boundary is a linear hyperplane of the form

$$[\vec{x}_o \cdot \vec{C} - D] = 0$$

where

$\vec{x}_o$ is any point on the hyperplane

$\vec{C}$ is a vector normal to the hyperplane

D is a constant which is the distance from the origin to the plane in units of the length of $\vec{C}$. In this program we normalize C to be of unit length.

If $[\vec{x} \cdot \vec{C} - D] < 0$, then $\vec{x}$ will be classified as A; otherwise $\vec{x}$ will be classified as B.

Once these boundaries are established between all pairs of signatures, classification proceeds as follows. Given a pixel, it is tested againgt the hyperplane between signatures 1 and 2, and one of these two classes wins. The winning signature is tested against the third, this winner against the fourth, etc. The ultimate winning signature thus will emerge, and the exponent value $(\vec{x}-\vec{\mu}_w)^t M_w^{-1}(\vec{x}-\vec{\mu}_w)$ will be computed. If the exponent is less than a specified threshold, the point will be tabulated as belonging to the winning signature class, but otherwise the point will be tabulated into the class "unclassified".

A Monte-Carlo technique is employed to generate the pixel from a given scene class. The production of a random pixel is as follows. We want $\vec{y}$ such that {y} is normally distributed with signature mean $\vec{b}$ and covariance R. First $\vec{x}$ is produced with each element normally distributed, so that it has mean 0 and covariance I (the identity, that is, channels, are uncorrelated). Then we want a transformation

$$\vec{y} = \vec{P}\vec{x} + \vec{b} \qquad \text{(XI-1)}$$

which we will apply to every $\vec{x}$ to get the corresponding $\vec{y}$. By definition, the covariance R can be written

$$R = E\{(\vec{y}-\vec{b})\ (\vec{y}-\vec{b})^t\}$$

where E { } or e( ) denotes the expected value of the enclosed term. Then

$$R = E\{(Px)(Px)^t\} = E(Pxx^tP^t)$$
$$= PE(xx^t)P^t = PIP^t = PP^t$$

By definition, P is the Cholesky decomposition of R. After computing P, each $\vec{y}$ is obtained quickly from Eq. XI-1.

REFERENCES

1. Skylab Program, EREP Sensor Performance Report Volume III (S-192) Engineering Baseline, SL2, SL3 and SL4, NASA Report MSC-05528, Houston, Texas, September, 1974.

2. Turner R. E. & M.M. Spencer, Atmospheric Model for Correction of Spacecraft Data, Proceedings of the 8th International Conference on Remote Sensing of Environment, Center for Remote Sensing Information & Analysis, Willow Run Laboratories of the Institute of Science and Technology, The University of Michigan, 1972.

3. Skylab Program, EREP Sensor Performance Evaluation Final Report, Volume III (S-192), Report No. JSC 05546, Johnson Space Center, Houston, Texas, May, 1975.

4. Braithwaite, J. and P. Lambeck, ERIM Contribution to the S-192 Sensor Performance Evaluation, Report 102800-51-F, Environmental Research Institute of Michigan, Ann Arbor, Michigan, January, 1975.

5. Morgenstern, J., J. Sarno, R. Nalepka, Skylab S-192 ADP Resources Requirements for an Agricultural Application, Report 104600-44-F, Environmental Research Institute of Michigan, Ann Arbor, Michigan, August, 1975.

6. Hasell, P., et al, Michigan Experimental Mapping System -- a description of the M7 Airborne Sensor and its Performance, Report No. 190900-10-T, Environmental Research Institute of Michigan, Ann Arbor, January 1974.

7. Mission Report, Earth Observations Aircraft Program, Mission 85M (Volume VII), NASA Project S456, Test Site 279, October 1973.

8. Horwitz, H. J. Lewis and A. Pentland, First Quarterly Report, Task IV: Proportion Estimation, Report No. 109600-3-L, August 30, 1974.

9. Coberly, W. Serial Correlation of Spectral Measurements, May 31, 1973 NASA:FM8/Mathematical Physics Branch.

10. Horwitz, H.M., J. T. Lewis and A.P. Pentland, Estimating Proportions of Objects from Multispectral Scanner Data, Report No. 109600-13-F, Environmental Research Institute of Michigan, Ann Arbor, May, 1975.

11. Henderson, R.G., G.S. Thomas and R.F. Nalepka, Methods of Extending Signatures and Training Without Ground Information, Report No. 109600-16-F, Environmental Research Institute of Michigan, Ann Arbor, May, 1975.

12. Malila, W. A., R. F. Nalepka, and J. E. Sarno, Image Enhancement and Advanced Information Extraction Techniques for ERTS-1 Data, Report No. 193300-66-F, The Environmental Research Institute of Michigan, Ann Arbor, Michigan, June 1975, Section 4.2.1.

13. Crane, R. B., Adaptive Processing with a Decision-Directed Kalman Filter and Feature Extraction of Multispectral Data, Report No. 190100-31-T, The Environmental Research Institute of Michigan, Ann Arbor, Michigan, July 1974.

14. Malila. W. A. and R. F. Nalepka, Atmospheric Effects in ERTS-1 Data and Advanced Information Extraction Techniques, Symposium on Significant Results Obtained from ERTS, Vol. 1, Goddard Space Flight Center, Greenbelt, Maryland, 1973.

15. Horwitz, H. M., R. F. Nalepka, P. D. Hyde, and J. P. Morgenstern, Estimating Proportions of Objects Within a Single Resolution Element of a Multispectral Scanner, Seventh International Symposium on Remote Sensing of the Environment, May, 1971.

16. Nalepka, R, and J. Morgenstern, Signature Extension Techniques Applied to Multispectral Scanner Data, Proceedings of the Eighth International Symposium on Remote Sensing of the Environment, October 1972.

17. Malila, W., R. Hieber and R. Cicone, Studies of Recognition with Remote Sensed Data, Report No. 109600-19-F, Environmental Research Institute of Michigan, June 1975.